University of Pardubice

Faculty of Chemical Technology

Effect of mechanical activation and thermal processing of Al/Ni mixtures on hydrodehalogenation of AOX dissolved in aqueous solution

Mgr. Michal Hegedüs

Doctoral thesis

2022

Prohlašuji:
Tuto práci jsem vypracoval samostatně. Veškeré literární prameny a informace, které jsem v práci využil, jsou uvedeny v seznamu použité literatury.
Byl jsem seznámen s tím, že se na moji práci vztahují práva a povinnosti vyplývající ze zákona č. 121/2000 Sb., autorský zákon, zejména se skutečností, že Univerzita Pardubice má právo na uzavření licenční smlouvy o užití této práce jako školního díla podle § 60 odst. 1 autorského zákona, a s tím, že pokud dojde k užití této práce mnou nebo bude poskytnuta licence o užití jinému subjektu, je Univerzita Pardubice oprávněna ode mne požadovat přiměřený příspěvek na úhradu nákladů, které na vytvoření díla vynaložila, a to podle okolností až do jejich skutečné výše.

Souhlasím s prezenčním zpřístupněním své práce v Univerzitní knihovně.

V Pardubicích dne 28. 6. 2022

Mgr. Michal Hegedüs

I am extremely thankful to my wife Andrea for her support, great care, and patience during my Ph.D. study. I´d like to dedicate this work to my first born daughter Victoria, who I hope will follow my footsteps in natural sciences one day. I am grateful to my dear friend Mgr. Katarína Gáborová for scientific and experimental help. Without her this work would not have been possible. Special thanks go to my supervisor Ing. Doc. Tomáš Weidlich, Ph.D. for his support, experimental ideas, and material support.

I would also like to thank my former colleague Ing. Petr Lacina, Ph.D. who actually made my way into the Czech Republic and introduced me to my supervisor. Last but not least, I acknowledge all my current colleagues from the Synthon, s.r.o. company for their time and help with various scientific challenges.

For proofreading of the thesis and grammar corrections, Mrs. Martina Roda and Mrs. Connie Massimino are acknowledged.

Efekt mechanické aktivace a termálního zpracování směsí Al/Ni na účinnost odstraňování AOX z vodních roztoků

ANOTACE

Předkládaná práce se zaobírá možností aplikace mechanicky aktivovaných směsí neušlechtilého kovu (konkrétně hliníku) a hydrogenačního katalyzátoru (niklu) pro hydrodehalogenační odbourávání aromatických halogenovaných látek z vod. Mechanická aktivace představuje časově a ekonomicky nenáročný proces, při kterém dochází mletím k aktivaci kovů, hlavně vlivem zvětšování specifického povrchu i vznikem různých defektů v jejich krystalové struktuře. Termicky upravené aktivované směsi Al-Ni můžou několikanásobně snížit celkové náklady na reduktivní dehalogenaci studovaných látek oproti doposud využívané komerčně dostupné Raneyho slitině (50:50 wt.% Al-Ni).

KLÍČOVÁ SLOVA

mechanická aktivace, binární slitiny, redukční dehalogenace, odstraňování polutantů

TITLE

Effect of mechanical activation and thermal processing of Al/Ni mixtures on hydrodehalogenation of AOX dissolved in aqueous solution

ANNOTATION

The presented thesis deals with the possibility of the application of mechanically activated metal mixtures (aluminum and nickel) for the removal of halogenated aromatic compounds from an aqueous environment. Mechanical activation is a process, in which the compounds are activated by milling, mainly due to an increase in a specific surface area and the formation of various defects in their crystal structure. Thermally treated activated Al-Ni mixtures may lead to a decrease in the total costs of reductive dehalogenation process for selected analytes in comparison with commercially available Raney type Al-Ni alloys; such as the 50:50 wt.% Al-Ni alloy.

KEYWORDS

mechanical activation, binary alloys, reductive dehalogenation, pollutants removal

CONTENT

LIST OF FIGURES AND TABLES

LIST OF ABBREVIATIONS

AOX – absorbable organic halides

API – active pharmaceutical ingredient

BPR – ball-to-powder ratio

BTEX – group name for benzene - toluene - ethylbenzene - xylene

CB - chlorobenzene

CBA – chlorobenzoic acid

DMCR - “Dehalogenation By Mechanochemical Reaction”

EU – European union

HDH – hydrodehalogenation reaction

MOF – metal organic framework

PAH – polycyclic aromatic hydrocarbon

PCA – process control agent

PCBs – polychlorinated biphenyls

PCDD – polychlorinated dibenzodioxin

PCDF – polychlorinated dibenzodifuran

POP – persistent organic pollutant

PSD – particle size distribution

PVP – polyvinylpyrollidone

SEM – scanning electron microscopy

XRPD – X-ray powder diffractometry

1 INTRODUCTION

Organic halogenated aromatics represent a large group of chemical substances vastly produced and used in the 20th century, mainly as solvents, dyestuffs, pigments, flame retardants, biocides, pesticides, or medical drugs. Their production was often connected to the leakage of unreacted starting materials/side products into waste- or groundwater, where they are still found due to their low biodegradability and high chemical stability of the C-X bond (X = F, Cl, Br, I). Since most of the halogenated organic compounds are classified as persistent organic pollutants (POPs) that can bioaccumulate in the environment and cause harm to living organisms, their production was eliminated or at least restricted (e.g. Stockholm convention on persistent organic pollutants [1]. Still, more than 300 000 sites are contaminated sites in the European Union. Of these, around 10% are reported to be contaminated by chlorinated organics [2].

Numerous methods for degrading of halogenated organics have been developed over the years. Whereas, in the case of simple aliphatic halogenated compounds (e.g. chlorinated ethylenes), oxidative dehalogenation was found to provide promising results, it showed only limited efficiency for halogenated aromatics degradation. Generally, the oxidation route is exhaustive because the C-H and C-C bonds are much more prone to oxidation. Thus, a significant excess of oxidizing agents is needed for the complete oxidation of organics down to inorganic products. On the other hand, reductive methods are more selective to the C-X bond cleavage. In the process, halogens are subsequently substituted with hydrogen atoms. Most of the times, catalysts based on precious metals have been utilized under high temperature and pressures [3] for reductive hydrodehalogenation. Other, more economically feasible solutions have been provided, too. These included metal sodium/potassium reduction or usage of strong reducing agents (e.g., $NaBH_4$, N_2H_4) [3, 4]. All of the mentioned processes are, however, technologically demanding. Thus, the focus of interest has turned to more simple alternatives. Zero-valent iron nanoparticles or their nanocomposites with Ni or Pd [5–9] have been proved to be efficient dehalogenation reagents. Several studies were also published on supported Pd/Mg catalysts applied at ambient conditions [10, 11]. While the catalyst showed acceptable removal rates and high removal efficiency of contaminants, it was found that the number of life cycles is relatively low. Moreover, only low levels of contaminants were tested.

A hydrodehalogenation reaction (HDH) using Al-Ni alloy (50:50 wt.% Al-Ni) has been found as one of the most efficient and cost-effective methods for removal of a broad range of

organic halogenated pollutants from an aqueous environment [12–19]. The mechanism of the reaction itself has not been described explicitly. Depending on the conditions and a compound being eliminated, it may slightly differ. It was found that the reductive strength of the alloy is even higher in dilute NaOH solutions, capable of reducing aromatics [20], or in specific cases cleaving the C-C bond [21].

In general, aluminum metal is leached out of the Al-Ni alloy in a basic environment followed by hydrogen gas evolution (equation 1) and the formation of the porous Raney Ni catalyst with a high surface area. The HDH reaction takes place in the next step (equation 2) on a freshly formed surface of the Raney nickel. The alloy acts both as a reagent and a source of the catalyst. After the reaction, the halogen atoms stay in the solution as inorganic halides.

$$2Al^{\mathbf{0}}/Ni^{\mathbf{0}}(s)\ (50{:}50\ wt.\%\ alloy) + 2NaOH(aq) + 6H_2O(l) \rightarrow 2Na[Al^{\mathbf{III}}(OH)_4](aq) + 3H_2(g)/Raney\text{-}Ni^{0}(s) \quad (1)$$

$$R\text{-}X(aq) + H_2(g)/Raney\text{-}Ni^{\mathbf{0}}(s) + H_2O(l) \rightarrow R\text{-}H(aq) + X^{-}(aq) + H_3O^{+}(aq) + Raney\text{-}Ni^{\mathbf{0}}(s) \quad (2)$$

The Raney type Al-Ni alloy is easy to handle and widely used to prepare the Raney Ni catalyst. Compared to the financially demanding heterogeneous catalysts based on precious metals (Pd, Pt, Rh), no special apparatus is needed for the HDH reaction. The reaction can be performed at room temperature and atmospheric pressure in open reaction vessels. The Al-Ni alloys of different compositions are as well air-stable materials. This property helps to overcome the pyrophoric Raney nickel or nano zero-valent iron storage problems. Its utilization in a basic environment also excludes the leaching of toxic nickel metal and other potential metallic impurities.

Despite the mentioned positives, several negative points such as a high excess of aluminum to substrate molar ratio, elevated temperatures, or long reaction times were reported previously for the complete hydrodehalogenation utilizing the Raney-type Al-Ni alloys. The major drawback of the technology is the cost of the Al-Ni alloy prepared via the metallurgical route, which requires working with high temperatures and molten metals. Moreover, pulverization of the formed ingots must be performed to isolate the alloy in the form of a powder. Therefore, the potential large-scale applicability of the Al-Ni alloys is, for now, economically unfavorable; especially in the case of low-contaminated waters. Even though the preparation process for Raney Al-Ni alloys is well-known and used worldwide, it can be effectively optimized via mechanical activation, making the process less energetically demanding and greener. Mechanical activation increases the reactivity of the starting metal mixtures. The mechanically activated

mixtures can then be processed at lower calcination temperatures and significantly shorter times needed for the crystallization of intermetallic phases (preferably below the melting point of aluminum).

In this work, the main goal was to apply mechanical activation of Al-Ni mixtures in a high energy planetary ball mill, followed by thermal treatment, to obtain Al-Ni alloys suitable for HDH reactions. The alloy preparation should avoid molten metals work-up and generally should be carried out at significantly lower temperatures. It might serve as an example of reducing the reagents cost to facilitate the implementation of the technology on a large scale.

2 THEORETICAL PART

2.1 Mechanical activation

The term *mechanical activation* refers to a process in which the reaction ability of a substance is significantly increased upon the action of mechanical energy on the studied substance. If a composition or a structure of the substance under investigation is changed in the process, it is referred to as a mechanochemical reaction/mechanical alloying. The properties of mechanically activated substances depend not only on the nature of the studied substances but mainly on the activation conditions that can vary considerably [22–25]. The most important properties that can be changed by mechanochemical activation are the reaction rate and the activation energy. These two parameters are closely connected with the formation of new surfaces and defects in a crystal structure (cracks and disordering). The mechanically activated substance is told to have a „captured" activation energy ΔE_{capt} (kJ/mol), which can be determined by calorimetry, differential thermal analysis (DTA), or the examination of the X-ray diffraction data. During the mechanochemical process, the distribution of "captured" activation energy is inhomogenous and is composed of several elements as follows

$$\Delta E_{capt} = \Delta E_{surf} + \Delta E_{grain} + \varepsilon\, \Delta E_{def} + \Delta H_{defrel} + f_{amor}\Delta H_{amor} + f_{chan}\Delta H_{change} + \text{heat loss}$$

where ΔE_{surf} = surface energy, ΔE_{grain} = grain boundary energy, ε = internal stress, ΔE_{def} = deformation energy, ΔH_{defrel} = enthalpy of short-live defects, f_{amor} = amorphization level, ΔH_{amor} = enthalpy of amorphization, f_{chan} = state of structural change, ΔH_{chan} = enthalpy of structural change.

The behavior of solids subjected to the effect of mechanical energy should be considered from the view-point of the three main aspects: structural disordering, structural relaxation, and structural mobility. All of these simultaneously affect the reactivity of the solid; structural relaxation being the most important. After interrupting the milling process, relaxation occurs for different states induced by the process (Figure 1). These can be either short-lived or long-lived states (e.g., surface area). According to this theory, the reactivity of activated solids cannot be influenced via states whose relaxation time is shorter than the time of the reaction itself.

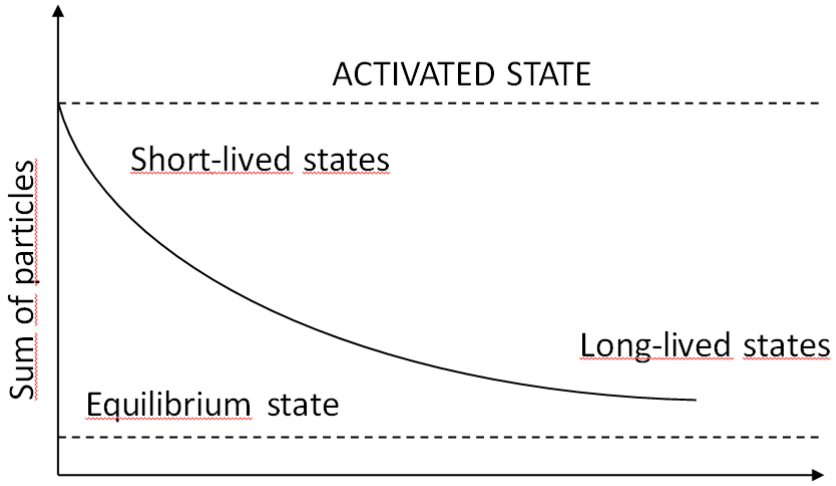

Figure 1. Generalized relaxation curve for the mechanically activated state showed as a function of time.

The energy demand on the physico-chemical and the structural changes decreases in the following order: bond cleavage, deformation, amorphization, formation of short-live defects, grain boundary formation, and surface changes. Due to the capability of energy capture inside the substance, many reactions of the solids can proceed at significantly lower temperatures. On top of that, some reactions can be observed only after the mechanical activation of solids. A few advantages of the mechanochemical activation are summarized below:

- Processing of materials from initial sources that are hardly processed by other methods.
- Performing high-temperature reactions at the acceptable rates and normal pressure/ambient temperature.
- Producing materials with properties unique to the mechanically activated solids [26].

2.2 Effects of mechanochemical activation

The primary effect of mechanochemical activation of solids is the particle size reduction followed by the formation of new surfaces, structure disordering, and commonly by polymorphism. A detailed study of these processes may explain the material´s properties and behavior. These effects occur due to the different types of stress applied to the materials. The main types are compression, shear (attrition), impact (stroke), or impact (collision) (Figure 2) [23].

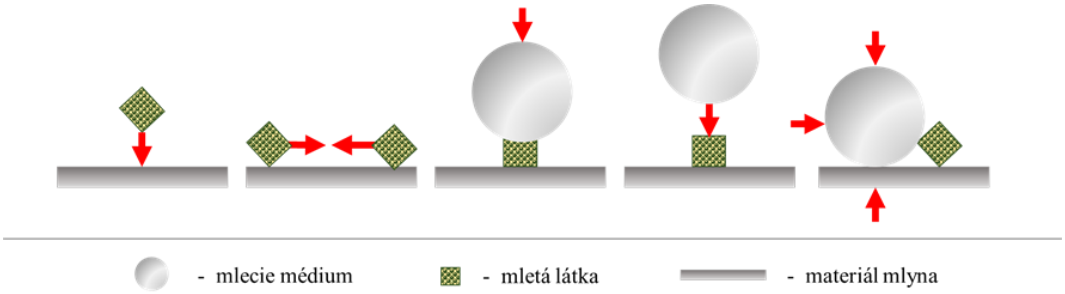

Figure 2. Different types of stress applied to the materials during ball-milling process [23].

2.2.1 Size reduction

Milling is a standard industrial operation for particle size reduction, also called grinding. Different types of mills may be utilized for particle size reduction depending on the material´s properties and demanded size class. Typically, ball mills, vibratory mills, rod mills, and jet mills are used to achieve particles less than 1 mm in diameter. For ultrafine dry milling (< 10 µm in diameter), vibratory ball milling, planetary ball milling, and air-jet milling are commonly used methods [27]. The utilization of these mills may lead to the formation of nano-powders [28, 29]. In many cases, particle size reduction is complicated by the aggregation and agglomeration of smaller particles into larger entities. Therefore, a gradual decrease in size reduction effectiveness is observed during the milling process. According to the literature [24], three stages of the milling process can be clearly distinguished:

a) The Rittinger stage – the interaction of particles can be neglected, and new surfaces are formed.
b) The aggregation stage – created surface area is not proportional to the energy input because of the particles interaction.
c) The agglomeration stage – dispersion first slowly drops and then remains almost constant upon further milling.

In stage b, particles are held together by weak van der Waals forces (0.04-4 $kJ.mol^{-1}$), whereas in stage c, chemical bonding of magnitude 40-400 $kJ.mol^{-1}$ exists.

Various analyses can study the effect of milling on the particle size and morphology. Scanning and transmission electron microscopy represent the most frequent techniques for studying morphology. Generally, upon grinding, the particles with no well-defined morphology are obtained. However, materials with various particle shapes may be prepared depending on the

conditions and the input material. Especially, solvent-assisted grinding or surfactants-assisted milling may result in well-crystalline materials. Figure 3 provides several examples.

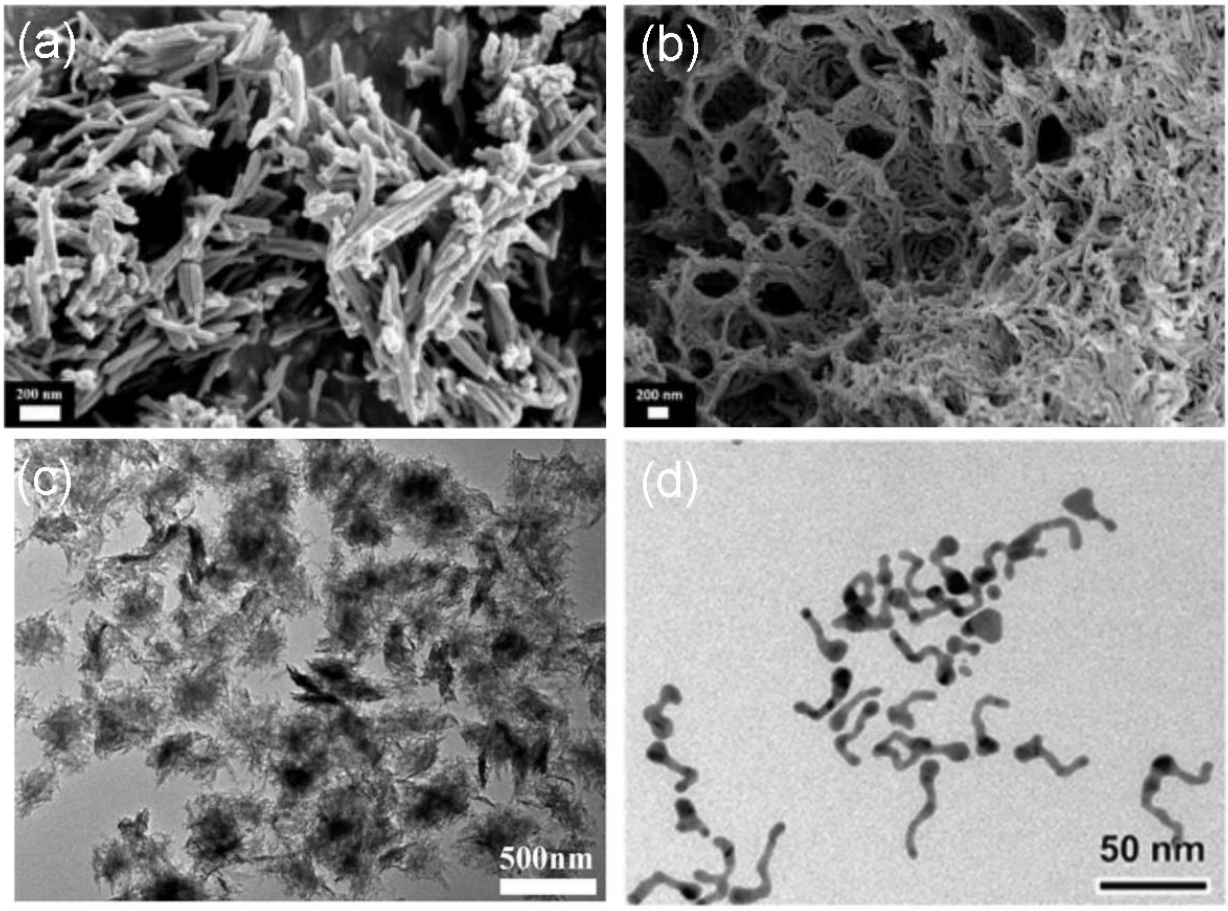

Figure 3. (a) and (b) Morphology of Fe-MILL-88A MOF after grinding synthesis utilizing water or triethylenegycol as co-grinding agents (ref. [30]**) (c) CuO nanoribbons formed by mechanical action on $Cu(OAc)_2$/NaOH mixture (ref.** [31]**) (d) the formation of Au nanotadpoles after PVP assisted synthesis of Au nanoparticles (ref.** [32]**).**

2.2.2 Amorphization

Amorphization is a widespread phenomenon connected with ball-milling [33]. Upon ball impact, point, line, or volume defects can be formed within a structure of a crystalline material. If the number of generated defects is high enough, the material undergoes a transformation into a so-called amorphous state where no long-range order of atoms can be found (short-range order might exist). The amorphous materials are metastable with an energy barrier preventing spontaneous crystallization. Whether or not the material is amorphous can be assumed based on a threshold level for amorphization ρ_α.

$$\rho_V + \rho_I > \rho_\alpha$$

The material is considered as completely amorphous in an area where the sum of the interstitial concentration (ρ_I) and the vacancy concentration (ρ_V) is above this level. Such a state represents the most energetic state of a material. Amorphous materials are characterized by having no defined diffraction lines in their XRPD patterns (Figure 4) and glass transition at T_g (= temperature at which reversible transformation into the rubber-like state from glass occurs) and crystallization temperature. These parameters can be determined by differential scanning calorimetry. There are several competing ideas to explain the mechanism of amorphization by milling. A commonly held view is that amorphization occurs via the generation of localized heating effects followed by quenching. Another says that milling leads to an increase in static disorder that adds to the intrinsic dynamic disorder up to the critical value at which the structure collapses [34]. In the case of metallic mixtures, for amorphization to happen, at least three criteria must be satisfied:

1. The system is an asymmetric diffusion couple (atoms of one metal diffuse through another metal at a significantly higher rate).
2. The system exhibits a negative heat of mixing since amorphization is thermodynamically driven.
3. The system possesses sufficient diffusivity at temperatures below the crystallization temperatures.

The crystal to glass conversion upon milling can take up several hours to be completed. The short milling time will only lead to a size reduction of the crystals. The amorphization process of amorphization has been only weakly studied regarding how amorphization is preceded by morphology change and defect formation in the solid-state [35]. It is also questionable how

the amorphous phase prepared via ball-milling differs in the properties from the one prepared by "conventional" techniques (e.g. melt quenching). In general, similar T_g points were reported for organic compounds but the long-term stability of the amorphous phase might change.

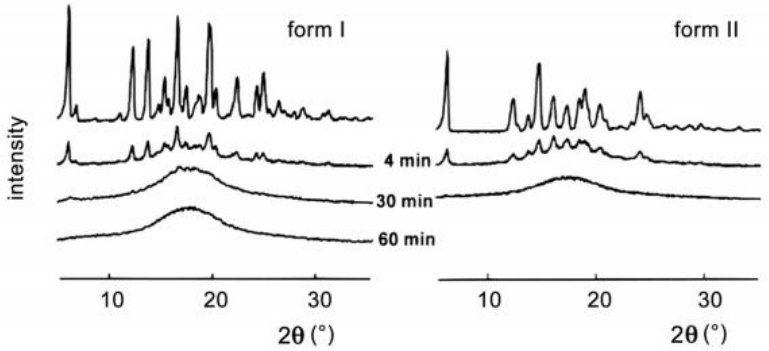

Figure 4. An example of amorphization of terfenadine drug upon ball-milling followed by XRPD (from ref. [33]**).**

Ball milling has been shown also an effective tool for the production of non-equilibrium glassy alloys. Compared to the rapid solidification, solid state amorphization might provide wider compositional range for many binary systems [36].

2.2.3 Polymorphism

Many compounds, either inorganic or organic can crystallize in different forms with special packing and molecular conformations in their crystal lattices. Such behavior is referred to as polymorphism. Different polymorphs possess different physicochemical properties such as density, melting point, dissolution rate, and physic-chemical stability, which makes the study of different polymorphs perspective. Mechanical activation can often transform material from one crystal structure into another [22, 37, 38]. Ball-milling as a polymorphic control tool has been widely studied for inorganic materials. For example, polymorphic transformations of the TiO_2 phase upon high energetic milling were studied by Ren et al. [39], who showed that inter-conversion of a different polymorphs takes place depending on the reaction time. Similar behavior can be observed for Gd_2O_3 milling, in which a transformation from a highly symmetric cubic phase into a monoclinic takes place in a planetary ball mill in several minutes (Figure 5). The polymorphism induced by ball-milling is becoming more popular in the field of APIs (active pharmaceutical ingredients) development, where crystallization of different polymorphs may be induced by amorphization of the material by ball-milling, optionally followed by thermal treatment.

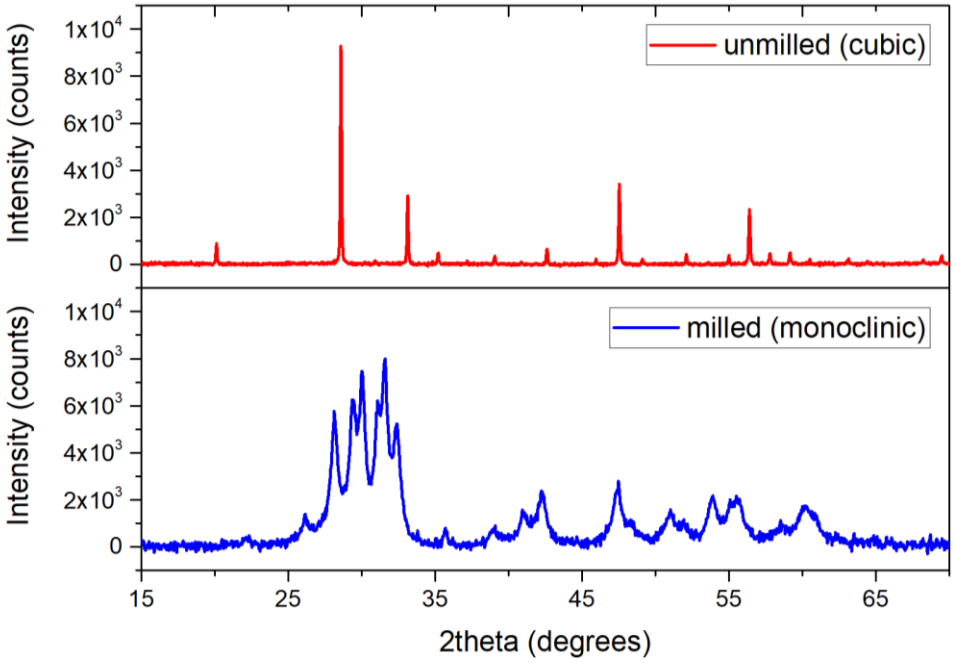

Figure 5. Polymorphic transition of Gd_2O_3 phase from the cubic to the monoclinic symmetry upon milling for 20 minutes in the planetary ball mill Fritsch Pulverisette 6 (unpublished results of the author).

2.3 Ball-milling as a tool for mechanical activation

In a typical mechanochemical experiment, the powder mixture is charged in the container (bowl, vial, jar) of a ball milling machine (a ball-mill), together with the milling balls (made of the same material as the milling container). The solid mixture is then subjected to high energetic collisions with the balls due to rotation or shaking of the milling containers. Therefore, a ball mill is an essential piece of equipment for mechanochemical process [24]. Depending on a specific application, several types of ball mills such as planetary ball mills, attritors, shaker mills, or horizontal ball mills might be utilized [40] (Figure 6). The principle of the operation is the same for various mills. It is believed that the critical parameter is to provide the correct impact energy for the requested outcome of the mechanochemical reaction. Depending on the tunable parameters of the milling process (type of mill, the material of milling media, ball-to-powder ratio, milling intensity, milling atmosphere, etc.), mills can work in different regimes (compression, shear, impact).

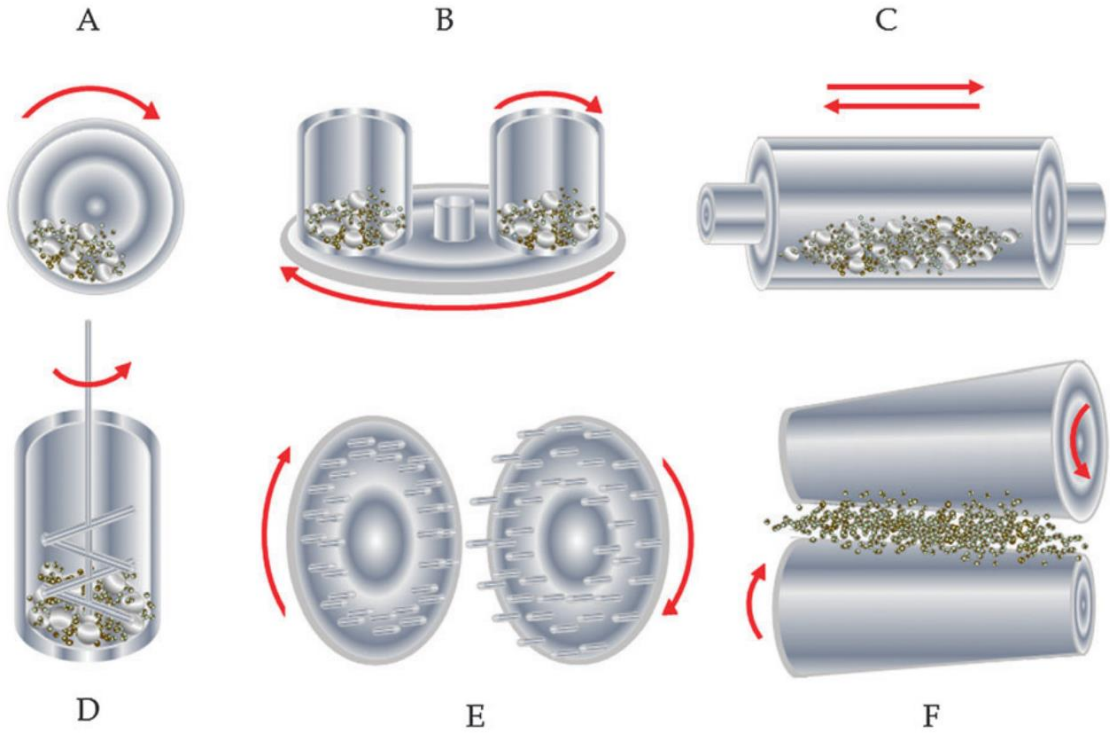

Figure 6. Types of ball mills with depicted movements: ball mill (a), planetary mill (b), vibration mill (c), attritor mill (d), pin mill (e), rolling mill (f) (From ref. [23]**).**

2.3.1 Planetary ball mills

Due to their high energy density, simple set-up, handling and cleaning, planetary ball mills represent the most popular milling equipment for laboratory purposes [41]. Only a tiny amount of the powders is required for their operation (typically gram amounts). A planetary ball mill consists of one rotation turn disc and two to four bowls. The turn disc rotates in one direction while the bowls move in the opposite direction, thus creating centrifugal force (acceleration up to 150 g) (Figure 7). The powder mixture is therefore ground either by the friction from the milling balls rolling on the bowl's inner wall or by the impacts where balls are lifted and thrown across the bowl to the opposite walls. The energy density is 100-1000 higher than the earlier used milling equipment. Usually high temperatures can be achieved upon high energetic impacts fast, which can sometimes promote reactions that would not be otherwise observed; but also to unwanted welding or thermal decomposition of the materials. Due to this fact, however, milling is usually performed for short times in cycles. Some modern systems can be modified to incorporate temperature and pressure controls for the mills (e.g., EASY-GTM from Fritsch company).

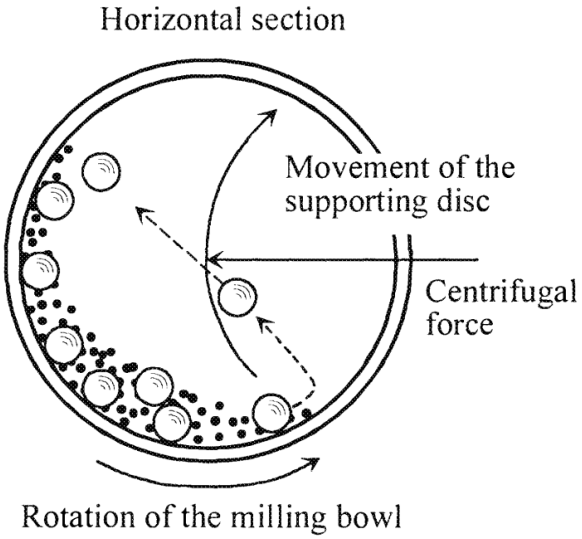

Figure 7. Schematic view of motion of the milling balls inside a planetary ball mill (From ref. [42]**).**

2.3.2 Shaker or mixer mills

Comparably to planetary ball mills, shaker mills are generally used to process small quantities of materials. These mills agitate powder mixture in three perpendicular directions at a high frequency. Compared to attritor and vibratory ball mills, shaker mills are classified as highly

energetic. High energy is secured by using high frequencies and amplitudes of motion. Ball velocity can reach up to 5 m/s. The most popular mill used in the USA for laboratory research purposes is the SPEX 8000 shaker mill (Figure 8).

Figure 8. Dual clamp high-energy shaker mill SPEX 8000D, typically used mill for lab-scale experiments.

2.3.3 Other types of mills

Several other types of mills are used at an industrial scale with different principles of operation [41, 43]. The *Conventional horizontal ball mill* rotates around a central horizontal axis. The maximum rotational speed is set just below the critical value that pins the balls to the wall. At such speed, the ball should fall down from the maximum height allowing for maximum energy. The diameter of the container for this type of mill should be greater than 1 m and thus is not suitable for laboratory purposes. For a low-energy mode, *magnet controlled horizontal ball mill* can be utilized. This mill allows the possibility of incorporating a magnetic field to act on ferromagnetic balls, thus controlling the balls' effective mass (which can be increased by a factor of about 80). The *Attritors* are mills (Figure 9b) in which many small grinding media are agitated by impellers, screws, or discs in a chamber. The central shaft rotates at high speed to collide with balls and generates collisions between the balls and the powder charge. The medium agitating mill is regarded as one of the most efficient devices for micronization. It has been widely used in mechanical alloying and for the size reduction of carbides and hard materials. Stirring the milling balls with a large surface area ensures a substantially higher degree of surface contact than in tumbling or vibratory mills. Milling takes place by impact and shear forces. Small attritors have

been utilized for research purposes. Since the milling container is stationary, additional cooling or heating can be applied to this type of mill. Depending on their design, attritor mills can be used in batch-, continuous, or circulation-type mills.

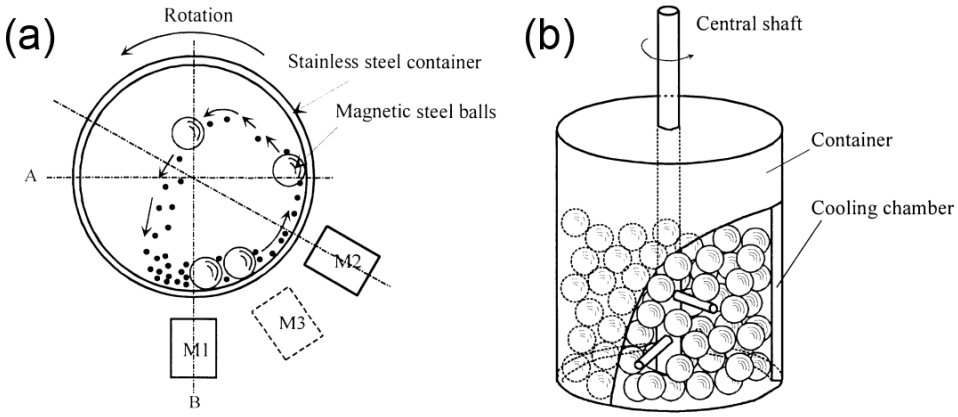

Figure 9. Illustration of a magnet controlled horizontal ball mill (a) and an attritor-type ball mill (b).

The *Vibration mill* working principle is based on a motion along a circular or elliptic trajectory by the rotation of out-of-balance weights (Figure 10). This motion involves four factors: the speed of the vibration, the horizontal and vertical amplitude, and the phase angle. Industrial vibration mills operate at frequencies 16-19 revolutions per second and amplitudes below 6 mm. The acceleration does not exceed 10g. The main disadvantage of this type of mill is its low output. The concept of an *eccentric vibration mill* was introduced by Gock *et al.* [44]. Unlike a conventional vibration mill, it performs elliptical, circular, and linear vibrations, thus increasing amplitude, and consequently energy.

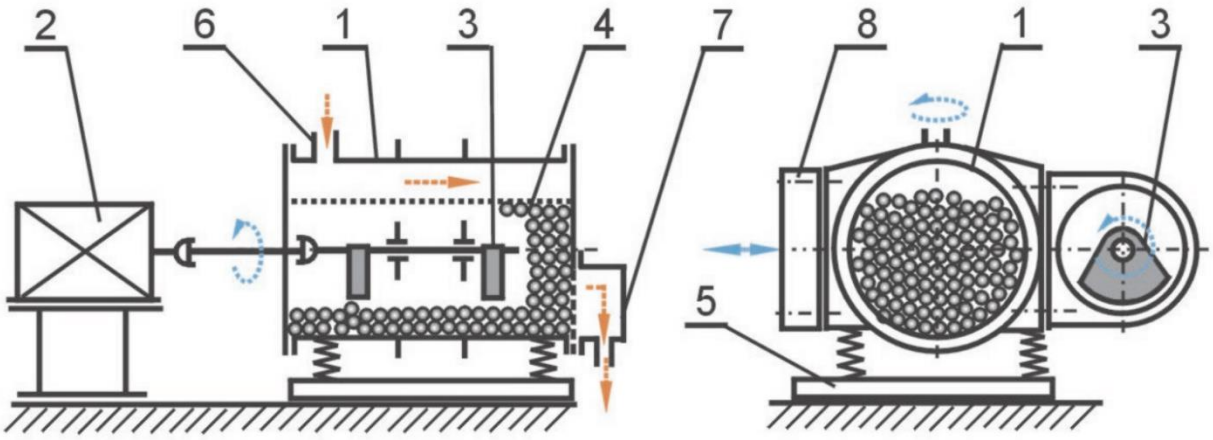

Figure 10. Schematic diagram of one-chamber single mass vibrator mill, with main parts 1 – chamber, 2-engine, 3 – eccenter, 4 – load (milling media and material) (From ref. [45]**).**

2.4 Mechanical alloying

Mechanical alloying is a ball-milling process where a metallic powder mixture placed in a ball mill is subjected to high energetic collisions from the milling balls [36, 46]. The process does not differ from mechanical activation but is mainly connected with metallic or ceramic powders [42]. Besides the standard processes for preparing alloys, this represents an alternative that came to attention during the 1970s. The two most important events are the repeated welding and fracturing of the material. The mechanical alloying can be continued only if the rate of one event balances the other and the average particle size stays relatively coarse. From the viewpoint of microstructure evolution, the mechanical alloying can be further divided into four stages:

a) *Initial stage* – during the initial stage, powder particles are usually flattened by compression forces due to the collisions of the balls. Almost no welding can be observed at this stage, only particle shape changes because of micro-forging. For the ductile-ductile system, a layered structure with separation between the two elements can also be observed. Significant variations in composition, particle size, and shape might be found for a very short milling duration. The hard particles usually remain untouched for ductile-brittle systems, and the ductile particles act as a binding agent to form agglomerates.

b) *Intermediate stage* – increasing the milling time, significant changes are observed. Cold welding becomes dominant, and more significant plastic deformations lead to pronounced layered structures forming. The random orientation of lamellae indicates fracturing, and their thickness is decreased. Even though dissolution might have appeared, the powder is not homogenous.

c) *Final stage* – in the final stage, no layering is observed anymore and the material becomes homogenous even at the micro-scale. The formation of a true alloy can have already taken place. Homogeneity of the prepared material is an outcome of the balance between fracturing and cold welding. The particle size is also the result of the balance of the forces that cold weld particles together and the forces required to fracture them. Depending on the system, crystallite size can reach nanometer size. Further decrease in crystallite size might be limited because very high deformation stress is needed, as given by the Hall-Petch relation

$$\sigma = \sigma_0 + kd^{-1/2}$$

where σ is the stress, σ_0 and k, constants, and d is the crystallite size.

c) *Completion stage* – extremely deformed metastable structure is formed, a true alloy is formed.

Material of milling media

Different types of milling media (milling chamber, vial, balls) are available on the market: stainless CrNi-steel, tungsten carbide (WC + Co), alumina (Al_2O_3), achate (SiO_2), zirconia (ZrO_2). Chambers made of these materials are usually made in different sizes. For the planetary ball mills 80, 250, or 500 mL chambers are the most common. The choice of the proper material is crucial due to the impact of the milling balls on the inner walls of the milling chamber. Generally, depending on the powder mixture´s chemical and physical properties, milling media is chosen. In some cases, contamination can occur due to abrasion of the milling media or by slow dissolution of the inner walls of the bowl (e.g. acetates are not suitable for milling in WC + Co bowls or hard/abrasive materials should not be milled in Teflon or PTFE bowl). To overcome contamination, the use of hardened milling tools should be considered. Milling tools having a composition similar to that of the powder mixture can be used. The contamination will have the same composition. Contamination is primarily critical for high-energetic milling and is not common for the reactions that are easily promoted at low impact energy.

Table 1. Typical material used for the production of milling media (chambers and balls).

Material	Main composition	Density (g/cm^3)	Abrasion resistance
Agate	SiO_2	2.65	Good
Alumina	Al_2O_3	3.8	Fairly good
Zirconium oxide	ZrO_2	5.7	Very good
Stainless steel	Fe, Cr, Ni	7.8	Fairly good
Tempered steel	Fe, Cr	7.9	Good
Tungsten carbide	WC, Co	14.7-.14.9	Very good

In specific cases, the choice of the milling media also depends on a purpose of a milling experiment. Materials translucent to the radiation must be selected for the experiments designed to monitor the course of a mechanochemical reaction. For this purposes, poly(methyl metacrylate) (PMMA) milling jars are frequently used. Custom-design milling chambers were also developed to provide better quality data from X-ray diffraction experiments [47]. Sometimes, the material of the milling media can directly catalyze chemical reactions, as well.

Milling atmosphere

Experiments can be performed in an inert atmosphere or vacuum to prevent the oxidation of the milled mixtures. If a mill is not attached to an atmospherically controlled chamber, the chamber is filled up with an inert gas in a glove box and sealed with rubber or Teflon. Commonly, purified argon gas is employed. Even though nitrogen is cheaper and very stable gas, at higher temperatures during ball milling, it reacts with most of the materials to form nitrides. Similarly, milling in a carbon dioxide atmosphere may lead to the chemical conversion of materials. If calcium oxide (CaO) is milled in a CO_2 atmosphere, fast transformation into $CaCO_3$ (calcite phase) is detected by XRPD (yet unpublished results of the author). Possibly, a reductive atmosphere may be introduced in the chamber.

Selection of process control agents (PCAs)

In a ball mill, powder metal particles are subjected to high energy collisions, which causes particles to cold weld together and fracture. As mentioned before, a balance between the two processes must be established to perform a successful alloying experiment. It can sometimes be hardly achievable when soft materials (or highly ductile) are used. For such cases, cold welding between the metal particles and milling media can become a serious problem. Two approaches may be taken to reduce excessive welding and promote fracturing. The first approach involves the modification of the metal particle surface by adding suitable organic material that prevents clean metal-to-metal contact. The second approach modifies the deformation mode so the particles fracture before they can deform to large compressive strains. For example, cryogenic milling can be utilized. The former approach is widely used and the surface agents are also called *process control agents* (PCAs). There exist numerous types of PCAs, most popular being stearic acid and alcohols (methyl alcohol, ethyl alcohol, polyethylene glycol). The most popular types of PCAs are stearic acid and alcohols (methyl alcohol, ethyl alcohol, polyethylene glycol) [40]. Added organic compounds should not represent any further obstacles, such as they are decomposed at relatively low temperatures during post-processing. PCAs can further also help to avoid agglomeration of the particles or promote crystallization of specific morphological types of crystal (Figure 11). Such stabilization may be either of electrostatic (charge or “inorganic”) or steric (“organic”) origin. The sterically bulky adsorbents that prevent close contact with particles can result in steric stabilization. On the other hand, electrostatic stabilization occurs by the

adsorption of electrically charged ions to the surface and forming the so-called electrical double layer.

Figure 11. Effect of methanol addition on mechanically activated aluminum-nickel metal mixture – 0 wt.% left, 5 wt.% right (photo by Bc. Andrea Hegedüs).

Ball-to-powder ratio

The ball-to-powder ratio (BPR) represents the mass of the milling balls compared to the mass of the powder mixture being processed. A wide range of BPR from 1:1 up to 220:1 was reported (typically 5-20:1). The higher the BPR ratio, the faster the mechanical alloying process is. It is because the number of collisions per time unit increases, increasing milling temperature and leading to faster diffusion. Usually, balls with the same diameter are used. To randomize the motion of the balls, the combination of bigger and smaller must be used.

Milling intensity

The milling intensity is a critical parameter affecting the behavior of a studied system and is the measure of the milling energy, which is proportional to the effective power transferred from the mill to the material. The milling intensity is increased by increasing the mass of balls or by increasing the speed/frequency of the mill. This parameter has a profound effect on the alloy formation and decrease in particle size. Overall, the kinematic analysis and the power transfer from the mill to the powders have been only scarcely studied, and not much attention has been paid to the predictability and parameterization of the mechanochemical reactions. Several models describing the input energy have been proposed.

Based on the Hertzian impact theory, a model proposed by Maurice and Courtney was introduced for powder-balls collision. According to the paper [48], the powder charged in the

milling jar only slightly alters the elastic collisions between the balls. The energy of elastic (U_E) and plastic (U_P) collision can be calculated for each collision as follows

$$U_E = 2\pi R\, r_h^2 p_{max}^2 / 3E$$

$$U_P = \pi r_h^2 h_0 up$$

where r_h is the contact distance between the two balls, k is the geometrical constant, ρ is density, E is the elastic modulus of the balls, and p_{max} is the maximum pressure developed during each collision. Both the plastic and the elastic energy increase exponentially with the frequency increase. The milling intensity is defined as the momentum transferred from the balls to the unit mass of powder per unit time and has the following expression [49]:

$$I = \frac{M_b V_{max} f}{M_p}$$

where M_b is the ball´s mass, V_{max} is the maximum velocity of the ball, f is the impact frequency and M_p the mass of the powder charge in the chamber.

A "hit" model was proposed by Burgio et al. in the 1990s [50] that was based on a theoretical-empirical approach. This model has been recently reevaluated and used for parameterization of the mechanochemical reaction [51]. This model proved highly reliable in assessing energy transferred from the mill to the material (for the planetary mills). This model assumes that the energy is only released by direct collisions between the balls and the walls, and it does not consider a temperature change or friction. The total power introduced into the system during collisions is expressed as

$$P = \varphi_b \Delta E_b N_b f_b$$

where, φ_b is an empirical coefficient, ΔE_b is the kinetic energy of the ball, $N_b$is the number of balls, and f_b is the frequency with which balls are launched defined as

$$f_b = K(W_p - W_v)/2\pi$$

where W_p is the angular velocity of the mill and the K is an empirical constant depending on the mill geometry (for planetary ball mills).

2.5 Alloys and mechanical alloying of the Al-Ni binary system

The phase diagram of the binary Al-Ni system is shown in Figure 12. In this system, several intermetallic compounds exist, namely Al_3Ni, δ-Al_3Ni_2, β-AlNi, Al_3Ni_5, γ'-$AlNi_3$; depending on the composition of the mixture. The Ni-rich solid solution is usually denoted as γ-Ni. Generally, the formation of aluminides is an exothermic event and it has been of significant concern for smelters due to the uncontrolled nature of the reaction. For this reason, the commercial-scale melting of Al-Ni intermetallic was limited. Later on, it was shown that the melting of aluminum solely is needed for the formation of intermetallic phases. Several investigators suggested that the production of aluminides at a larger scale can be successfully performed by combustion- or reaction-synthesis techniques [52]. To optimize the process for production, the Exo-Melt^{TM} process was developed [52]. Even though this process provides several advantages over conventional processes for aluminides formation, such as lower energy demand, shorter required time, and fewer impurities present, the melting route will always represent a safety risk. Thus, in this paragraph, some general knowledge of the Al-Ni binary system is provided along with the characterization of the intermetallic phase and a novel approach to nickel aluminides via mechanical alloying.

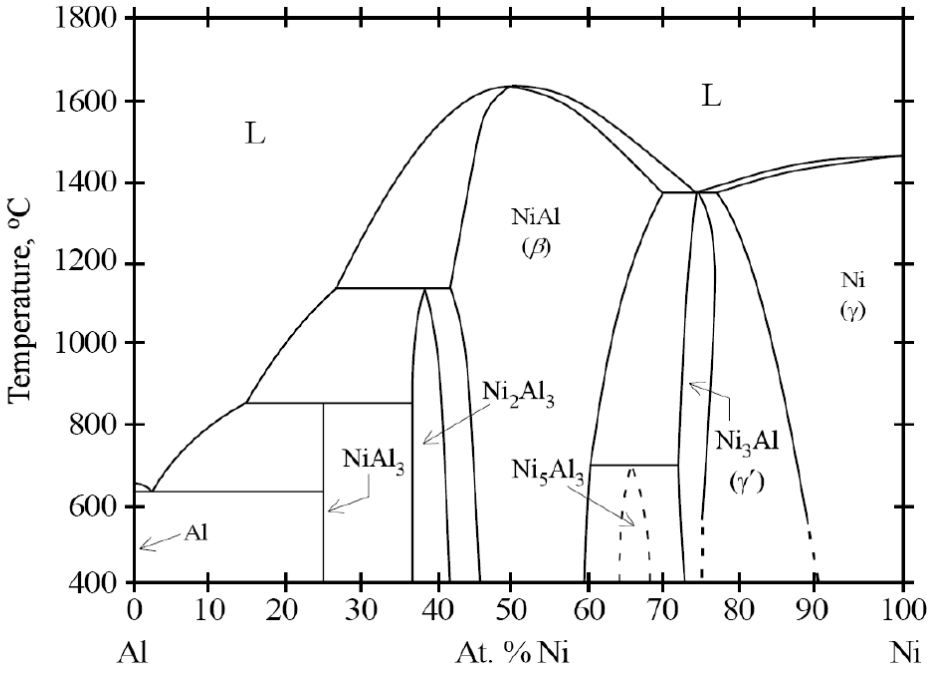

Figure 12. The binary phase diagram for Al-Ni system (ref. [53]**) showing the phase composition in the range of 0-100 At.% of Ni.**

In the system, stable and metastable eutectics are formed close to 75 at.% of Ni. As seen, the solid metastable eutectic consists of β and γ phases. Some of the mentioned phases have become of significant interest in terms of their potential industrial application. To meet the objectives of the thesis, the properties of those having an Al-rich composition are further discussed (β-AlNi, Al_3Ni_2, and Al_3Ni).

Table 2. A list of possible phase present in the Al-Ni binary system, their symmetry, and melting points (from ref. [52]**).**

Phase	Composition (wt. % Ni)	Space group	melting point (°C)
(Al)	0 - 24	*Fm*-3*m*	660
Al_3Ni	42	*Pnma*	854
Al_3Ni_2	55.9 – 60.7	*P*-3*m*1	1133
AlNi	61 – 83.0	*Pm*-3*m*	1639
Al_3Ni_5	79 - 82	*Cmmm*	-
$AlNi_3$	85 – 87	*Pm*-3*m*	1395
(Ni)	89.0 - 100	*Fm*-3*m*	1453

The intermetallic compound β-AlNi is characteristic of its low density (5.9 g/cm^3), oxidation resistance, and good thermal/electrical conductivity. According to Al-Ni binary phase diagram, the β-AlNi phase can exist in a wide compositional range (45 to 60 at.% Ni). At the stoichiometric composition, it forms a cubic (CsCl type) structure which can be described by two simple interpenetrating sublattices (a = 2.8810 Å, space group *Pm*-3*m*) [54] (Figure 13). Aluminum atoms occupy 1a Wyckoff position (0, 0, 0), whereas Ni atoms are located at 1b (½, ½, ½). In the Ni-rich β-AlNi, larger aluminum atoms are replaced by nickel atoms, a drop in a cell parameter is observed and the density increases. On the contrary, Al-rich composition is dominated by vacancies on nickel sites up to 25%. Depending on its composition, the melting point of β-AlNi can reach as high as 1638 °C. Due to the high melting point of the β-AlNi phase, it has been extensively studied in the field of ultra-high temperature applications [52].

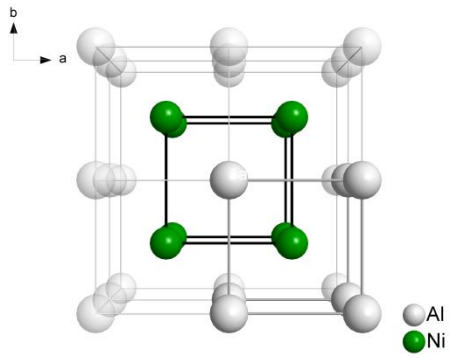

Figure 13. The crystal structure of the β-AlNi phase with cubic symmetry, the two interpenetrating lattices are shown in the picture.

More to the left side of the phase diagram, at 43 at.% nickel, the stoichiometric δ-Al_3Ni_2 is formed in which vacant nickel sites are ordered [55]. The crystal structure of δ-Al_3Ni_2 can be derived from β-AlNi by removing Ni atoms of every third plane perpendicular to the diagonal of the β-AlNi cube (Figure 14). The ordering reduces the crystal symmetry from cubic to trigonal and additional lines assigned to the vacancy superlattice are produced in the X-ray pattern (see Figure 16 for a comparison of the XRPD patterns).

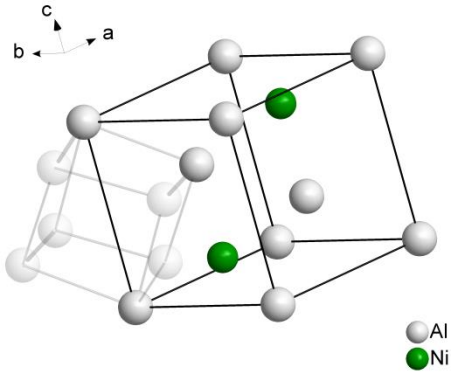

Figure 14. The unit cell of the δ-Al_3Ni_2 phase derived from β-AlNi (deformed cubic cell depicted) by ordered Ni vacancies.

The Al_3Ni phase with 58 wt.% aluminum crystallizes in the orthorhombic crystal system (Fe_3C structure type) [56] (Figure 15). This phase constitutes a significant fraction of the 50:50 wt.% Al-Ni alloy. The other phase found in this alloy is δ-Al_3Ni_2, which forms prior to the β-AlNi. After aluminum leaching, these two phases provided a well-known Raney nickel hydrogenation catalyst.

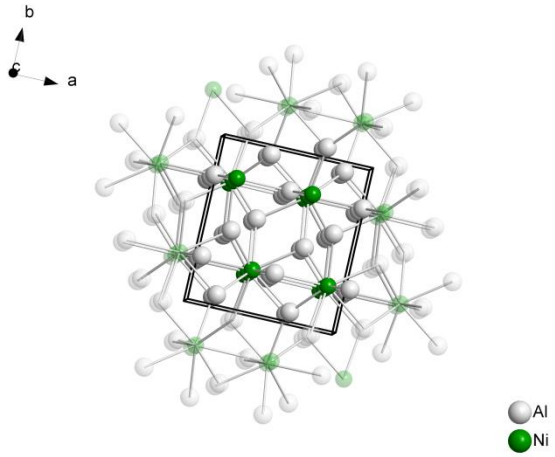

Figure 15. The crystal structure of the aluminum-rich Al_3Ni phase with Fe_3C type structure (the unit cell is highlighted).

$$Al(s) + OH^-(aq) + 3H_2O(l) \rightarrow Al(OH)_4^-(aq) + 3/2H_2(g)$$

It has been found that leaching kinetics is strictly dependent on the nature of the resulting porous nickel after aluminum atoms are removed from the alloy [57]. A striking difference is observed between the two nickel aluminides. Alkaline leaching of the Al_3Ni phase at temperatures higher than 293 K shows linear kinetics. A high tendency of the leached product to disintegrate occurs from the very beginning. Thus, the process continues at an unvarying rate. On the contrary, Al_3Ni_2 shows slow parabolic kinetics due to the formation of a coherent Ni layer. Even though the found liquid-phase diffusion of hydroxyl ions is fast enough for the observed rate constants, it was concluded that it is not the rate-determining process.

Nonetheless, the preparation of phases from the Al-Ni binary system is an energetically demanding task because of the relatively high melting point of elemental aluminum and the exothermic character of the reaction. Typically, all of the mentioned intermetallics are prepared by pyrometallurgical methods. As previously published, mechanical alloying can overcome this obstacle [58]. Due to a highly negative mix enthalpy of Al and Ni (-71 kJ/mol at 298 K), the preparation of β-AlNi via ball milling should be accompanied by an abrupt increase in temperature after short milling. Before this reaction occurs, layers of Al and Ni should be observed because of the low diffusion coefficient between the two metals. No gradual compound formation is observed, which also proves why the formation of another intermetallic compound from the Al-Ni system is not detected. The crystallization of Al_3Ni or Al_3Ni_2 phases is hindered by the fact that at a given composition, these rapidly recrystallize to the β-AlNi phase. Another

explanation could be that the reaction enthalpy is the largest for the β-AlNi phase. In the work of Atzmon et al. [59], an explosive character of the equimolar Al-Ni reaction was proven upon milling for only 120 min. A thorough explanation of the reaction mechanism was proposed. The alloy is thought to be melted in the explosion and solidified on cooling. Another paper by Cardellini [60] demonstrated the preparation of the same phase with slightly changed milling conditions in 3 hours confirming the explosive character under defined conditions. The utilization of mixer mill SPEX 8000 must be emphasized. Up to date, the mechanical alloying using another type of mill was done by Rafiei [61] but many parameters of milling were not provided (milling chamber volume, ball size), which is the main drawback of many published papers. Also, a paper was published by Naeem, who reported successful preparation of the β-AlNi phase after 4 hours of milling in the planetary ball mill Fritsch Pulverisette 5 [62]. Several other papers were published on mechanical alloying of the $AlNi_3$ phase, which are however not of particular interest for the hydrodehalogenation application.

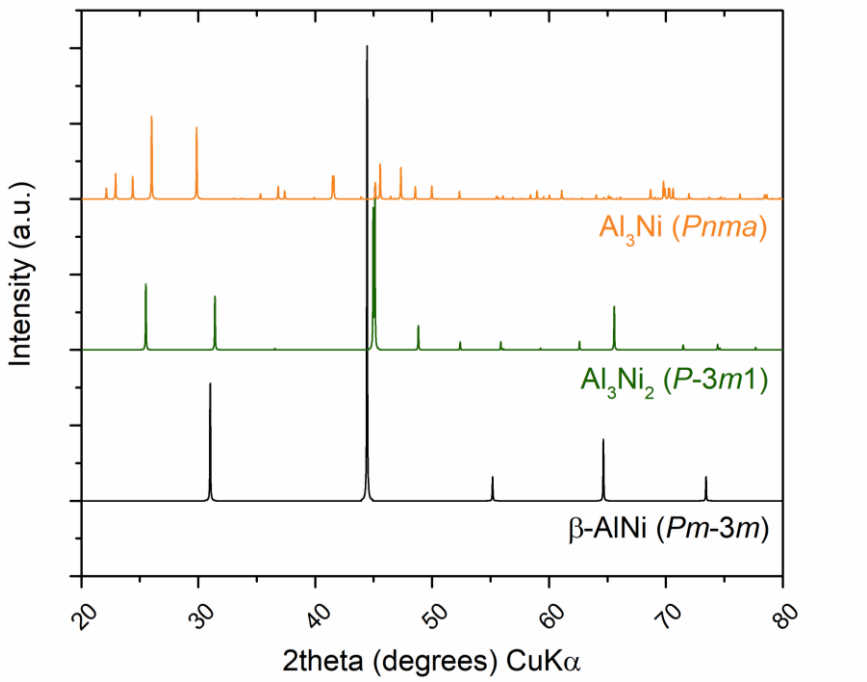

Figure 16. Simulated XRPD patterns of the Al-rich intermetallic phases form the binary Al-Ni system.

2.6 Chlorinated organics as emerging contaminants

Chlorinated organic pollutants represent a wide range of chemical entities, of which the majority is classified as persistent organic pollutants (POPs). POPs, in general, are organic compounds that resist degradation (photolytic, biological, or chemical). Along with chlorinated hydrocarbons, polycyclic aromatic hydrocarbons (PAHs) and all other halogenated organic compounds (fluorinated and brominated) are also classified as POPs [3]. The chlorinated organic pollutants can be further divided into three main categories; depending on their chemical structure:

a) Aliphatic (chlorinated methanes and ethanes; with relatively short half-lives).
b) Aromatic (chlorinated benzenes, chlorophenols, biphenyls, dioxins, furans, etc.).
c) Polycyclic (chlorinated PAHs; formed as byproducts of combustion processes) [63, 64].

Even though some of the chlorinated organic pollutants can emerge from natural sources, e.g. metabolites of polychaete species [65], they mainly originate entirely from anthropogenic activity (targeted or unintentional emission). The sum parameter characterizing the level of organically bound halogen atoms present in soil or water matrix is called AOX (adsorbable organic halides) and is usually given in mg/L [66]. The measure of POPs persistence in the environment is usually defined as the time needed to break down the compound into a less hazardous one (or the one more prone to degradation). In the case of POPs, half-lives ($t_{1/2}$) are usually six months and more.

However, two other factors add more emphasis to the early detection and tracking of POPs. Mostly, POPs have low water solubility and are highly lipophilic (preferably dissolved in fats and lipids), leading to their bioaccumulation in fats. This tendency causes bioconcentration of the compounds and their biomagnification up through the food chain. The phenomena of bioconcentration and biomagnification result in the highest exposure to the organisms at the top of the food chain.

Moreover, some of these compounds (especially the higher halogenated congeners) might be semi-volatile, which allows them to be transported for long distances due to significantly increased mobility. Long-range transport of the chemicals is mediated by the atmosphere as the primary medium. Volatilization is supported via surface use of the chemicals (pesticides on plants and soil) and is highly dependent on several meteorological parameters such as temperature and pressure. Thus, these substances may volatilize from hot areas, condense and remain in colder regions.

Short-term exposure of a living organism to high concentrations of POPs may result in acute illness or, in some cases, death. Long-term exposure to POPs may also be associated with a various adverse health and environmental effects. Investigation of the environmental impact of POPs revealed that they might be involved with such phenomena as endocrine disruption, immune and reproduction system dysfunction, and neurobehavioral and development disorders [67].

Chlorinated organic compounds are historically significant with many applications as starting reagents, solvents, or intermediates in organic chemistry or other industries [3]. They have been proven resistant to degradation and have had the expansive production, use, and release characteristics of all halogenated hydrocarbons. Historically, the trichloroacetaldehyde was one of the first organochlorines to be synthesized in 1832. This was later used as a key reagent in the production of strong insecticide 1,1,1-trichloro-2,2-bis(4-chlorophenyl)ethane, known as DDT. During the world wars, chlorine-based toxic gases, such as chloropicrine (CCl_3NO_2), diphosgene ($ClCOOCCl_3$), and phosgene ($COCl_2$), were developed and used in large quantities. The production of chlorinated benzenes started in 1909 in England and rapidly increased during World War I. Back then, chlorinated benzenes were used as intermediate products to phenols; used as explosives. Twelve individual compounds represent this group of halogenated aromatic substances, out of which a few have become of great industrial importance [68]. No natural sources of these compounds exist and their occurrence in nature is therefore exclusively connected with their industrial production. Monochlorobenzene is widely used in the manufacture of pesticides and as an intermediate compound to other chemicals. Even though its production in the US has declined, it is still listed as a high-volume chemical (over 450,000 kg annually by 2012). Other higher chlorinated benzenes, such as 1,2,4-trichlorobenzene, penta- or hexachlorobenzenes mainly were used as lubricants, decreasing agents, or intermediate compounds in herbicide production [69]. Acyclic short-chain organic halides have been widely used as solvents or degreasing agents; the principal representatives being the chlorinated solvents methylene chloride, tetrachloroethylene, and trichloroethylene. In the 1940s early organochlorine pesticides, usually with cyclodiene-type or cyclobornane-type structures, emerged. For example, aldrin, dieldrin, heptachlor, chlordane, or lindane were produced in vast quantities [70]. Despite being later identified as severely harmful to humans, they also helped to save millions of lives.

For example, in some countries, dichlorodiphenyltrichloroethane (DDT) is still used to control the mosquito population [71].

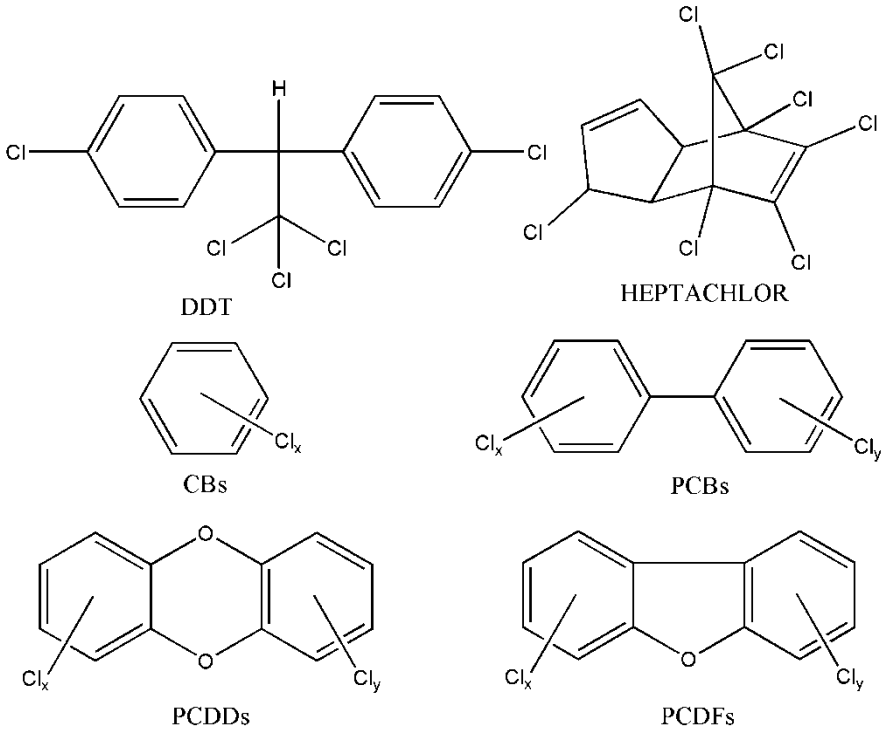

Figure 17. The structures of the two selected organochlorine pesticides (DDT and Heptachlor) and general formulas of the most common organochlorine aromatic pollutants.

In contrast to the chemicals mentioned above 2,3,7,8-tetrachlorodibenzo-*p*-dioxin is considered to be *"the most toxic man-made chemical"*; being more toxic than strychnine or sodium cyanide. Also, it is the most potent cancer promoter known. Chlorinated dioxins and furans are generated in the combustion process of municipal or chemical waste. 2,3,7,8-TCDD was also present as an impurity in the production of a defoliating agent, the so-called Agent Orange during the Vietnam war and led to severe health issues in soldiers.

Among others, during the interwar decades, polychlorinated biphenyls were created. Polychlorinated biphenyls are represented by a group of 209 congeners containing diphenyl core, to which 1-10 chlorine atoms are attached [67]. The congeners substituted at the 3,4-ortho-positions were the most toxic. Their physical properties depend primarily on a degree of chlorination and cannot be generalized. Due to their excellent properties, such as high thermal stability, non-flammability, high electrical resistivity, and dielectric constant, it found worldwide use as oil in capacitors or dielectric in capacitors [72]. Their acute toxicity is low (0.5 g/kg to

11.3 g/kg of body weight), and most effects result in chronic exposure to the PCBs. As for chlorinated benzenes, no natural source of PCBs is known. In the 1970s, their production stopped gradually due to evidence of adverse environmental effects.

Chlorobenzoic acids (CBAs) represent a newly emerging class of POPs, which can be released into the environment from various sources [73]. For example, 2,3,6-trichlorobenzoic acid (TCBA or *trysben*) or 3,6-dichloro-2-methoxybenzoic acid (*dicamba*) have been widely used as herbicides (synthetic auxins) in agriculture [73, 74].

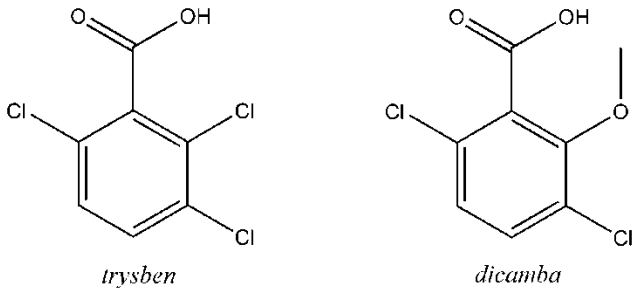

Figure 18. Chemical structures of the two organochlorine pesticides – *trysben* and *dicamba* - with auxin-like activity derived from benzoic acid.

Other CBAs can be formed by microbial degradation of higher chlorinated congeners, by the degradation of various pharmaceutical compounds (e. g. indomethacin, bupropion), or as the final products of degradation of other chemicals; such as polychlorinated biphenyls or DDT [75]. In many cases, 4-chlorobenzoic acid has been identified as the intermediate or the final product of these substances, as in the degradation pathway of indomethacin. It was reported that some CBAs can persist in soils from months to several years [76, 77] and can be found in effluent waters or groundwater. Especially, *trysben* was found to persist in the upper parts of soils for a prolonged period [78].

In nature, many different specimens of bacteria, such as *Pseudomonas*, *Alcaligenes*, *Nocardia*, or *Azobacter*, capable of decomposing CBAs were found and described [79]. The natural decomposition of CBAs can either occur under aerobic or anaerobic conditions. In anaerobic conditions (sulfogenic or emthanogenic), reductive dehalogenation is the first step prior to the ring cleavage and further degradation resulting in CO_2/CH_4 products. The halogen atoms are released as gaseous hydrogen halide. The degradation can also proceed via the benzoate-CoA pathway. Under these conditions, CBAs are utilized by both consortia of

microorganisms and pure cultures. fluorobenzoic acids, however, were never found to be reductively dehalogenated [79].

For aerobic conditions, the mechanisms vary significantly, such as different strains of bacteria developed various strategies for the degradation of CBAs. Mainly, halogenated benzoates are degraded by dioxygenation (1,2-dioxygenase) of the aromatic ring, which results in the formation of halocatechols. After the ring cleavage by the *ortho* route, halo-cis and cis-muconates are produced. However, the meta cleavage provides halo-2-hydroxymuconate semialdehydes. These represent toxic intermediate compounds for the organisms.

Even though CBAs can be degraded microbially, this process is slow (from days up to months) and, to a great extent, depends on a compound structure, a microbial strain involved, and environmental conditions. Besides, some intermediate products may represent reaction inhibitors, slowing down or stopping the degradation completely. Especially in the case of aerobic degradation, many halogenated intermediates that can affect degradation rates are formed along the reaction pathway [73]. Despite the mentioned drawbacks of bioremediation, almost no effort has been put into searching for an alternative technology. Only a few studies have reported on CBAs removal/degradation by chemical or physical approaches [81-84]. These included catalytic ozonization using nanosized ZnO particles [81], Fe-MCM41 composite material [82], or goethite FeOOH material [83]. Photocatalytical degradation in an anoxic environment using TiO_2 was also demonstrated [84]. The methods showed fast degradation rates under optimized conditions; however, the decomposition products were not analyzed or discussed.

2.7 Reductive dehalogenation using the Al-Ni alloys

2.7.1 Principle of the HDH reaction using Al-Ni alloys in an aqueous environment

The proposed HDH reaction is based on heterogeneous catalytic hydrogenation on a surface of the Raney Ni catalyst, which is produced *in-situ* during the reaction. The Raney nickel is a much-employed hydrogenation catalyst representing a cheap alternative to Pd and Pt catalysts. It can be prepared easily from Raney type Al-Ni alloys (typically 50:50 wt.% Al-Ni composition) by leaching out aluminum and washing the catalyst to remove alkali. The main phases for the preparation of Raney nickel are:

1. Pyrometallurgical preparation of the Al-Ni alloy by addition of nickel into molten aluminum (exothermic event).
2. Pulverization of the produced alloy to obtain a powder.
3. Extraction of aluminum in alkaline medium at elevated temperature.
4. Washing and storing the air-sensitive catalyst.

The properties of the catalyst depend on the conditions such as duration of leaching, temperature, and alkali concentration [68]. The leaching step can be written as

$$Al(s) + OH^-(aq) + 3H_2O(l) \rightarrow Al(OH)_4^-(aq) + 3/2H_2(g)$$

The main difference between conventional hydrogenation reactions and the proposed HDH technology lies in the use of hydrogen gas being evolved during the leaching step (Figure 19). As the Raney Ni catalyst is being generated consecutively during the leaching, evolved hydrogen gas can be immediately used for HDH reaction with contaminant already present in an alkaline medium. To the best knowledge of the author, no efforts have been made globally to implement this technology; even though our group has published several papers on the topic [13, 15–17, 69]. The technology itself being low-cost however still has some drawbacks:

1. Excess of alkali is needed to leach out aluminum effectively out of the 50:50 wt.% Al-Ni alloy.
2. Alkali needs to be neutralized after the reaction is done, which leads to the formation of a large amount of salt (preferably sodium sulfate).
3. Pre-treatment of water is needed if it contains easily reduced compounds (i.e. unsaturated C-C bonds) or catalytic poisons.

The strategy proposed within this thesis utilizes mechanochemical activation of the Al-Ni mixtures with subsequent thermal treatment. Mechanical activation of the metal mixture leads to enlargement of the active surface area and provides close contact/interdiffusion of metal particles. This approach can dramatically cut overall

technology costs because it eliminates the need for high-temperature pyrometallurgical preparation of the Al-Ni alloys. According to the analyses, the mechanically activated mixture rapidly reacts to form an alloy, providing even higher efficiency than commercial products, as will be discussed in the experimental part.

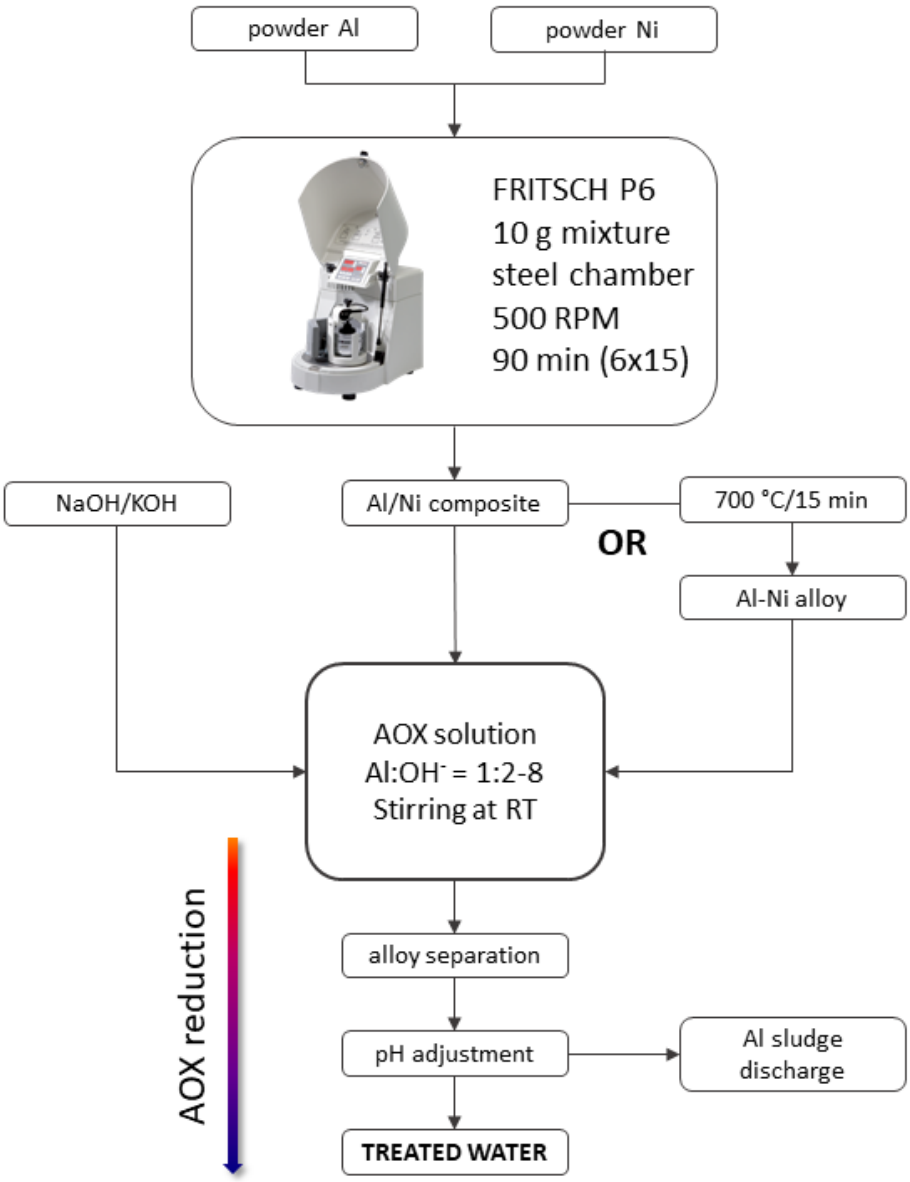

Figure 19. A schematic representation of the proposed hydrodehalogenation technology utilizing ball-milled Al-Ni samples or mechano-thermally.

2.7.2 The HDH reaction mechanism

The reaction mechanisms for hydrodechlorination via heterogenous metal-based catalysts such as Cu^0, Fe^0, Ni^0, or bimetallic couples Pd/Ni or Fe/Ni were studied before by numerous researchers [9, 70–74]. These mechanisms were reviewed and summarized by Mitoma et al. [75]. Despite many interpretations published, the mechanism seems to be compound and catalyst specific. In general, two possible mechanisms were outlined – either an indirect reduction mechanism, where catalytical hydrogenation promoted by adsorbed activated hydrogen H* over the surface of the metal (Ni, Pd) takes place, or a direct electron transfer (DET) upon oxidation of the used metal (Cu^0) [70, 71]. A direct reduction in the case of chlorinated aromatics was proven as an effective pathway only for the systems where the conjunction of the aromatic ring *pi* system with the metal´s surface could be achieved.

The former explanation for the Raney-type Al-Ni alloy is much more plausible since aluminum as a reducing agent cannot reduce chlorinated aromatics [13, 14, 16]. Also, the reaction was found to be not stoichiometric regarding the number of electrons provided by the oxidation of aluminum from Al^0 to Al^{3+}. The molar excess of aluminum (and consequently the amount of the alloy) is needed for complete dehalogenation, such as the HDH reaction is competitive with the evolution of H_2, which due to the vigorous reaction progress cannot be completely utilized for dehalogenation. A porous Raney Ni catalyst formed by leaching of the Raney-type Al-Ni (50:50 wt.%) alloy serves as a hydrogenation catalyst. The substitution reaction takes place immediately on a fresh surface of the porous Ni catalyst and the halogen atoms are released in the form of halide ions. Generally, the reaction can be written for compound as follows

$$2Al^{\mathbf{0}}/Ni^{\mathbf{0}}(s)\ (50{:}50\ wt.\%\ alloy) + 2NaOH(aq) + 6H_2O(l) \rightarrow 2Na[Al^{\mathbf{III}}(OH)_4](aq) + 3H_2(g)/\text{Raney-}Ni^{\mathbf{0}}\mathbf{(s)}$$

$$R\text{-}X(aq) + H_2(g)/Ni^{\mathbf{0}}(s) + H_2O(l) \rightarrow R\text{-}H(aq) + X^-(aq) + H_3O^+(aq) + \text{Raney-}Ni^{\mathbf{0}}(s)$$

To support the suggested mechanism, the paper published by Weidlich, where glucose as an additive was used for the HDH reaction using the Raney Al-Ni alloy, can serve as an example [15]. Lowering the amount of the alloy needed for completion of the reaction can be observed only when the alloy in a basic environment acts as a hydrogenation catalyst. If the direct electron transfer from aluminum reduced compounds, the reaction would be slowed down without impacting the total alloy consumption.

2.7.3 Examples of the HDH reaction using Al-Ni alloys

Even though the HDH reaction using the 50:50 wt.% Al-Ni alloy as a possible way for organic synthesis of deuterated compounds was outlined by Tashiro et al. in the 1980s [78, 79]; not much attention had been paid to this technology for environmental clean-up till the late 1990s. Tashiro showed that under specific conditions, various halophenols could be reduced not only to dehalogenated phenol but also to cyclohexanol at elevated temperature [76] (Figure 20). Moreover, the same paper showed that using Al-Cu Raney-type alloy instead of the Al-Ni alloy leads only to one product.

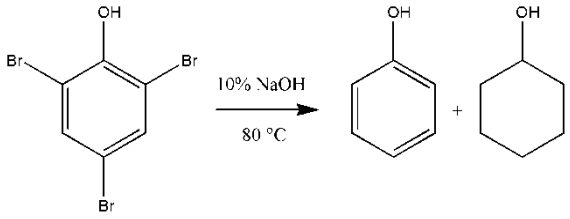

Figure 20. Cyclohexanol as a side-product of tribromophenol reduction using the 50:50 wt.% Al-Ni alloy.

Similar results were obtained with halobenzoic acids, which could be successfully dehalogenated to corresponding deuterated benzoic acids at 80 °C [77]. The substrate-catalyst binding mechanism was proposed that the distance from the surface of the Ni catalyst generated in-situ to each position might decrease in order *ortho* > *meta* > *para*. It explained the resistance of hydrogen-deuterium exchange in the ortho position and as will be later on shown in this thesis, it might as well explain the removal rate of chlorine atoms from different positions in halobenzoic acids. Their further works showed how the temperature and used reagents affect the reaction products. Reducing haloacetophenones with the Raney Al-Ni alloy in a 10% NaOH-ethanol mixture, ethylbenzene is obtained at 90 °C. Decreasing temperature to 50 °C and the concentration of NaOH leads to the formation of either 1-phenylethanol or halo-1-phenylaethanol (if Al-Cu was used instead of Al-Ni) [78]. Ultrasound has been shown effective in the acceleration of the reaction but was tested only for the Al-Cu alloy. However, a similar effect could be achieved with the Al-Ni alloy with respect to the properties of the Raney nickel catalyst obtained by Al-Ni alloy leaching [80]. Other work by Tashiro et al. demonstrated possible dehalogenation of haloanilines, halonapthalenes, and halo-*m*-toluidines using the Al-Cu alloy. Such results firmly pointed to the applicability of the HDH reaction to a wide range of halogenated compounds. The Raney-type Al-Ni alloy and its analogues with copper and iron showed good efficiency and reaction selectivity. These findings regarding the reactivity of the compounds concerning the used reagents and the reaction conditions become a promising background for further research. It focused on

halogenated organics as a source of environmental pollution. Liu did this in 1998, presenting the first dehalogenation of PCBs congeners without any organic solvent [20]. Monochlorobiphenyls were dehalogenated at different conditions using the 50:50 wt.% Al-Ni alloy in very diluted hydroxide solutions (as low as 0.1 wt.% NaOH). At elevated temperatures, such diluted solution provided phenyl-cyclohexane in addition to biphenyl. When a more concentrated solution of NaOH was used, biphenyl was obtained as the only product. It proved the solid reducing power of the alloy at low base concentrations. The technology was concluded to be operationally simple since it does not require high temperatures, high pressure, hydrogen atmosphere, or special apparatus. Again, ultrasonic irradiation accelerated the reaction significantly as expected from their previous experiments with the Al-Cu alloy. Moreover, besides the strong reducing capability of the alloy, cleavage of C-C bonds was observed when debromination of TBBPA was approached [21] (Figure 21). While a bond cleavage is known to occur in bisphenyl A under different conditions (thermolysis above 150 °C, photodegradation, enzymatic reaction), this was the first report of such a process taking place at relatively mild conditions to yield a mixture of cyclohexanol, phenol, 4-isopropylcyclohexanol, hydroxy-bisphenyl A, and dihydroxy-bisphenyl A.

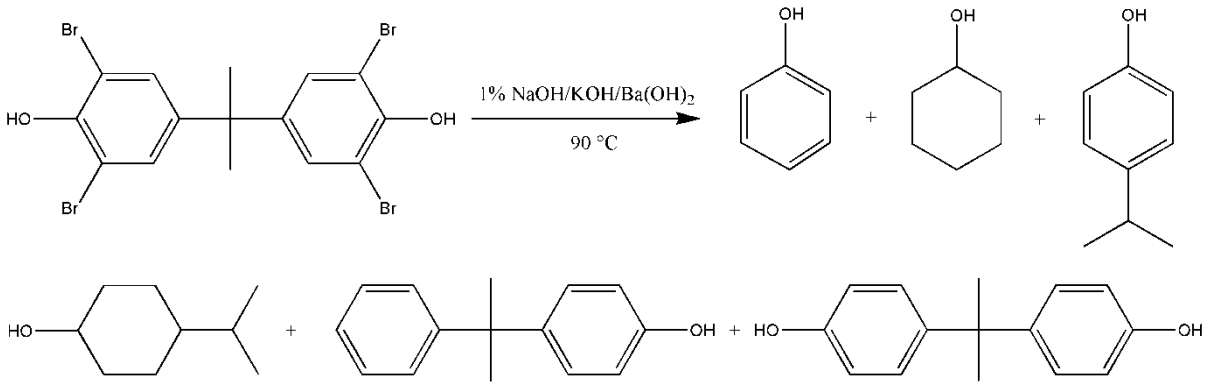

Figure 21. A mixture of products obtained by dehalogenation of tribromobisphenol A by the Raney 50:50 wt.% Al-Ni alloy showing its ability for C-C bond cleavage.

The composition of the mixture was highly dependent on reagent dosage. Since the reactions are parallel, this might represent a further disadvantage of the technology with the Raney alloy being used up for unwanted side reactions such as hydrogenation of aromatic rings. This phenomenon can be, however, controlled up to a large extent. Similarly, the reduction of halogenated phenols and trihydroxybenzenes at the same reaction conditions led to a mixture of products [82]. The authors used a very acceptable alloy dosage of 500 mg/mmol of the substrate. Finally, Liu and his group focused on the dehalogenation of halogenated biphenyls A (tetrabromo- and tetrachloro-) using the 50:50 wt.% Al-Ni alloy in

the presence of different bases, such as Na_2CO_3, K_2CO_3, Cs_2CO_3. All of the experiments at a temperature of 90 °C showed full dehalogenation of the studied compounds. In the case of salts such as sodium acetate, sodium oxalate, or ammonium chloride, only a small fraction of the studied compounds reacted after 12 hours. It was also found that whereas the Raney Al-Ni alloy showed complete dehalogenation, Cu-Al and Fe-Al alloys provided only minimal effect on the decomposition of TBBPA [83]. Based on the previous finding, it is evident that the Al-Cu alloys will be much more compound-specific than the Al-Ni binary alloys.

In the early work of Weidlich et al. [12], the dehalogenation of halogenoanilines (namely 4-bromo, 4-chloro, 4-fluoro and 3-chloro) using powdered 50:50 wt.% Al-Ni alloy was demonstrated at room temperature. The group studied the minimum excess of alloy needed for complete dehalogenation of the corresponding compounds in edetane buffer at pH 10.9. Also, the decomposition rate for each contaminant was determined in this buffer and it followed the C-X bond strength in the case of 4-substituted anilines as expected. They also showed that the reaction efficiency in other buffer solutions is limited by the solubility of aluminum species formed with other ions present in the solutions (e.g. in $NaHCO_3/Na_2CO_3$ buffer, slightly soluble sodium dihydroxy aluminum carbonate is formed. A relatively small molar excess of aluminum (2.5) was needed for complete dehalogenation of all contaminants, except for fluoro-derivate. To overcome the problem with solubility in buffers, the authors used NaOH instead. The leached alloy re-used with hydrogen gas did not show the same efficiency. Another paper by Weidlich, focusing on the dehalogenation of halogenoanilines, showed that the order exists for the Al-Ni alloy reducing ability in the solutions of different bases. The order was set as follows - $NaOH = KOH > K_3PO_4 = Na_2CO_3 = K_2CO_3 > Mg(OH)_2 > CH_3COONa > NaHCO_3$. That should not be generalized for other compounds. In the case of G-NH-Ar-X_n aniline-type compounds dissolved in dimethoxymethane, complete dehalogenation was observed. Interestingly, 2-amino-5-chloro-2'-fluorobenzophenone was fully dehalogenated down to 2-benzylaniline, 4-chloro-2-trifluoromethylaniline was reduced only to o-trifluoromethylaniline; with trifluoromethyl group not intact. It could be caused more probably due to steric hindrance reasons by densely packed fluorine atoms in the fluoro-methyl group (Figure 22). A similar drawback of technology should be observed for polyfluorinated acids with densely packed $–CF_2-$ groups. A significant structural aspect of the bound halogen was demonstrated for the first time [13].

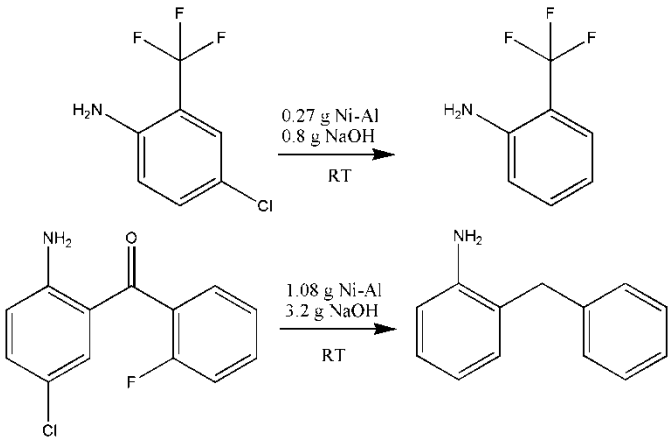

Figure 22. Comparison of the two reactions involving the C-F bond containing compounds; trifluoromethyl group is left intact.

In their following papers, possible reuse of spent Al-Ni alloy or combination of the alloy with other reducing agents was investigated. A significant effect on lowering the Al-Ni dosage necessary for complete dehalogenation of monohalogenated anilines was observed if glucose was used [14]. The amount of the Al-Ni alloy could be reduced by half in the presence of glucose in sodium hydroxide solutions (Figure 23). The effect's origin remained unknown; it was proven that glucose itself could not reduce haloanilines. However, a slightly higher amount of dissolved nickel (around 1.5 mg/L) was present in the filtrates after the reaction. The filtrates were yellowish, and nanoparticles of nickel with volume average hydrodynamic diameters around 70 nm and 390 nm were identified. These could serve as high surface area hydrogen saturated particles for better utilization of hydrogen gas. Based on the observed behavior, the authors successfully dehalogenated several industrially important ortho- or meta-substituted chloroanilines with only 1.2 mol equivalents of aluminum per C-X bond. Reducing the Al-Ni reagent's needed amount to an almost equal ratio represents a big step for potential large-scale application.

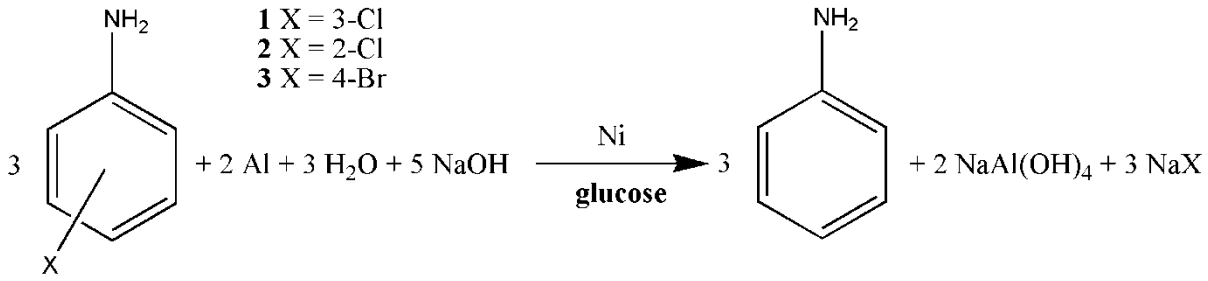

Figure 23. A graphical scheme for conversion of monohaloanilines into aniline at low Al:substrate ratio in the presence of glucose.

Besides the most basic halocompounds occurring in the environment, the hydrodehalogenation reaction using the Raney Al-Ni alloy was also tested for decomposition of triclosan (5-chloro-2-(2,4-dichlorophenoxy)phenol) and chlorophene (2-benzyl—4-chlorophenyl); used as antimicrobial agents [16] (Figure 24). The experiments confirmed superior properties of the Raney Al-Ni alloy over Devarda´s or Arnd´s alloy, which showed zero removal efficiency of the two studied compounds. Again, a very feasible metal-to-substrate ratio of 2.5-5:1 was calculated for the complete dehalogenation of both compounds into the corresponding reaction product. In the case of chlorophene, if an excess of Al-Ni reagent was used, reduction of aromatic ring was observed at room temperature. If weaker bases were used (NaF, Na_3PO_4, Na_2CO_3), triclosan was dechlorinated at a much slower rate and different intermediates could be detected in the reaction mixtures.

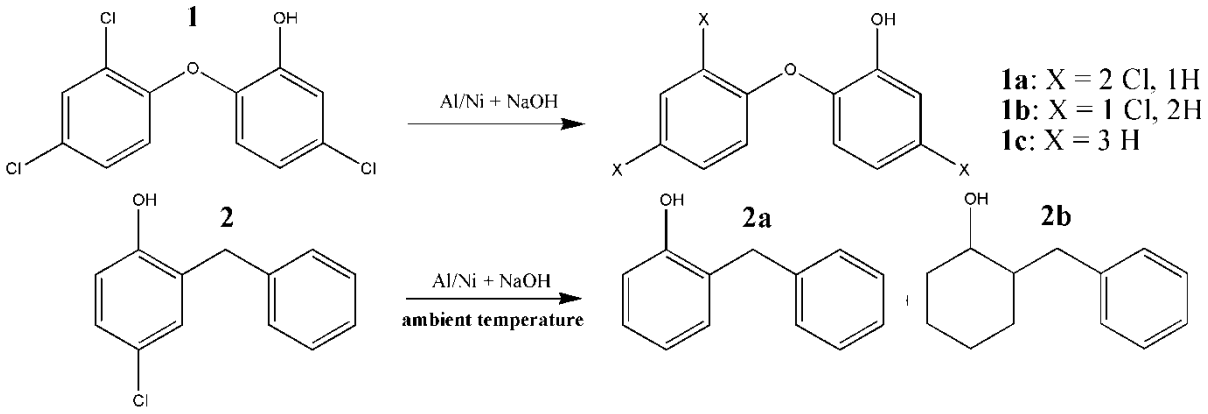

Figure 24. Dechlorination of commercially available antimicrobial agents utilizing the 50:50 wt.% Al-Ni alloy leading to partial or complete dehalogenation of the compounds.

In the latest paper published by Weidlich et al. [18], the hydrodehalogenation reaction utilizing both Raney Al-Ni and Devarda´s alloy (Al-Cu-Zn) was compared at ambient pressure. It was tested on 12 different chlorinated anilines. No regioselectivity or bound halogen selectivity was observed when Al-Ni alloy was utilized, except for the C-F bonds in trifluoromethyl groups. For Devarda´s alloy, substantially higher regioselectivity was found. For example, 4-chloroaniline showed 0% conversion into aniline upon reaction with the alloy. Reaction rates for degradation of 2-chloro- and 3-chloroaniline were determined for Raney Al-Ni alloy without and with co-action glucose addition. It was previously proved that adding glucose significantly alters the minimum dosage of Al-Ni needed for complete conversion. Despite this advantage, it was shown that reaction is also slowed down approximately four-fold. Dechlorination of chlorobenzenes in water/methanol mixtures provided benzene as the only product of the reaction for the Raney Al-Ni alloy and the mixtures of different

chlorobenzenes in the case of Devarda´s alloy. As expected, dichlorobenzenes' kinetic rates were higher than those of trichloro-derivates. In the case of chlorinated phenols, Devarda´s alloy, compared with Raney Al-Ni, failed as a dehalogenation reagent.

Table 3. A brief overview of up-to-date published papers on the HDH reaction of aromatic pollutants utilizing the 50:50 wt.% Al-Ni alloy.

Compound	Al:substrate eq.	Temperature (°C)	Time (h)	Reference
Monochlorobiphenyl	4-40	60-90	2-8	[20]
TBBPA	18-46	90	4-8	[21]
TBBPA, TCBPA	9.5-46	60-90	5-8	[85]
X-PhOH	5-18.5	90	4-6	[86]
XAN	2.5-5	25	17	[13]
TBP	3-5	25	16	[14]
Triclosan, Chlorophene	4-20	25	o/n	[16]
2-CP	100-1500	25	1	[87]
2-CP	500	25	0.75	[88]
Cl-B	480	25	o/n	[18]

TBBPA = tribromobisphenol A, TCBPA = trichlorobisphenol A, X-PhOH = halogenated phenols, XAN = halogenated aniline, TBP = tribromophenol, 2-CP = 2-chlorophenol, Cl-B = chlorinated benzenes; o/n = overnight

The robustness of hydrodechlorination using the 50:50 wt.% Al-Ni alloy was also tested on a sample of natural wastewater. Weidlich utilized the technology for hydrodehalogenation of the technological aqueous stream obtained from the production of azo pigments based on the reaction of 2,5-dichloroaniline [18]. It was also partially contaminated with different chlorinated phenols and low concentrations of chlorinated biphenyls, azobenzenes, and aminobiphenyls. The reaction was done with co-action of a commercial mixture of 12 wt.% $NaBH_4$ in 14M NaOH. $NaBH_4$ can be a possible co-reductant for reducing easily reducible groups, such as azo- group. The reaction output was identified by GC-MS chromatography and AOX parameter determination. While a significant decrease in AOX value and chlorinated contaminants was found, chemical oxygen demand stayed almost identical. Similar values for the sample before and after dehalogenation prove that adsorption on separated insoluble Ni plays a minor role in the process.

Another paper by Hegedüs [17] demonstrated an on-site removal of chlorobenzenes present in groundwater using a pump and treat technology at a 150 L scale. The water containing a mixture of chloro- and dichlorobenzenes exceeding several thousand µg/L was

successfully decontaminated during 8 hours long operation at a temperature under 22 °C. The process was monitored with temperature, pH, and ORP probes. Although almost all monitored compounds were successfully degraded to benzene (detected by GC-MS as the only product of the reaction), the AOX parameter was only reduced by ca 60%. It might suggest the presence of other chlorinated or brominated compounds, which cannot be dehalogenated under given conditions. The process in which hydrogen gas is evolved also helped to strip out toluene, which was also present in a considerable amount. A decrease in benzene levels was also observed. In terms of metal contamination after the reaction, the neutralization step using diluted sulfuric acid was implemented, which led to a decrease in aluminum concentration below 1 mg/L. The nickel level slightly increased after neutralization but did not exceed the value of 1.5 mg/L. Thus, the only byproduct of the reaction, sodium sulfate, led to a slight increase in sulfate levels, which is not considered toxic and can serve as a source for sulfur-reducing bacteria, further improving the biodegradation of contaminants.

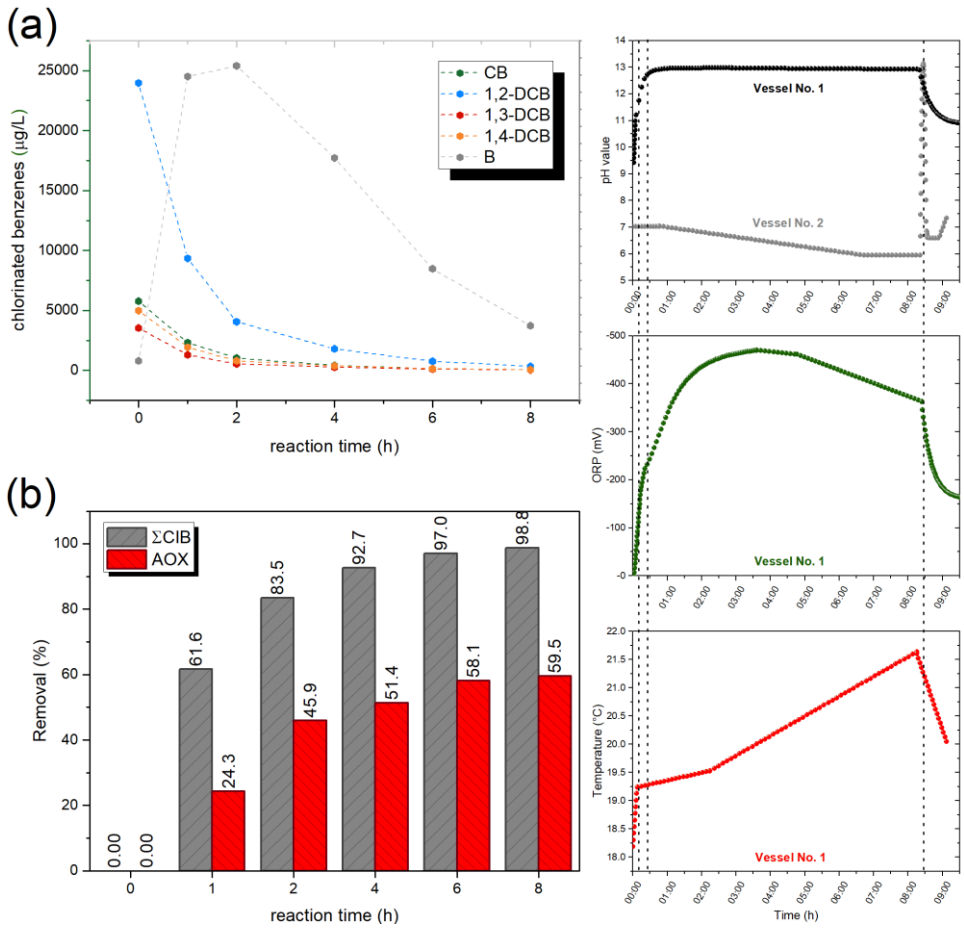

Figure 25. The results obtained from a pilot-scale application of the Raney alloy for dehalogenation of groundwater contaminated by chlorinated benzenes; (a) evolution of CB levels and benzene as the only product of the reaction, (b) % removal of CBs and reduction in the AOX parameter. On the right side, followed physical parameters are given.

2.7.4 Direct reductive dehalogenation via ball-milling/mechanochemistry

Apart from the scope of the presented thesis, the author insists on shortly mentioning the ball-milling technique as a powerful direct method that can be used directly for the dehalogenation of POPs in solid state (DMCR = "Dehalogenation By Mechanochemical Reaction"). An exhaustive review on this topic was written by Cagnetta et al. in 2016 [89]. Regarding reduction techniques, the halogenated organic pollutants can be degraded using zero-valent metals (preferably Mg, Na, or Fe) as in the case of solution chemistry. These reactions need the presence of H-donors (such as alcohols, and amines). Zero-valent metals are cheaper compared to hydrides. Such reactions are thought to proceed via organometallic intermediates, which readily react with H-donors due to their essential character. If metallic hydrides are used (such as CaH_2, $NaBH_4$, $LiAlH_4$), the reagent acts as both the reducing agent and H-donor. The reaction mechanism is the nucleophilic substitution of H^- ion with the halogen atom and can have an explosive character. Lewis bases (e.g., CaO or MgO) can be used for mechanochemical conversion of various halogenated compounds. The former has been studied the most for dehalogenation purposes. The reduction proceeds via the formation of radical species. Even though this novel approach can be advantageous, sometimes prolonged milling time is needed and the technology can become expensive. The process of dehalogenation by mechanochemical approach proceeds via two different types of bonds-rupture:

1. Involves disordering and amorphization of the material (activation of surfaces).
2. Includes the rupture of bonds and bond reformation (cleavage of the C-X bond).

There have been numerous studies published on successful mechanically induced dehalogenation reactions. For example, Birke [90] and Nah [91] demonstrated the dechlorination of PCBs via ball-milling with elemental magnesium and zinc in the presence of hydrogen donors in two different types of mills.

$$R\text{-}X + Mg/Zn + \text{“H”}\ (\text{hydrogen donor}) \rightarrow R\text{-}H + Mg(Zn)Cl_2$$

Eggshell waste as a source of CaO was shown to reduce chlorinated dioxins in fly ash as a co-grinding agent. Baláž et al. demonstrated the solid-state dechlorination of polyvinylchloride (PVC) with eggshells. In this study, the milling parameters were optimized to obtain the highest conversion in the shortest possible time. The dechlorination was followed by an increase in the concentration of inorganic chlorides [92].

$$PVC + CaCO_3 \rightarrow [\text{-}CH{=}CH\text{-}]_n + CO_2 + H_2O + CaCl_2$$

3 OBJECTIVES

The objective of this thesis is to further develop and optimize the hydrodehalogenation technology based on the reduction of halogenated organics using the Raney Al-Ni alloy. This technology for degradation of a vast spectrum of halogenated organic compounds was first mentioned back in the 1990s and since then it had been mostly overlooked by scientists. Even though it provides a cheaper solution than most of the precious metal-based catalysts and its realization does not require high pressures, temperatures, or complicated technological devices, it still possesses several disadvantages. First, utilization of aluminum must be increased because only a fraction of the metal is leached during the reaction. Second, as the Raney Al-Ni alloy acts both as a reagent and a catalyst, the way for its recycling and re-use must be developed; its market price is too high for a single-use operation. We aim to reduce the cost of this technology by the optimization of the Raney Al-Ni alloy solid-state preparation/properties and by possible route for its recycling. The following is the list of the partial tasks to achieve this goal:

1. Preparation of intermetallic phases from Al-Ni binary system, namely Al_3Ni and Al_3Ni_2 phases (or their mixture), via mechanical activation followed by subsequent thermal processing.
2. Characterization of the prepared materials by common techniques for solid-state materials characterization, such as X-ray diffractometry, scanning electron microscopy, particle size distribution, etc.
3. Demonstration of robustness and applicability of the HDH reaction using Al-NI alloys.
4. Testing of prepared materials for their hydrodehalogenation properties on model solutions of chlorinated contaminants.
5. Demonstration of scale-up experiment with the selected organic pollutant.
6. Designing the possible way for the alloy recycling and reuse via ball milling.

4 EXPERIMENTAL PART

4.1 Used chemicals

All chemicals were bought and used without further purification. The powdered metals (aluminum and nickel) were obtained from Fichema company (Czech republic) in technical grade purity (98+). The commercial samples of 50:50 wt.% Al-Ni alloy (Sigma-Aldrich, Germany, mesh 300) and Al_3Ni phase (American elements, USA, mesh 150) were also purchased for comparison with the in-house prepared materials. Halogenated aromatic compounds used within the thesis were obtained from different suppliers and are listed in the table below (Table 4) along with their basic physic-chemical properties.

Synthesis of 2,3,6-trichlorobenzoic acid

2,3,6-trichlorobenzaldehyde (1 g, 4.77 mmol) was placed into a 10 mL reaction vial. To this, magnetic stirring bar and 10 mL of hydrogen peroxide solution (3.5-3.7 %) were added. The vial was enclosed and heated to 190 °C in a microwave reactor for 35 minutes while stirred at 600 RPMs. The vial was cooled to 55 °C. A formation of yellowish oil was observed at the bottom. The mother liquor was separated and freeze-dried to obtain white solid. The yellowish oil was let to crystallize over the weekend and then purified via salt formation as follows: The entire obtained mass was put into 20 mL glass vial, to this, 20 mL of sodium hydroxide solution (0.2 g in 20 mL) was added, and the mixture was stirred for 10 minutes. The yellowish solution was separated by filtration. The clear solution that resulted was stirred with active charcoal (roughly 100 mg) for 10 minutes and then separated via filtration through diatomite. The solution was acidified using 1M HCl solution (pH not measured) and cooled to 6 °C overnight. Approximately 100 mg of solids were obtained upon filtration. The next fraction was obtained by concentrating the solution at 55 °C and 40 mbar, and cooling the solution down to 0 °C. Separate fractions were mixed together to yield approximately 350 mg of the product in total.

Table 4. Summary list of chlorinated compound used for hydrodehalogenation tests along with their basic physico-chemical properties.

Compound	Formula	Molecular weight	Melting point (°C)	Water solubility* (mg/L)	Supplier
chlorobenzene	C_6H_5Cl	112.56	-45	500	Synthesia, CZ
1,2-dichlorobenzene	$C_6H_4Cl_2$	147.01	-17	100	Synthesia, CZ
4-chlorophenol	C_6H_5ClO	128.56	43	2,700	Appolo Scientific, UK
2-chlorobenzoic acid	$C_7H_5ClO_2$	156.57	142	2,090	Sigma-Aldrich, DE
2,6-dichlorobenzoic acid	$C_7H_4Cl_2O_2$	191.01	138-139	100-1,000	Sigma-Aldrich, DE
2,3,6-trichlorobenzoic acid	$C_7H_3Cl_3O_2$	225.45	125	7,700	in-house
2-methoxy-3,6-dichlorobenzoic acid	$C_8H_6Cl_2O_3$	221.04	114-116	6,100	Glentham life sciences, UK
3-amino-2,5-dichlorobenzoic acid	$C_7H_5Cl_2NO_2$	237.08	194-197	700	Sigma-Aldrich, DE

*approximate values from the Internet are provided for informative purposes, given for 20 °C

4.2 Mechanical activation of the Al-Ni system

A mixture of elemental aluminum and nickel in the corresponding weight ratio (either 50:50 or 58:42 Al-Ni wt.%) was co-milled in the Fritsch Pulverisette 6 planetary ball mill at 500 rpm in argon atmosphere at ambient temperature for different times. A milling chamber (250 cm^3 in volume) and balls (10 mm in diameter) made of hardened steel were used. The ball-to-powder ratio was set to 10:1. A small amount of methanol/stearic acid (1-5 wt.%) was used as a process control agent (PCA) in order to avoid extensive welding of the material. The milling chambers were cool to room temperature overnight before opening.

4.3 Thermal processing

The pre-milled metal mixtures were further processed by annealing either in air or in argon atmosphere for 15 minutes in alumina crucibles at either 500 °C or 700 °C. A tube furnace equipped with a quartz glass tube was used.

4.4 Reduction of halogenated organics

Each of the laboratory hydrodehalogenation experiments was carried out at ambient temperature using 100/250/500 mL Erlenmeyer flask enclosed by a drying tube filled up with 5 grams of granulated active carbon. Constant stirring was maintained during the reaction process. Typically, freshly prepared aqueous solution containing desired concentration of the studied contaminant was placed into the flask. Then, sodium hydroxide either in a form of solid or a solution was added and the resulting mixture was homogenized by stirring for 5 minutes. To this mixture, different amounts of the commercial Al-Ni 50-50 wt.% alloy, Al-Ni ball-milled mixtures, or mechano-thermally prepared alloys (of 50:50 wt.% Al-Ni or 58:42 wt.% Al-Ni) were added. The reaction mixtures were sampled through 0.45 μm nylon filters and acidified by concentrated nitric acid to prevent aluminum precipitation for ICP-OES analysis.

4.5 Characterization techniques

X-ray diffractometry (XRPD)

The qualitative identification of the phase composition was performed by XRD method with Panalytical Empyrean (Malvern Panalytical, UK) working in Bragg-Brentano geometry with $CuK\alpha_{1,2}$ doublet radiation. Rietveld refinements of the XRPD data were performed using the *Fullprof* program. The XRPD line broadening was analyzed by the

refinement of regular Thompson–Cox–Hastings function parameters. In order to obtain proper geometry set-up and to eliminate instrumental broadening, the instrumental resolution function was determined by refinement of LaB_6 standard specimen. The JCPDS PDF database and Crystallography Open Database implemented in Match! software were utilized for phase identification.

Scanning electron microscopy (SEM)

SEM images of the samples were recorded using a MIRA 3 FE-SEM microscope (TESCAN, Czech Republic) equipped with EDX detector (Oxford Instrument, United Kingdom).

Difference scanning calorimetry (DSC)

Thermal behavior of ball-milled mixtures was carried out using a STA 449 Jupiter thermal analyzer (Netzsch, Germany). Approximately 85 mg of the sample was placed into an Al_2O_3 crucible and heated from ambient temperature °C up to 700 °C under argon atmosphere with a rate of 30 K/min.

Particle size distribution (PSD)

The particle size distribution was determined with the use of Malvern Mastersizer 3000. Demineralized water and IGEPAL CA-630 as a dispersant were used. The sample was directly added into the dispersion unit with stirring set up to 2,800 rpm and internal sonication with intensity 80% for 60 s was applied on sample before measurement. The Fraunhoffer calculation model was used for evaluation of the final PSD from raw data.

Specific surface area (SSA)

The analysis of the specific surface area was performed with the use of gas sorption analyzer Quantachrome Autosorb iQ. Each sample was degassed at 250°C for at least 240 min and subsequently the adsorption isotherm (11 equidistant points in range 0.05-0.30 p/p0) of N2 at 77 K was measured. The Brunauer-Emmett-Teller (BET) theory was used for determination of the specific surface area.

Gas chromatography (GC)

Water samples for analysis of volatile compounds (chlorobenzene (CB), dichlorobenzenes (DCBs), and benzene (B)) were taken to the 100 mL dark glass containers and filled up to the brim so that there were no bubbles in the container after closing. After this, containers were cooled and transported to the analytical laboratory. The analysis of these compounds was carried out by headspace GC/MS. 6 mL of the water sample was transferred to a 10 mL vial, placed to the heating box of headspace system and incubated at 40 °C for 10 minutes. Released volatile compounds were analyzed by GC/MS Thermo trace GC Ultra

system equipped with Restek RtX-624 capillary column (dimensions: 60 m × 0.25 mm × 1.4 μm). The carrier gas was ultrapure helium (99.9999 %) set at the constant flow mode (1.5 mL/min). The temperature program was as follows: 10 min at 40 °C, then with heat ramp 1 °C/min to 50 °C and held for 10 min. The mass spectrometer with a single quadrupole (Thermo MS Trace DSQ) was operated in the electron-impact mode at 70 eV. The quadrupole operated in the scan mode in a range of molecular weights from 50 – 650. The temperature of ion source was set at 200 °C.

High-performance liquid chromatography (HPLC)

The levels of selected compounds were determined by liquid chromatography using the Shimadzu Prominence HPLC machine equipped with a UV-Vis 2-channel detector and the Gemini C6-phenyl 3 μm 100 x 3 mm chromatographic column (Phenomenex, USA) at a flowrate of 1 mL/min. 0.1% aqueous solution of phosphoric acid (solvent A) and acetonitrile (solvent B) were used as mobile phases. Analyses were performed at a room temperature (24-25 °C) with pre-defined injection volume of 1.3 μL. The compounds were detected at 230 nm. The calibration was performed in the range of 0-1 mmol/dm^3.

AOX (Adsorbable organic halides) determination

The AOX levels were determined using AOX XPlorer analysator (TE Instruments, Netherlands). The samples for measurement were prepared as follows: 100 mL of homogenized sample is placed into 100 mL Erlenmayer flask and 5 mL of 0.2 M sodium nitrate solution are added. The pH value is then adjusted below 2 by addition of 65% nitric acid. One measuring cap of active charcoal is added and the mixture is shaken for 1 hour. The charcoal is filtrated through XPrep-3 filtration system and washed thoroughly by 25 ml of wash solution (0.01 M sodium nitrate). The sample is subsequently burned in an oven at 1000 °C followed by evolution of HX gases which are trapped in the titration cell by a reaction with acetic acid. The amount of halogenides was determined by coulometric titration with standardized $AgNO_3$ solution.

Inductively coupled plasma optical emission spectrometry (ICP-OES)

The levels of selected metals in the real water sample were determined utilizing ICP-OES Spectrometer iCAP 7400 D (Thermo Scientific, Germany) equipped with CID86 detector. The instrument was calibrated on the certified reference material AN 9090(MN) representing a mixture of metal ions stabilized in 5% HNO_3 (v/v). For experiments performed with model solutions the levels of toxic elements before and after the adsorption were determined by atomic absorption spectroscopy (AAS) using spectrometer 240 RS/2400 (Varian, Australia).

5 RESULTS AND DISCUSSION

The scientific part of the doctoral thesis can be divided into two subparts. The first comprises of ball-milling experiments and the solid-state characterization of the prepared alloy materials via available analytical techniques. The second part describes the materials´ application and the comparison of their efficiency with their commercially available analogs (Raney type Al-Ni alloys either 50:50 wt.% or 58:42 wt.% - refer to the materials part). Emphasis is put on the subsequent utilization of the prepared materials for hydrodehalogenation reactions, which plays a bridging role between the research in environmental chemistry and industrial chemistry areas. This part objectively reports on the Al-Ni alloys utilization for hydrodehalogenation of organic pollutants in waters and its possible drawbacks.

5.1 Mechanochemical activation and processing of the materials

At the beginning of this research, numerous mechanochemical experiments were carried out in the Fristch Pulverisette 6 planetary ball-mill equipped with 250 mL stainless-steel milling jars. These experiments followed the pioneering works in the field of mechanical alloying of the Al-Ni system [58–60]. In these works it was shown that some intermetallics from the binary Al-Ni system (e.g. β-AlNi or Al_3Ni) can be prepared directly by co-milling the two elements or by a combined mechano-thermal approach. However, prevalently mixer mills (e.g. SPEX 8000) were utilized in these studies. The research was mostly focused on the general behavior of the Al-Ni system without detailed description of neither of the material properties or their application. This type of ball-mills is usually only used for small-scale synthesis.

Moreover, experimental details were often missing (material of the milling equipment, the volume of jars used, and the frequency). For potential large-scale fabrication of materials, it was inevitable to investigate whether the same outcome could be obtained in another type of mill with higher material throughput. Generally, transferring the fabrication process between two types of mills may represent a challenge. Recently, it has been shown that the planetary or vibratory ball-mills can be successfully utilized for the scale-up of mechanochemical synthesis up to 100 g per batch [93, 94]. It is possible that the industrial scale mills could provide kilogram quantities of materials.

Within this thesis, attention was focused primarily on 50:50 wt.% Al-Ni system (equal to $Al_{69}Ni_{31}$ molar composition), as this Al-Ni alloy solely has been used for

hydrodehalogenation applications before [13, 14, 16–18]. However, other Al-rich compositions of the Al-Ni alloys (specifically 58:42 wt.% Al-Ni equal to $Al_{75}Ni_{25}$) were investigated due to their promising properties, as well. The summary of the selected ball-milling experiments is given in Table 5.

Table 5. The summary table of the selected performed ball-milling experiments in the binary Al-Ni system.

Al:Ni wt.%	t_m (min)	PCA (wt.% amount)	Appearance of the product	XRPD
50:50	15	-	coarse grains	reactants
50:50	15	MeOH (2.5)	coarse grains	reactants
50:50	30	MeOH (5)	fine powder	reactants
50:50	60	MeOH (5)	fine powder	reactants
50:50	90	MeOH (5)	fine powder	reactants (or + IM)
50:50	180	MeOH (5)	fine powder	reactants
50:50	90	stearic acid (2.5)	fine powder	reactants + IM*
50:50	90	stearic acid (5)	fine powder	reactants + IM*
58:42	15	MeOH (5)	fine powder	reactants
58:42	30	MeOH (5)	fine powder	reactants
58:42	60	MeOH (5)	fine powder	reactants
58:42	90	MeOH (5)	fine powder	reactants
58:42	180	MeOH (5)	fine powder	reactants

IM = intermetallics (Al_3Ni_2 + Al_3Ni), the mixtures were milled at 500 RPM with a ball-to-powder (BPR) ratio of 10 under argon atmosphere, *combustion took place during the isolation step of material

Although most of the studies that were published on the topic of the mechanical alloying of the Al-Ni system did not suggest the use of a process control agent (PCA), under the studied conditions (please refer to the experimental part), dry milling led to immediate welding of aluminum which then agglomerated upon cooling. Particles over 1 mm in size were obtained by this approach. Temperatures above the melting point of aluminum were achieved upon high-energetic impact of milling balls or cold welding dominated over the fracturing process. To avoid this phenomenon, methanol was added to the mixture as a commonly used PCA. It was found that at least five wt.% must be used to fully overcome welding of the material. These experiments led to the formation of highly homogenous dark grey microcrystalline powder. Self-combustion after the milling process could be observed several times (during the isolation step). It was initially believed that the organic PCA agent is oxidized rapidly upon exposure to the air. Another possible explanation was that the formation of pyrophoric metal particles upon high-energetic milling might have initiated exothermic surface oxidation when removed from the argon atmosphere. Such an exothermic event could

have subsequently promoted the crystallization of alloy between the two metals homogenized at the nanoscale. Both Al_3Ni and Al_3Ni_2 were reported to have highly negative formation enthalpies [95, 96]. In the previous studies, a less energetic SPEX mixer mill was utilized for β-AlNi or Al_3Ni phase, and no such behavior was reported for any of the systems studied. Generally, in a mechanically activated system, the crystallization of intermetallic phases takes place at lower temperatures, as reported before by Cardellini et. al [60]. The conditions at which the spontaneous exothermic reaction takes place remain unknown and more research must be carried out to explain this phenomenon.

5.2 Solid-state characterization of the prepared materials

The prepared ball-milled samples and the samples of mechano-thermally prepared alloys were characterized in detail by X-ray powder diffractometry. The X-ray powder patterns of 50:50 wt.% Al-Ni metal mixtures milled for 15 to 90 minutes are shown in Figure 26a. The qualitative phase analysis of the measured patterns using JCPDS database [97] revealed the presence of starting reagents – elemental aluminum (JCPDS card no. 01-1180) and nickel metals (JCPDS card no. 71-4655) – in all samples; regardless of the milling time. The identical result was obtained for the 58:42 wt. % Al-Ni system (Figure 26b) after 90 minutes of ball-milling. No other phases from the Al-Ni binary system or metal oxides could be detected.

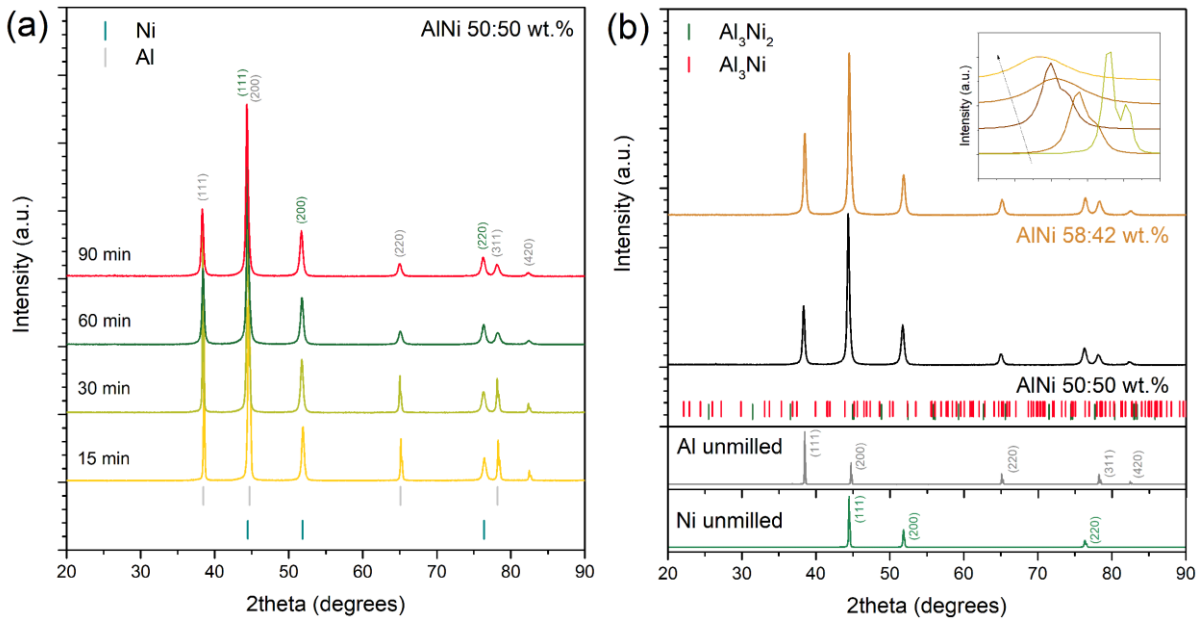

Figure 26. The evolution of the XRPD patterns for the ball-milled 50:50 wt. % Al-Ni mixture from 0 up to 90 minutes (a); the comparison of the XRPD patterns for 90 min activated mixtures (two different compositions) and the inset showing the evolution of aluminum (111) crystallographic plane – the arrow shows time progress.

Therefore, the formation of intermetallic phases was excluded at short milling times even at relatively high impact energy compared to the shaker mills. It is noteworthy that MeOH, 5 wt.%, was used as PCA in all experiments.

An in-depth analysis of the patterns revealed valuable information about the impact of mechanical treatment on the studied system. A closer look on the (111) aluminum crystallographic plane for the 50:50 wt.% Al-Ni metal mixture (Figure 26b; inset) suggested that the process of Al-Ni system activation could proceed via two separate stages:

1. In the first stage of milling, up to 30 minutes of milling, most of the provided mechanical energy was used for homogenization of the mixture and disintegrations of aluminum precursor particles, as there was no pronounced broadening of the Bragg reflections corresponding to this phase observed. This well fits the observed particle sizes for the input material (aluminum $d_{90} \leq 60$ μm).

2. In the second stage of milling, after 60 minutes, a decrease in the crystallinity of the aluminum metal became more pronounced as it was followed by a significant increase of full-width-half-maximum (FWHM) values for all diffraction lines. Based on the Rietveld refinement results, the nano-crystalline character of both aluminum and nickel were found with the crystallite size below/close to 50 nm at the end of the milling process. The change in the crystallite size was more pronounced for aluminum metal. Such small crystallite size may drastically enhance the solid-state reactivity of materials as it is usually observed for the ball-milled materials. The calculated wt.% composition of the milled mixtures corresponded to the theoretical values with great accuracy and the final R_{wp} were around 10%.

Table 6. The calculated phase composition of the ball milled sample along with the crystallite size of aluminum and nickel metals followed in time.

sample	compositions wt.%		crystallite size (nm)		R_{wp} (%)
	Al	Ni	Al	Ni	
Al-Ni 50:50 0 min	48.1	59.1	216(3)	76	11.42
50:50 15 min	50.6	49.4	112(1)	37	10.10
50:50 30 min	50.8	49.2	134(2)	35	9.65
50:50 60 min	48.4	51.6	49	32	8.28
50:50 90 min	47.2	52.8	42	33	8.26
average	**49.25**	**50.75**			
58:42 15 min	56.7	43.3	150(2)	41.4	9.52
58:42 30 min	55.4	44.6	89(2)	34.4	9.65
58:42 60 min	58.7	41.3	120.2	33.8	10.54
58:42 90 min	55.3	44.7	63.2	33.4	11.22
average	**56.53**	**43.47**			

Increased reactivity of ball-milled materials was proved by the DTA measurements (Figure 27). For the unmilled Al-Ni mixtures, a sharp exotherm was observed in the pattern. This event was found to have a maximum at around 635 °C, slightly below the melting point of pure aluminum metal (Figure 27a), and was assigned to the crystallization of the alloy. The result was verified by XRPD measurement and the presence of intermetallic phases was confirmed (with no unreacted material left). The Al-Ni alloy with coarse grains could be prepared even without mechanical activation of a given mixture of metallic particles. Due to its inhomogeneity, the material is not applicable for the hydrodehalogenation purposes presented in the next chapters. Instead, highly homogenous ball-milled samples showed disappearance of the sharp exothermal peak, with thermal events shifted to a lower temperature range (below 500 °C). The broad, overlapped, exothermic events, according to the Cardellini et al. are assigned to the crystallization of intermetallics [60]. First, the materials were processed at 700 °C for 15 minutes to secure the complete crystallization of the requested alloy. Following the results of DTA measurements, the low-temperature method for the crystallization of 58:42 Al-Ni wt.% mixtures at 500 °C was later used. It is important to note that the optimal milling conditions (rotational speed and ball-to-powder ratio) were also supported by DTA data. Because the main goal was to develop a fast and low-temperature process, decreasing these two parameters would lead to the prolongation of the ball-milling process itself and increased operational costs. An exciting observation connected to the behavior of the mixtures was made. Whereas annealing of a non-activated metal mixture resulted in the formation of alloy; to our surprise, the coarse-grain welded sample ball-milled without the PCA agent did not represent an alloy. This could be explained by a far-from-equilibrium state of matter during the high energy ball milling and inability of the material to nucleate the intermetallics phases (even when progressive cold welding already took place).

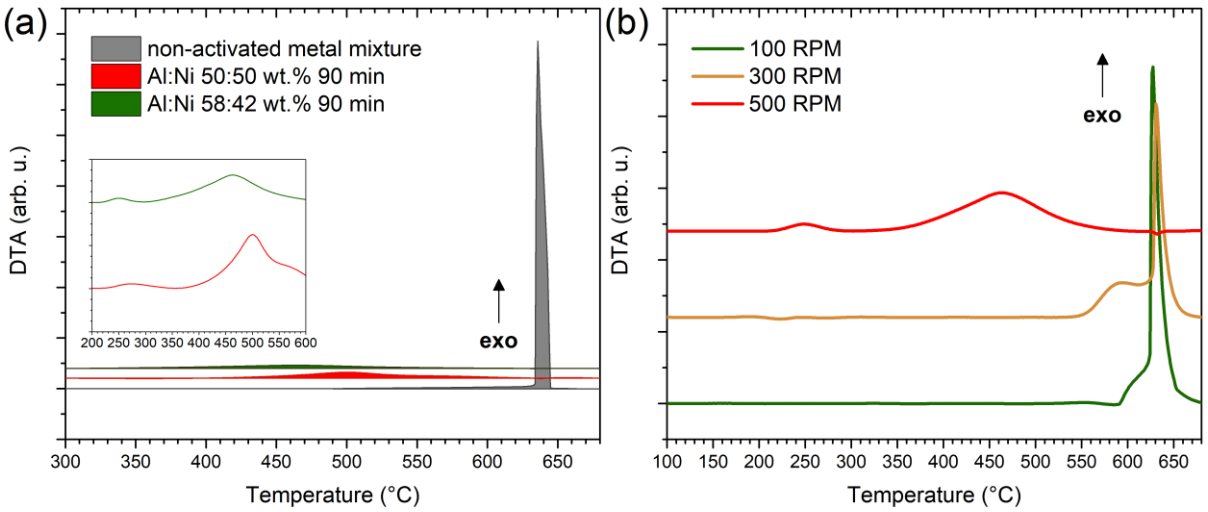

Figure 27. The comparison of DTA pattern for an unmilled Al-Ni mixture and the mixtures of corresponding compositions activated for 90 min (a); the disappearance of sharp exotherm at around 635 °C followed by DTA as a function of increasing RPM at fixed milling time 90 min for 58:42 wt. % composition (b).

The XRPD patterns of the metal mixtures activated for 90 minutes after the thermal treatment are presented in Figure 28. The formation of new phases in the system and disappearance of elemental powder reflections is, even after short annealing at 500 °C/ 700 °C, self-evident. The Le-Bail analysis was performed starting with the expected phase composition to prove the formation of predicted intermetallic phases (shown for 50:50 wt. % Al-Ni system, Figure 28c). The presence of orthorhombic Al_3Ni phase (JCPDS card no. 02-0416) with the unit cell parameters of a = 6.62 Å, b = 7.37 Å, and c = 4.82 Å and rhombohedral Al_3Ni_2 phase (JCPDS card no. 03-1052) with the unit cell parameters of a = 4.05 Å and c = 4.90 Å was confirmed. The presence of cubic β-AlNi phase was not detected. The obtained pattern was compared to that of the commercial Raney 50:50 wt.% Al-Ni alloy sample and showed only minor differences, such as the commercial alloy contained a nominal amount of unreacted aluminum. The quantification of each phase in the alloy materials was, in general, complicated by non-trivial preferred orientation of Al_3Ni_2 phase. For the 58:42 wt. % composition of Al-Ni mixtures (corresponding to Al_3Ni intermetallic phase), processed at the same conditions, an admixture of Al_3Ni + Al_3Ni_2 was formed. The phase composition was calculated to be approximately 80/20 wt.% Al_3Ni/Al_3Ni_2 based on a semi quantitative analysis in the EVA software (according to the provided corundum numbers). Please refer to Table 7 for the phase analysis of alloy materials used within the thesis and the corresponding crystallite size. The Al_3Ni_2 phase was also found to be present in the commercial 50:50 wt.% Al-Ni material. The coexistence of the two phases is in the agreement with the phase diagram. It might be connected to the crystallization pathway or to

the local inhomogeneity caused by ball milling. The repetition of the milling experiments or prolonging the milling time to 3 hours did not seem to affect the final alloy phase compositions. It will be still necessary for the effect of the preferred orientation to be taken into account.

It is noteworthy that the observed phase composition for prepared materials is a good match with the phase diagram and previous studies. The presence of Al_3Ni_2 phase in 58:42 wt.% mixtures (equal to Al_3Ni) composition might have resulted from local inhomogeneity of the material. Contradictorily to this, for the crystallization of the alloys purely from ball-milled systems, the β-AlNi phase has been found to crystallize even from aluminum-rich compositions [60]. The β-AlNi phase has the most negative formation enthalpy out of all intermetallic phases in the binary Al-Ni system [98], which might explain such observation. The results provided were however not uniform across the literature. The milling experiments carried out in these studies took hours to be done, as well. Even on a small scale.

Table 7. The quantitative phase analysis of the Al-Ni alloy materials and the average crystallite size for the two intermetallic phases. Commercially available materials are shown for comparison.

sample	compositions		crystallite size (nm)		R_{wp} (%)
	Al_3Ni	Al_3Ni_2	Al_3Ni	Al_3Ni_2	
50:50 commercial*	42.9	54.8*	115	114	21.5
50:50 mechano	31.2	68.8	100	129	15.6
58:42 commercial*	90.5	8.2*	120	65	20.7
58:42 mechano	80.9	19.1	105	92	19.0

*the commercial material contained small amounts of unreacted aluminum metal.
higher observed R_{wp} factors were caused by severe preferred orientation of Al_3Ni_2 phase

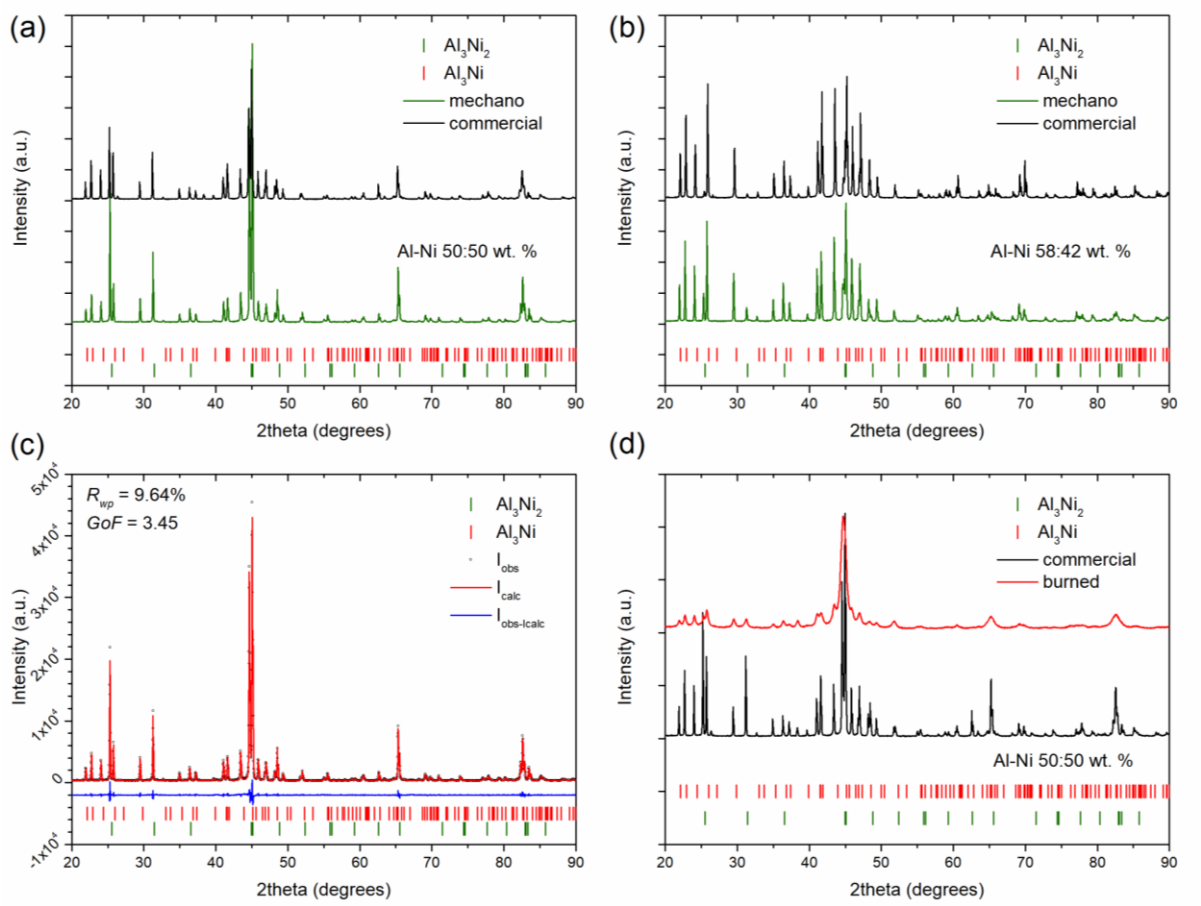

Figure 28. The XRPD patterns of Al-Ni mixtures ball-milled for 90 min after thermal processing – 50:50 wt.% (a), 58:42 wt.% (b), the graphical output of LeBail analysis showing a good match with standards of Al_3Ni and Al_3Ni_2 phases (c), XRPD pattern of burned material after the milling compared to the commercial Al-Ni alloy (d).

As previously outlined, in some cases a spontaneous crystallization of the alloy was observed even at ambient temperatures. It was usually accompanied with sudden self-combustion during the isolation step. Initially, no attention was paid to these materials. After the materials were analyzed by XRPD to determine their phase composition, however, the formation of nano-crystalline alloy was confirmed (Figure 28d). The intermetallic phases were accompanied with variable amounts of unreacted metals. The spontaneous crystallization of the Raney type Al-Ni alloys is an interesting future challenge for our research group. If controlled properly, such process can lead to the preparation of extremely reactive particles of Raney Ni. The determination of exact conditions at which the self-combustion takes place is the crucial parameter.

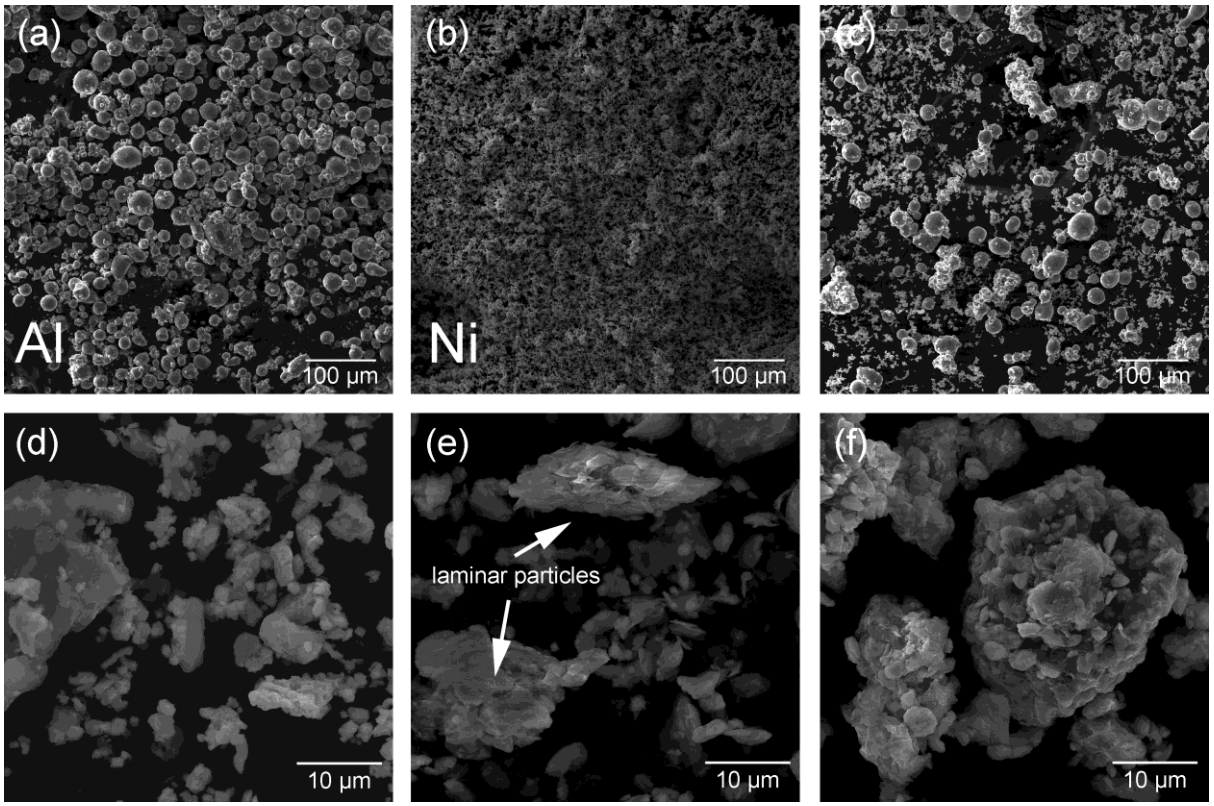

Figure 29. SEM images for precursor materials (a, b), their physical mixture (c), and the mechanically activated Al-Ni mixtures for 15, 30, and 60 min respectively (d, e, f).

Furthermore, the process of the ball-milling was followed by scanning electron microscopy (SEM) to explore the microstructure of ball- milled samples. The evolution of the ball-milled system is demonstrated on the 50:50 wt.% Al-Ni mixture. Selected SEM images of non-milled elemental precursors and milled metal mixtures are shown in Figure 29. The powders of aluminum and nickel showed a significant difference in their particle size and morphology. This corroborates the findings from the XRPD measurements (average FWHM values of diffraction lines for the starting metals were higher for a nickel metal). The un-milled metal mixture (Figure 29c) consisted of spherical aluminum particles up to 60 µm in diameter (60 mesh), whereas nickel was found in micrometric agglomerates of small, submicronic crystallites (electrolytically prepared material, d_{90} n.d.). The observed difference is the result of different preparation routes for the two metal powders but clearly represents an advantage for the mechanical activation process. This, so-called "micro-nano", approach in the field of mechanochemistry was demonstrated previously [99]. It showed faster transformation rates or, in the case of starting reagents prepared by different methods, and an even more explosive character of the reactions [100]. Therefore, combining bigger particles of malleable aluminum metal with relatively hard nickel submicronic particles is beneficial for the process in general. For short milling times (15 min), slight deformation of originally

spherical aluminum particles was observed, but the sample was not homogenous as seen in energy dispersive analysis (EDS) image (Figure 30a). Further milling of the mixture for additional 15 minutes led to slight homogenization of the mixture (Figure 30b) and the disappearance of spherical aluminum particles. Due to the shearing effect typical for planetary ball-mills and ductility of aluminum, these acquired a laminar shape after 30 min (Figure 29e). At 60 min, it became challenging to distinguish between the elements. The fine nickel particles became hammered into the aluminum particles and the roughness of the particle´s surface increased significantly. Narrowing of the particle size distribution was observed due to the agglomeration effect. The particles became more homogenous in the shape and their morphology could be described as rather quintessential for ball-milled samples (Figure 29f). Progressive inter-diffusion of metals is presumed at this stage such it is almost impossible to detect separate metal particles by EDS analysis (Figure 30c). No contamination from abrasion of milling equipment was detected and the powders were only slightly oxidized on the surface. The presence of oxide phases could not be detected by X-ray powder diffractometry. Only negligible surface contamination is presumed with no effect on the reactivity of the materials. Even though the starting mixture contained 50:50 wt.% Al-Ni, most of the spectra pointed to aluminum rich composition (on average 60 wt.% of aluminum). It is suspected that the result might be connected with the structural features of the materials and the penetration depth of the electron beam, where submicronic nickel particles are attached to the aluminum core. When analyzed by handheld X-ray fluorescence analyzer (XRF), the composition of powders was very close to the original mixtures. The used XRF analyzer also detected low amount of impurity metals such as iron and copper (below 5000 ppm). These originate from starting nickel metal but are of no concern, since the materials are only applied in very basic conditions. Further inspection of the materials by transmission electron microscopy is expected in the near future. It might provide a better insight on the nanostructure and to reveal a possible mechanism for the self-combustion phenomenon.

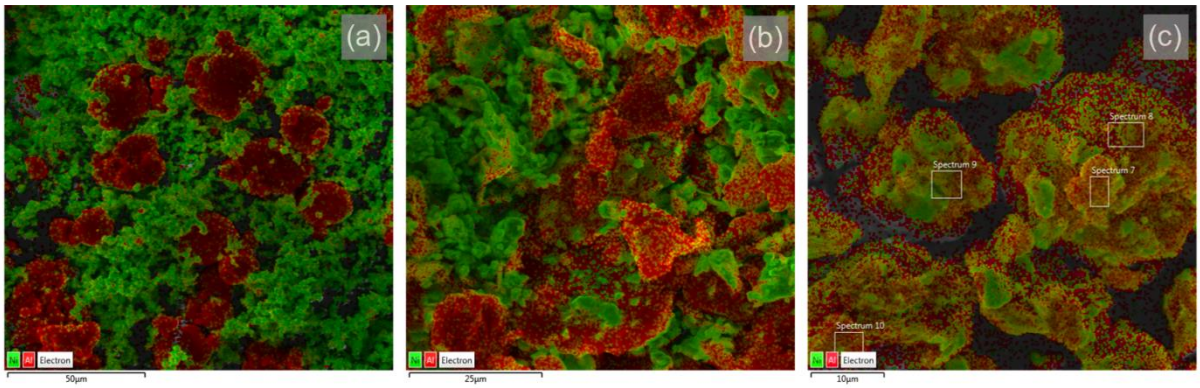

Figure 30. The energy dispersive analysis (EDS) results for the unmilled Al-Ni 50:50 wt.% mixture (a) and for the ball milled samples – 30 min (b) and 60 min (c), respectively. Aluminum is shown in green color, nickel in red.

To secure full homogenization of the mixture, the milling time was increased to 90 minutes. The materials were then isolated from the chambers and processed in a tube furnace under argon atmosphere (at 500/700 °C). The alloy materials are composed of Al_3Ni_2 and Al_3Ni phases, as confirmed by XRPD, of 50:50 wt.% Al-Ni and 58:42 wt.% Al-Ni compositions were analyzed both by SEM and PSD analyses. The microstructure of mechano-thermally prepared materials, which will be shown to have a pronounced effect on the hydrodehalogenation, is depicted in Figure 31a a 31b. After thermal treatment, the materials retained their characteristic microstructure (aggregates composed of submicronic crystallites). The crystallization of the intermetallics, which is a highly exothermic event, might have promoted short-lived melting of the material, judging from the smooth edges of individual particles (Figure 31a). The materials have rough surfaces compared to their commercial analogues. Industrially, Raney-type Al-Ni alloys are prepared by a conventional cast-and-crush method – crystallization of the intermetallics from a melt; followed by crushing of the ingots (a three step process). Materials prepared via this method have comparably lower surface area and their morphology is dominated by sharp edges resulting from material fractures during the milling process. The surface of the particles is relatively flat and covered with a fraction of the small size class particles. In addition the top of that, the process of fracturing must be energetically demanding, as the Al-Ni alloys are in general hard materials.

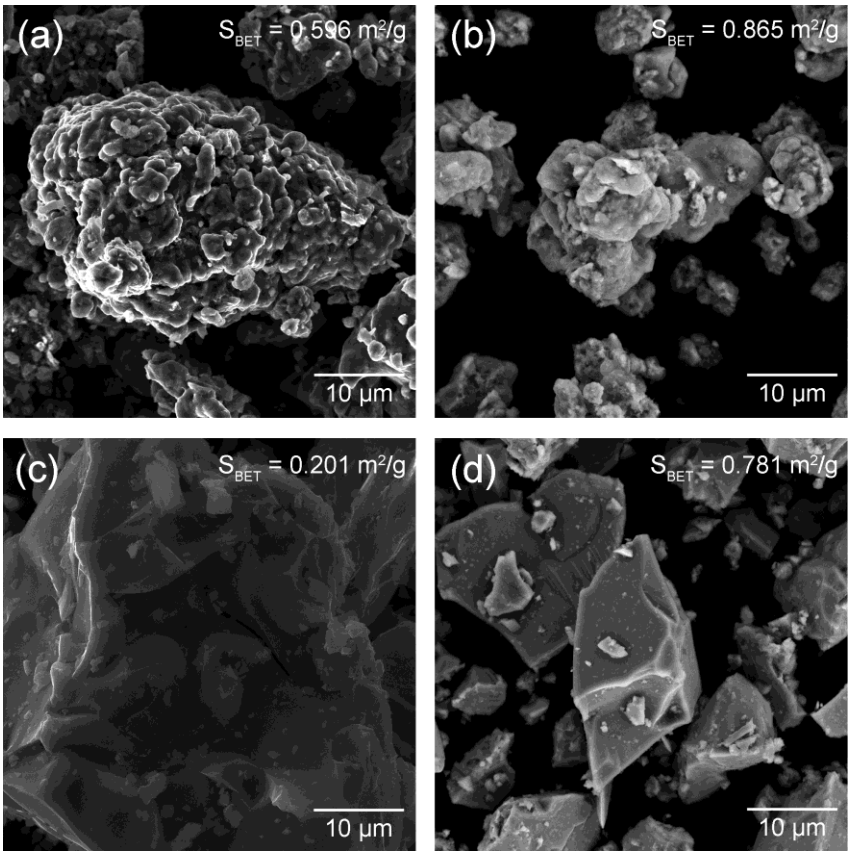

Figure 31. High-resolution SEM images of the mechano-thermally prepared Al-Ni alloys (a, b) compared to their commercially available analogues (c, d) at the same magnification with the measured S_{BET} surfaces.

The particle size distribution measured for the alloy materials correlated well with the observation from the SEM analysis and surface area measurements. For the 50:50 wt.% alloy, a bimodal PSD curve was observed. While d_{50} value was determined to be around 36 µm, due to the agglomeration effects, a small fraction of the material contained bigger particles as well, in the size range of 200-1000 µm. The materials, after milling and the subsequent thermal treatment, were not further processed (via sieving). Therefore, this might be also considered as a deviation caused by inhomogeneity. According to the measured d_{90} value, most of the particles are smaller than 180 µm. For comparison, the commercial material showed rather narrow particle size distribution, with the d_{50} value significantly shifted to bigger size class (around 100 µm). According to the measured data, the material can be assigned mesh300 quality (not specified by vendor). In this case, the d_{50} value and increase in the surface are decisive factors as will be presented in the dehalogenation part. On the other hand, material with the composition adjusted to 58:42 wt.% had the particle distribution size almost identical to the commercial sample of the alloy. The values d_{50} and d_{90} for the two materials were on average 37 and 107 µm, respectively. These values were also very close to

the mechano-thermally prepared alloy with the 50:50 wt.% composition. Similar particle size distribution was beneficial for further comparison of the materials in terms of their catalytic properties. If compared to the other studies published for low-temperature synthesis, such as LTCA method, the particle size distribution of mechano-thermally material is broader and particles are slightly larger [101, 102]. Nevertheless, the fact that particle size classes below 100 μm can be directly obtained without a need for additional fractionation of the material is in favor of the proposed mechano-thermal approach. If applied at large scale, the process could be optimized to obtain uniform PSD curves with defined particle size range as requested. It is highlighted that within the present thesis, other surfactants were not explored. Surface active components could affect the output particle size distribution and the morphology of the particles to a great extent.

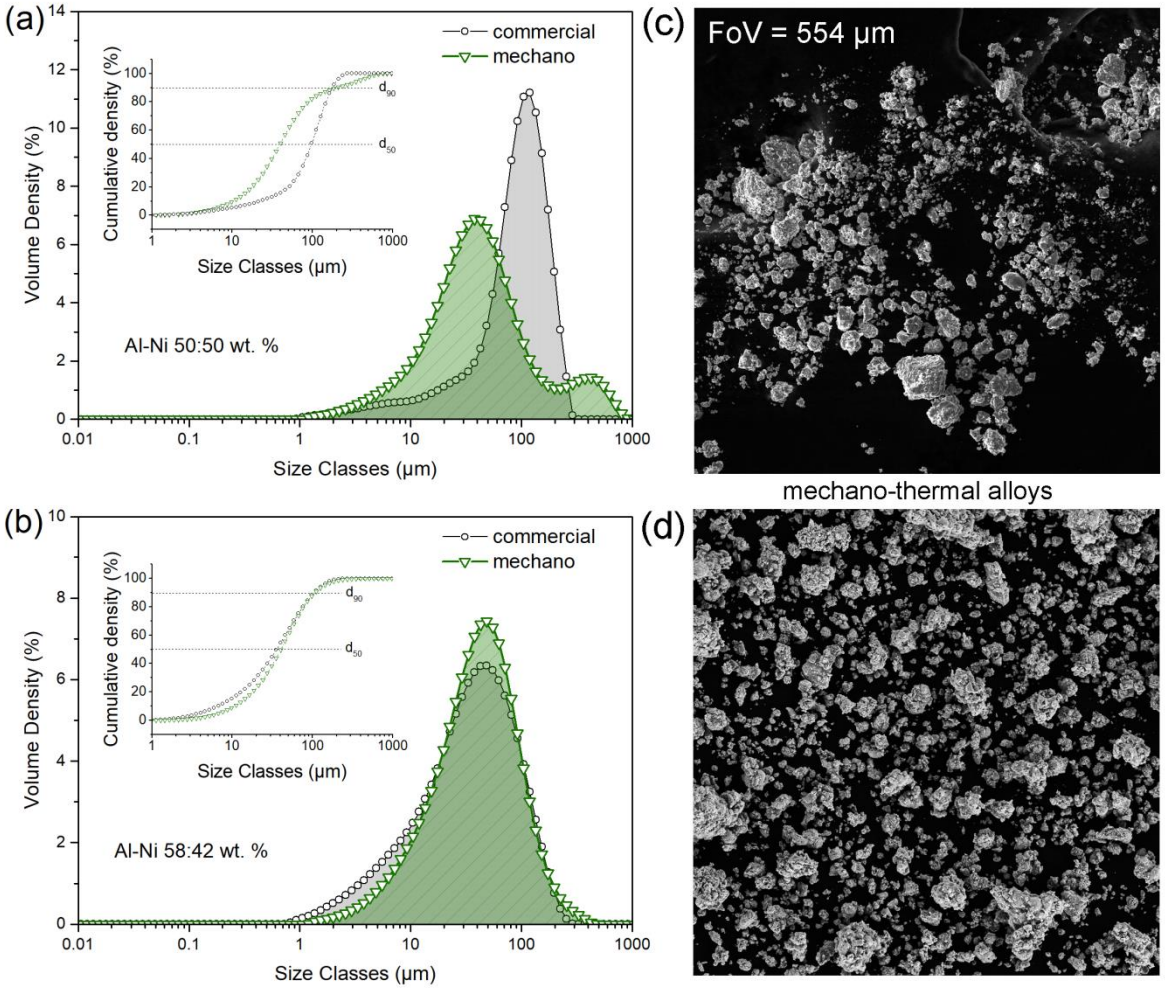

Figure 32. The particle size distribution (PSD) curves of mechano-thermally prepared alloys, compared to the commercially available analogues. SEM images at low magnification are shown in figures (c) and (d).

Based on the collected data, it was concluded that the process of mechanical activation in the binary Al-Ni system can be transferred to different types of the mills. The milling conditions for such process must be optimized beforehand (RPM, ball-to-powder ratio, PCA selection) to obtain materials with requested properties. The formation of intermetallic phases at short milling times (up to several hours) cannot be expected, as this was only shown to take place after tens to hundreds hours of milling in higher throughput mills (e.g. attritor). In general, mechanical activation favors interdifussion of the metals and promotes the crystallization of intermetallics below the melting points of pure elements. Therefore, nanocrystalline ball-milled Al-Ni metal mixtures processed at temperatures <700 °C will provide the materials with requested phase composition and catalytic properties. This temperature range is comparably lower to the one used for industrial production of the Al-Ni alloys (exceeding 1200 °C). It also allows for the downsizing of the materials, providing materials with high reaction surfaces and reactivity.

The mechano-thermal process thus has several advantages - reduced fabrication time, significantly lower working temperatures, no need for further processing of materials (e.g. crushing and sieving). On a large scale, for the process itself, vibratory ball mills or continuous feed screw mills could be applied. High throughput industrial mills can accommodate tens to hundreds of kilos of solids [44]. The total time may vary depending on the input material size and the energy input from the mill.

In this case, the process was carried out under protective atmosphere of argon gas and took around 4 hours in total. The repeatability of the preparation route was verified by numerous runs, in which, over 300 grams of the materials were prepared. On a tested lab scale (10-20 g per batch), the resulting materials were composed of Al_3Ni/Al_3Ni_2 phases in different ratio; depending on the starting mixture compositions. The materials prepared by mechano-thermal way showed broad particle size distribution (3 orders) and were composed of agglomerated non-porous nanocrystallites. The particles size distribution measurements confirmed d_{90} value for the final alloy materials to be around 100 μm. The mechano-thermally prepared alloy materials, compared to the commercially available materials, showed higher surface areas, essential for good reactivity and formation of highly active Raney Ni catalyst. The analyzed materials were used for hydrodechlorination tests.

5.3 Dehalogenation tests

5.3.1 Robustness of hydrodehalogenation reaction using commercial Raney Al-Ni 50:50 wt.% alloy

5.3.1.1 Hydrodehalogenation of model compounds (chlorobenzenes and 4-chlorophenol)

Robustness of the HDH reaction was verified in the first step using commercially available Raney type Al-Ni alloy (50:50 wt.% Al-Ni) on the model samples of the simplest chlorinated aromatic contaminants - monochlorobenzene (CB) or 1,2-dichlorobenzene (1,2-DCB), which were widely used in the past as solvents due to their degreasing properties. The tests were also performed on solutions of 4-chlorophenol, which belongs to a diverse POPs group of chlorinated phenols. 4-chlorophenol is typical model compound for hydrodehalogenation tests (up to date 84 hits for combination of keywords 4-chlorophenol AND hydrodechlorination; Science direct). The tests were performed using an excess of alloy and the main goal was to demonstrate robustness of the technology (selective C-Cl bond reduction, and high removal rates at normal conditions). No optimization was done at this stage as the commercial alloy was further used only for comparison with mechanically activated or mechano-thermally processed alloy materials. The initial tests were followed by scale-up and optimization solely on the samples containing 4-chlorophenol dissolved in distilled water.

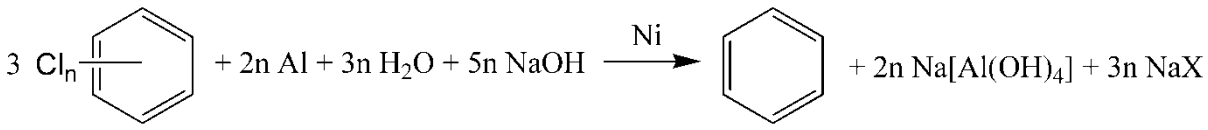

Figure 33. General hydrodehalogenation scheme for decomposition of chlorinated benzenes using the Al-Ni alloys.

In table 8 below, the results of initial tests performed on model solutions of CB and 1,2-DCB are shown. The loads of alloy powders were set to 260 mg for each experiment using several-fold molar excess of sodium hydroxide (compared to the molar amount of pollutant). The results clearly showed that decomposition of monochlorobenzene (CB, Entry **#1**) is rapid and runs to completion in less than one hour. As the only product, benzene (B) was detected but was not quantified due to its high volatility. Same behavior was observed for 1,2-dichlorobenzene (1,2-DCB, Entry **#2**), which is less soluble in water. Its decomposition rate was somewhat slower due to double molar amount of chlorine atoms present in the molecule. As it will be shown later, the number of bound halogen atoms is

decisive for the rate of removal under the same reaction conditions. After 90 minutes, removal of 1,2-dichlorobenzene was almost complete with over 96% of the compound being converted into benzene or to the intermediate compound; which was determined as monochlorobenzene (CB). When the reaction time was increased to 180 min, the complete conversion took place and the intermediate compound was degraded as well. The last example shown was a mixture of the two discussed chlorinated benzenes (CB and 1,2-DCB) in approximately 2:1 weight ratio (Entry **#3**).

Table 8. The results of initial experiments on model solutions of monochlorobenzene (CB), 1,2-dichlorobenzene (1,2-DCB), and their mixture.

Entry #	**commercial 50:50 wt.% alloy (Sigma-Aldrich)**				
	reaction time (min)	1,2-DCB *(µg/L)	CB (µg/L)	Al (µg/L)	% removal*
1	0	-	178,310	0	0
	5	-	34,473	29,700	61.3
	15	-	10,458	45,600	88.3
	45	-	43	115,200	99.9
	90	-	<LOD	175,400	>99.9
2	0	45,310	0	0	0
	5	19,360	28	25,400	14.5
	15	12,070	70	50,600	24.7
	45	7,784	119	105,900	65.6
	90	1,563	209	163,200	96.6
3	0	29,040	13,000	0	0
	5	8,565	4,713	22,900	27.5
	15	7,051	3,546	45,700	45.5
	45	5,407	2,601	98,200	60.0
	90	2,860	1,546	155,500	90.1

reaction conditions: 25 °C, 500 RPM, 100 cm^3 of stock solution + 100 cm^3 of NaOH (0.12 M) + commercial Raney Al-Ni 50:50 wt.% alloy (260 mg)
due to volatility of the compounds and measurement conditions, 5% deviation might be observed, determination of CB and DCB levels should be considered as informative-only
*4-fold lower levels of 1,2-DCB were given by the limited solubility of the compound in water.

For higher chlorinated congeners of chlorinated benzenes (hexachlorobenzene, trichlorobenzenes), please refer to paper of Hegedüs et al. [17], where a summary table for decomposition of these compounds was presented. The reactions with chlorinated benzenes undeniably confirmed that despite different chemical structures of the compounds and different number of chlorine atoms present, the HDH reaction will generally lead to one single product. This is the halogen free molecule (benzene in this case). Later on, it will be

shown that this also applies to chlorinated analogs of benzoic acids. However, due to benzene volatility (as a product of CB and DCBs degradation), uncertainty in the quantification is high and it will be biased to the sampling process and subsequent processing for analysis. Thus, the data presented here should be considered informative only and another compound (4-chlorophenol) was selected for optimization and scale up tests.

Regarding the hydrodechlorination of 4-chlorophenol (4-ClP), since the input concentrations of the compound were significantly decreased compared to CB/1,2-DCB (or less molar amount of chlorine was present), the dosage of the Al-Ni alloy was decreased to 1 g/L. Table 9 shows that the alloy was able to successfully dechlorinate all amount of 4-chlorophenol (4-ClP, determined as AOX) in 4 hours run. Since AOX parameter refers to organically bound halogen atoms, the reaction product must have been a chlorine free molecule. This was presumed to be a halogen free phenol molecule. Such reaction pathway is in accordance with previously published results. For example, Zhang et al. published dechlorination of 4-ClP using Ni/Fe bimetallic particles. However, they implemented a dosage of the metallic mixture of 5 g/L and 2.5 times lower concentration of 4-ClP solution [103]. Cu/Fe bimetallics showed even lower efficiency at 100 g/L concentration [71], which is not economically feasible. On the other hand, more promising results are obtaining with Pd or Rh based materials, but at higher material costs [8, 72]. A similar dosage of the catalyst (1 g/L) was found to 4-chlorophenol in higher amounts but at higher cost. These technologies often require multistep synthesis of the catalyst, external source of hydrogen gas, or increased temperature. These factors profoundly affect the applicability of individual catalysts and favor the application of the Raney type Al-Ni alloys for the HDH reactions in aqueous basic environment. For the initial experiment, pseudo-first kinetics rate constant was calculated to be 0.0328 min^{-1} (based on the entries **#1-6** from Table 9).

Table 9. The results of the hydrodechlorination of 4-chlorophenol 50 mg/L solution using commercial Raney Al-Ni alloy.

Entry #	**commercial 50:50 wt.% alloy (Sigma-Aldrich)**			
	reaction time (min)	AOX (mg/mL)	Removal (%)	Al (µg/L)
1	0	13.40*	0	0
2	60	1.10	91.80	135,000
3	120	0.170	98.60	185,200
4	180	0.100	99.20	210,800
5	240	0.079	99.40	238,000

reaction conditions: 25 °C, 500 RPM, 500 cm^3 of 50 mg/mL 4-chlorophenol solution + NaOH (2.96 g) + commercial Raney Al-Ni 50:50 wt.% alloy (500 mg, 1 g/L)

5.3.1.2 Hydrodechlorination of 4-chlorophenol, optimization, and scale-up

The optimization on a laboratory scale was performed on a model solution of 4-ClP (50 mg/L). The tests were carried out similarly to the experiment showed in Table 10. Dosage of the Raney Al-Ni alloy was varied along with the amount of sodium hydroxide. The molar ratio of contaminant (4-ClP) to aluminum present in the alloy varied from 4.5 up to 45. In general, using the AOX parameter as a dehalogenation efficiency parameter, the results were not as consistent as the HPLC results. Significant variability in the final values, especially for the reacted mixtures (90% removal and more) might have been caused by the interference with inorganic halides released during the HDH reaction. As for Entry **#1** in Table 10, total removal of the studied compound was expected, since a half dose of the alloy showed better results. The lowest suitable dosage of the alloy was found to be 0.5 g/L (ca 25 molar excess). While the excess of the used reagents was still high, the Al:substrate molar ratio can be considerably lowered and herein observed values were up to large extent caused by the used alloy material, limited reaction time, and set up of the experiment.

Table 10. The results of the hydrodehalogenation performed on model solution of 4-chlorophenol under various reaction conditions.

Entry #	commercial 50:50 wt.% alloy (Sigma-Aldrich)			
	alloy (g/L)	NaOH (g/L)	AOX (mg/L)	Removal (%)
1	1	4.45	1.49	89
2	0.50	2.96	0.61	96
3	0.50	2.22	1.41	89
4	0.50	1.49	2.90	79
5	0.25	1.85	12.1	11
6	0.10	0.74	10.8	20

reaction conditions: time 240 min, temp 20-23 °C, 500 RPM, 500 cm^3 of 50 mg/L 4-chlorophenol solution (equal to 13.5 mg/L AOX) + NaOH (see table) + commercial Raney Al-Ni 50:50 wt.% alloy (see table)

In the next step, 10 L reaction apparatus was designed in cooperation with ASIO, a.s. company and it was used for optimization of the HDH reaction using 4-chlorophenol as a model contaminant (Table 11). For the experiment, an overhead stirrer with a 3-blade propeller set to 1200 RPM was implemented to achieve homogenous dispersion of the alloy in the reaction mixture. The reaction kinetics was followed, evaluated, and compared to the small-scale experiment under identical reagent dosages. It is clear from Figure 34 that the reaction at small scale proceeded much faster. The pseudo-first order kinetics rate constant of 0.009 min^{-1} for 10 L scale represented two-and-half reduction in the kinetics of decomposition (0.025 min^{-1} respectively for the 0.5 L scale). The relatively low R^2-factors for the chosen

model were caused by the uncertainty in AOX parameter determination as mentioned before (R.S.D. up to 20%). For comparative purposes, measured data are provided here, as stirring is one of the most critical parameters in alike heterogeneous systems. The leached fraction of aluminum followed exponential function and reached.

Table 11. The results of 10 L scale hydrodechlorination experiment performed with an automatized station.

Entry #	commercial 50:50 wt.% alloy (Sigma-Aldrich)			
	reaction time (min)	AOX (mg/mL)	Removal (%)	Al (µg/L)
1	0	13.00	0	0
2	120	2.71	79	137,000
3	240	1.46	89	186,200
4	360	0.75	91	220,800
5	720	0.10	98	229,600

reaction conditions: temp 20 °C, 1200 RPM (mechanical stirring), 10 dm^3 of 50 mg/mL 4-chlorophenol solution (equal to 13.5 mg/L AOX) + NaOH (44.5 g,) + commercial Raney Al-Ni 50:50 wt.% alloy (10 g, 1g/L)

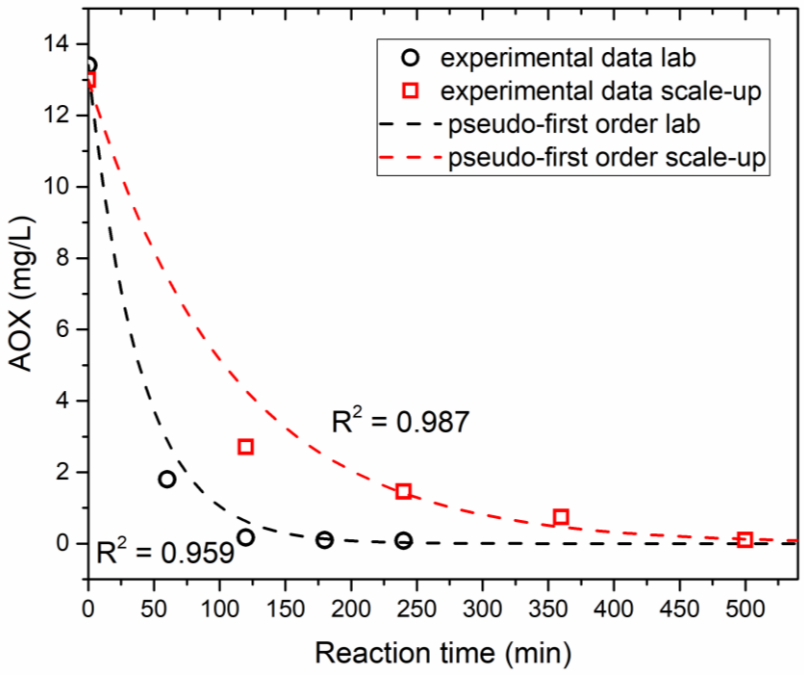

Figure 34. Comparison of the hydrodehalogenation of 4-chlorophenol (4-ClP) at 0.5 L scale and 10 L scale under the same experimental conditions, except for stirring utilized.

5.3.1.3 Hydrodehalogenation of chlorinated benzenes in real wastewater, optimization, and scale up

The applicability of the HDH technology based on the reduction with the Al-Ni alloys in a basic environment is largely dependent on its reducing power in the real conditions. Real waste- or groundwater samples main contain, besides the halogenated pollutants, a wide range of ions and other compounds - all these species may potentially act as competing substrates or catalytic poisons. To prove the high potential of the technology, laboratory experiments on model samples were transferred to the real groundwater samples. The samples of water were obtained from the area of the unnamed Czech industrial factory where the groundwater was found to be highly contaminated with chlorobenzene and dichlorobenzenes. A few runs to test optimal dosages of the reagents are given in Table 12. Clearly, an alloy concentration of 1 g/L showed the best results, with 5-fold reduction in AOX parameter and close to 98% removal of chlorinated benzenes. Varying the concentration of sodium hydroxide in an acceptable range showed no further increase in aluminum leaching or increased removal efficiency. The promising laboratory-scale results led to a design of pilot-scale on-site application of the HDH technology.

Table 12. The hydrodechlorination of the chlorinated benzenes in real groundwater sample (continuation on the next page).

Entry#	**commercial 50:50 wt.% alloy (Sigma-Aldrich)**				
	reaction time (min)	CB (µg/L)	1,2-DCB (µg/L)	1,3-DCB (µg/L)	1,4-DCB (µg/L)
	0	1,296	3,592	308	456
1	60	1,151	3,263	266	395
	120	1,174	3,205	268	390
	180	1,028	2,905	244	353
	240	970	2,832	221	332
	Al (mg/L) = 3; AOX (mg/L) = 2.30; benzene (µg/L) = 62				
2	60	1,158	2,202	187	288
	120	719	1,981	170	266
	180	599	1,885	158	246
	240	584	1,731	145	226
	Al (mg/L) = 49; AOX (mg/L) = 1.60; benzene (µg/L) = 892				
3	60	553	1,812	154	244
	120	348	1,194	109	178
	180	157	649	62	103
	240	145	605	58	100
	Al (mg/L) = 117; AOX (mg/L) = 0.88; benzene (µg/L) = 1512				
4	60	215	776	76	132
	120	120	535	48	88
	180	45.2	266	22	43

	240	14.9	85	11	23
	Al (mg/L) = 209; AOX (mg/L) = 0.50; benzene (µg/L) = 1834				

reaction conditions: temp 25 °C, 400 RPM (magnetic stirring), 1 dm^3 of fresh real groundwater sample
reagent dosage: #1 = 0.1 g/L Raney Al-Ni 50:50 wt.% alloy + 0.3 g/L NaOH, #2 = 0.25 g/L Raney Al-Ni 50:50 wt.% alloy + 0.74 g/L NaOH, #3 = 0.5 g/L Raney Al-Ni 50:50 wt.% alloy + 1.48 g/L NaOH, #4 = 1 g/L Raney Al-Ni 50:50 wt.% alloy + 2.97 g/L NaOH.

The pilot application was performed in the area of the unnamed Czech industrial factory, where the groundwater is highly contaminated by chlorobenzene and dichlorobenzenes. This contamination is the result of leaks from tanks of a former warehouse of chlorinated benzenes historically placed on the site. The warehouse with the tanks has been removed, but the groundwater contamination persists. The area has the status of an old ecological burden. For a more complex evaluation of the performed experiment, full physico-chemical parameters were determined for each water sample. Selected parameters (CBs, BTEX, AOX, aluminum, nickel, and sulfate levels) are given in Tables 13 and 14. The alloy dosage of 0.5 g/L, molar $Al:OH^-$ ratio of 1:2, and the reaction time of 8 hours was selected for the experiment; following up previous laboratory results [17].

Table 13. The evolution of contaminants levels during an on-site pilot application (October, 2020).

Reaction time (h)	Contamination levels (µg/L)					
	CB	1,2-DCB	1,3-DCB	1,4-DCB	B	toluene
0	5,774	23,970	3,548	4,993	31	39,825
1	2,332	9,342	1,298	1,937	1,691	36,400
2	1,025	4,054	544	795	1,753	33,520
4	405	1,806	258	380	1,215	30,650
6	139	761	99	147	568	17,350
8	53	329	41	61	236	7,278
neutralized	40	253	30	45	163	5,095

Table 14. Evolution of metal leaching and sulfate content in analyzed samples of real wastewater.

Reaction time (h)	Contamination levels				
	AOX	Al (µg/L/)	Ni (µg/L/)	SO_4^{2-} (mg/L)	pH
0	7.4	119	37.7 (<0.01)	52.5	5.84
1	5.6	27,700 (11)	2.1 (<0.01)	53.1	12.51
2	4	40,500 (16.2)	1.86 (<0.01)	83	12.56
4	3.6	63,500 (25.4)	1.74 (<0.01)	61.8	12.58
6	3.4	82,500 (33)	3.00 (<0.01)	53.8	12.59
8	3.1	90,200 (36.1)	2.24 (<0.01)	70.1	12.60
neutralized	3	46.4 (<0.01)	1300(<0.01)	5,880	6.84

Some of the physico-chemical parameters were measured during the experiment in-situ to examine the reaction course in more detail. The change of the pH value in Vessel No. 1 (the reaction vessel) in the very beginning is caused by pH adjustment and the addition of an equivalent amount of sodium hydroxide for the hydrodehalogenation reaction. Adding the reagent led to a slight increase in temperature which is in general favorable for the aluminum leaching and thus for the hydrodehalogenation process. The alloy was added simultaneously along with sodium hydroxide. As hydrogen gas started to evolve, a drop in the ORP parameter (Figure 35a) and another temperature rise was observed. After reaching the minimum ORP value of -450 mV at 3:30 hours, the parameter slowly began to rise again (less negative values). This is in accordance with decreasing leaching rate of aluminum. As the excess of sodium hydroxide was used, the pH value stayed almost constant. The sharp peak appearing in Figure 35 (gray line) is connected to the transfer of the treated water to the Vessel No. 2 (neutralization vessel) and immediate neutralization by sulfuric acid. The total temperature rise may be a due to a combination of two factors – exothermic character of the process and an increase in outside temperature during daytime (maximum temp. recorded on 10/15/2019 was 21.1 °C at the location).

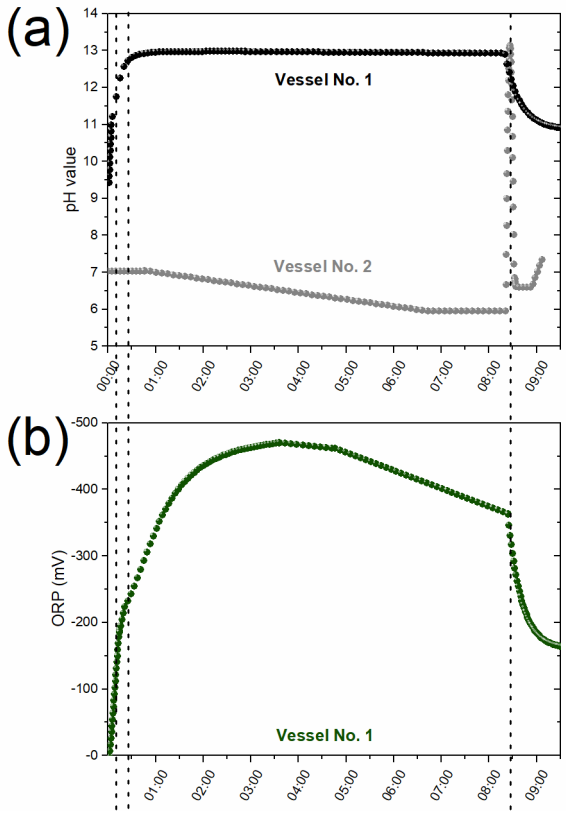

Figure 35. The evolution of selected physical parameters, pH (a) and ORP (b), during an on-site pilot application of the HDH technology in the real wastewater.

5.3.2 Mechanically activated Al-Ni mixtures and their thermally processed analogues

Following the previous paragraphs discussing the robustness of the HDH technology, newly prepared materials from the Al-Ni system (ball-milled bimetallic mixtures) were applied for the HDH of the same model compounds – monochlorobenzene, 1,2-dichlorobenzene, and 4-chlorophenol. Because bimetallic metal couples have shown potential for reductive dehalogenation, the removal power of ball-milled Al-Ni samples was evaluated before thermal treatment as well. The results for the dehalogenation of the studied compounds are summarized in Tables 15, 16, and 17. The efficiency of the material prepared by combined approach (milling and annealing) was tested on the same model solutions as in the case of activated metal mixtures. Due to limited analytical support at the time, the results were compared with the data provided in previous paragraphs for the commercial Al-Ni 50:50 wt.% alloy and were not repeated. Nevertheless, the input levels of contaminants were of the same order and thus the data were considered comparable (namely for 1,2-DCB).

From gathered data several important observations were made. Monochlorobenzene could be removed easily by the mechano-thermally prepared material within 45 minutes and the kinetics of decomposition (k = 0.1623 min^{-1}) is close to that of the commercial alloy (k = 0.1784 min^{-1}). Bimetallic, ball-milled mixtures, showed also progressive removal of the pollutant (Table 15, Entry **#1**). Due to the highly volatile nature of the compound and strong effervescence of hydrogen gas, it could not be decided whether the bimetallic couple solely promoted the hydrodehalogenation (benzene was not determined for the reaction mixtures). The puzzle was solved when we applied the materials for the HDH of 1,2-DCB. In Table 16, for the ball-milled mixture, a significant amount of monochloro derivate (CB) was detected.

Therefore, based on the presence of the intermediate, the bimetallic Al-Ni couple (as determined by XRPD) is able to reduce halogenated compounds. Nevertheless, the reaction of nanocrystalline ball-milled particles is rapid and most of the hydrogen gas is not utilized, which eventually led to the interruption of the process (removal of 44% 1,2-DCB). Even though the removal of 1,2-DCB is a two-step process (via monochloro derivate), the removal of almost 99% was achieved with the mechano-thermally prepared alloy material after 45 min (k = 0.1671 min^{-1}), which is 30% more than in the case of the commercial 50:50 wt.% Al-Ni alloy. This fact is closely connected to the dissolution rate of aluminum during the experiment and it is affected by the average particle size and phase composition of the alloy material. What appeared to be suspicious is the kinetic rate constant for 1,2-DCB decomposition. It was comparable to that of monochlorobenzene (Figure 36). It could have been caused by a poorly homogenized first batch of the mechano-thermally prepared material.

Table 15. Dehalogenation of CB using mechanochemically prepared Al-Ni powder and the commercial 50:50 Al-Ni wt.% alloy.

Entry #	sample	mechanically activated (90 mins)		
	reaction time (min)	CB (µg/L)	Al (µg/L)	% removal
1	0	178,310	0	0
	5	46,763	430,000	47.6
	15	23,783	454,600	73.3
	45	10,458	478,800	88.3
	sample	mechano-thermally prepared		
2	0	184,680	0	0
	5	66,360	46,800	64.1
	15	23,348	125,000	87.4
	45	116	265,000	99.9
	sample	commercial (Sigma-Aldrich)		
3	0	178,310	0	0
	5	34,473	29,700	61.3
	15	10,458	45,600	88.3
	45	43	115,200	99.9

reaction conditions: 25 °C, 500 RPM, 100 cm^3 of aqueous CB solution (1.5 mmol) + 100 cm^3 of NaOH (0.12 M) + Al-Ni (260 mg)

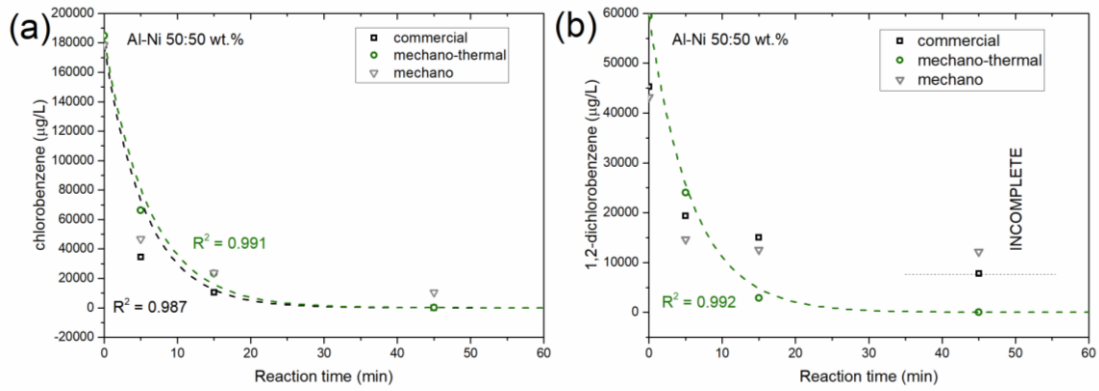

Figure 36. Comparison of decomposition kinetics for monochlorobenzene (a) and 1,2-dichlorobenzene (b) between ball-milled Al-Ni mixture, thermally treated mixture, and the commercial 50:50 wt.% alloy.

Finally, the ball milled mixture was tested against alloy materials for decomposition of 4-chlorophenol. Since 4-chlorophenol is non-volatile substance, the result in Table 17, Entry 1 supported our previous observation with 1,2-DCB. While relatively low efficiency was achieved for the ball-milled metal mixture (accounted for high excess of reagents), the reaction progressed in time and removal reached 30% after 6 hours. For mechano-thermally prepared alloy material and the commercial 50:50 Al-Ni wt.% alloy, removal reached around 90% within the same time frame.

Table 16. Dehalogenation of 1,2-DCB using mechanochemically prepared Al-Ni powders and the commercial Al-Ni 50:50 wt% alloy.

sample	mechanically activated (90 mins)			
reaction time (min)	1,2-DCB (µg/L)	CB (µg/L)	Al (µg/L)	% removal
0	43,190	0	0	0
5	14,640	459	386,400	32.21
15	12,560	628	431,200	41.83
45	12,170	696	460,100	43.64
sample	mechano-thermally prepared alloy			
0	59,410	0	0	0
5	24,040	24	52,000	59.52
15	2,868	56	132,000	95.17
45	794	30	221,000	98.66
sample	commercial (Sigma-Aldrich)			
0	45,310	0	0	0
5	19,360	28	25,400	14.54
15	15,070	70	50,600	24.69
45	7,784	119	105,900	65.64

reaction conditions: 25 °C, 500 RPM, 100 cm^3 of aqueous solution 1,2-DCB (0.3 mmol) + 100 cm^3 of NaOH (0.12 M) + Al-Ni (260 mg)

The pseudo-first kinetic constants could be determined and the values favored the mechano-thermally prepared alloy. The kinetic rate constant (k = 0.0076 min^{-1}) was comparably higher to that of the commercial alloy (k = 0.0046 min^{-1}), opposite to the data calculated for CB decomposition. We hypothesize that due to easy removal of ClBs, leaching kinetics differences between the materials was not a significant factor. Whereas, for 4-chlorophenol, which in general shows much slower kinetics of dehalogenation under the same conditions, we could spot dominant properties of mechano-thermally prepared material. Although the reactions did not reach 100% removal after 6 hours of the reaction time, we note that significantly milder conditions were applied than in previous experiments (see Table 8 for comparison of the reaction conditions). Based upon this observation and estimated deviation of AOX parameter deviation, the reaction can be considered to be complete at over 90% determined efficiency.

A brief comparison of the three materials under investigation gave a hint for their potential applicability. While for the commercial Al-Ni 50:50 wt.% alloy was already proven a powerful reducing reagent (under different conditions and for various samples contaminated with chlorinated aromatics), now it was demonstrated that simply prepared ball-milled Al-Ni mixtures can also provide partial dehalogenation. A rapid reaction of aluminum with hydroxyl ions is however not feasible, especially in the case of hardly removable pollutants. Because of

this, thermally unprocessed were removed from the experimental design. The mechano-thermally prepared material of the same elemental composition (50:50 wt.% Al-Ni), showed superior properties compared to the commercial alloy. Subsequently, the next chapter was devoted to this material. The alloy with different wt.% Al-Ni composition was prepared and tested as well (see Chapter 4.2).

Table 17. Dehalogenation of 4-ClP using mechanochemically prepared Al-Ni powders and the commercial Al-Ni 50:50 wt.% alloy.

sample	mechanically activated (90 min)*	
reaction time (min)	AOX (mg/L)	% removal
0	13.50	0
120	12.20	9.6
240	10.40	23.0
360	9.54	29.3
sample	mechano-thermally prepared alloy	
0	13.3	0
120	5.98	55.0
240	2.6	80.5
360	0.85	93.6
sample	commercial (Sigma-Aldrich GEOtest)	
0	13.30	0
120	7.91	40.5
240	4.93	62.9
360	1.81	86.4

reaction conditions: 25°C, 500 RPM, 500 cm^3 of aqueous solution of 4-chlorophenol (0.4 mmol) + NaOH (0.05 mol) + Al-Ni (260 mg)
*for the tests, mechanically activated mixture of Al-Ni (50:50 wt.%) was prepared using lower amount of surfactant (methanol, 2.5%) in order to increase particle size and achieve slower dissolution of aluminum

5.3.3 Mechano-thermally prepared alloys as hydrodehalogenation reagents

To further explore dehalogenation properties of the prepared alloy materials, chlorobenzoic acids and their derivate were chosen as non-volatile, moderately soluble, substances with good HPLC detectability. The most of the reactions were performed on 1 mM model aqueous solution. This represents hundreds of milligrams of pollutants per liter of solution. The concentration range lies in the solubility region for the substances in distilled water. All of the reactions were carried out at normal conditions (atmospheric pressure and ambient temperature) in basic environment of sodium hydroxide; as an optimal leaching agent. The sodium hydroxide dilute solutions (0.5-1 wt.%) were found to produce the environment with the pH levels well above 12.5, which secures high aluminum solubility and enough OH^- anions for the reaction with aluminum. The general scheme for decomposition of chlorinated benzoic acids is shown below (Figure 37).

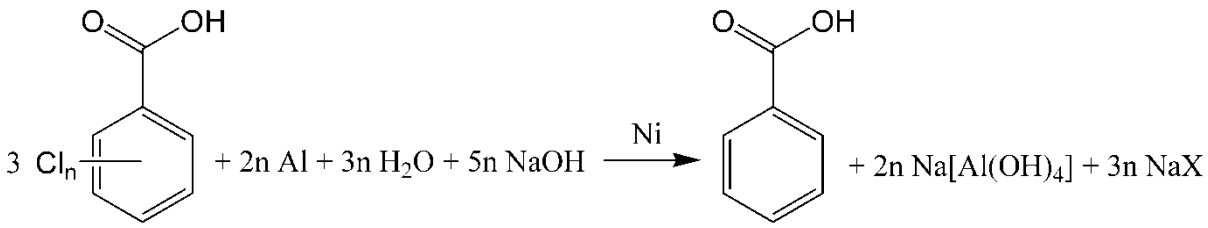

Figure 37. general scheme for dehalogenation of chlorobenzoic acids with the Al-Ni alloys in basic environment of sodium hydroxide.

First, decomposition of the simplest chlorinated derivate of benzoic acid (2-chlorobenzoic acid) was explored. The results were compared to those of commercially available Al-Ni alloys of the same Al-Ni wt.% compositions (Table 18). 2-chlorobenzoic acid (2-CBA) was easily dechlorinated under studied conditions and benzoic acid as the only product was determined by HPLC in the reaction mixtures. The amount of alloy needed for conversion of over 90% for the pollutant was 0.8 g/L (15 mol eq.) in the case of 50:50 wt.% alloys and 0.4 g/L (9 mol eq.) for 58:42 wt.% alloys. The often considered molar ratio of Al vs. contaminant, for the HDH reaction, typically lies in the range of 1-10. For lower dosages, even after 5 hours of stirring, the mixtures of benzoic acid with unreacted 2-chlorobenzoate formed. When the reaction time was increased, no further reaction progress was observed. The observed difference in efficiency can be unambiguously assigned to the leachability of aluminum from alloys materials. On average, around 25% more aluminum could be leached from mechano-thermally prepared alloys of 50:50 wt.% Al-Ni composition. Al-rich alloys, mainly consisting of Al_3Ni phase, showed difference of only 5% in aluminum leachability.

Better leachability of mechano-thermally alloys, in general, was also promoted by higher surfaces areas and considerably smaller crystallite size. The leachable fraction of aluminum is connected to the mass of evolved hydrogen gas utilized in the HDH reaction.

This finding is in a good match with previously reported data on leaching of the two intermetallic phases [57, 80]. It is noteworthy however that the aluminum solubility is limited in aqueous solutions and highly dependent on the pH level. In a few cases precipitation of insoluble $Al(OH)_3$ phase took place when 58.42 wt.% alloy was utilized. $Al(OH)_3$ precipitate in general acts as the HDH reaction inhibitor by the "glueing" of the alloy particles. Therefore, maintaining pH over 12 is crucial for fast and complete progress of the HDH reactions.

According to the measured kinetics data and the results obtained from experiments shown in Table 18, an important finding was made. Comparing entries **#4-5** ad **#6-7** from Table 18, half the amount of alloy resulted in incomplete degradation of 2-CBA. Whereas 0.8 g/L dose of 50:50 wt.% Al-Ni mechano-thermal alloy was found to fully dechlorinate also 2,6-dichloro (Figure 38c). Recalculated for the molar amount of halogen atoms removed from aromatics, this results in four time higher efficiency by doubling the initial dose of the alloy. For the reaction to reach the completion there is a minimum amount of the alloy that must be utilized. It does not, however, reflect maximum molar number of halogen atoms removed during the reaction. The observed dependence can be explained simply by considering not only the fraction of aluminum leached but also the available catalyst surface for the reaction.

The kinetics of the decomposition was determined at a fixed reagent dosage (0.8 g/L alloy and 1 g/L of NaOH). The kinetics was evaluated based on the pseudo-1st order reaction model (Figure 38) shown below. The chosen model provides a good approximation to the second order kinetics because an excess of the reacting species compared to the studied chlorobenzoates is assumed during the whole reaction time.

$$\frac{d[A]}{dt} = -k[A][B] \; where \; [B]_0 \gg [A]_0 \; therefore \; [B]_0 \cong [B]$$

$$[A] = [A]_0 e^{-k.t}$$

The degradation of 2-chlorobenzoic acid (2-CBA) was considerably faster in favor of the 58:42 wt.% Al-Ni alloy (both the commercial and mechano-thermally prepared materials). Using the mechano-thermally product, regardless of their elemental composition, close to full

degradation was achieved in under 3 hours of the reaction time. The short reaction times are highly beneficial for the water treatment application as more contaminated wastewater could be cleaned per time unit.

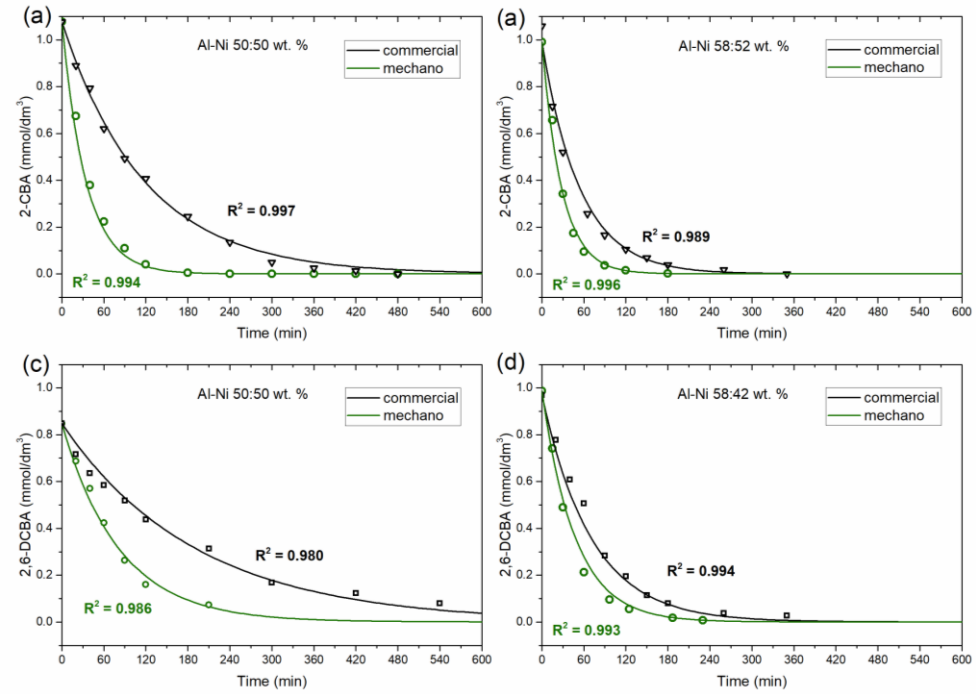

Figure 38. Decomposition kinetics of 2-CBA (a, b) and 2,6-DCBA (c, d) by mechano-thermally prepared alloys of two Al-Ni alloys with different wt.% composition under identical reaction conditions (compared with their commercially available analogs).

For degradation of 2,6-dichlorobenzoic acid (2,6-DCBA), a similar trend was observed. Higher efficiency was obtained for the 58:42 wt.% Al-Ni alloy materials. Here, the minimum amount of alloy needed for decomposition of contaminant favored the mechano-thermally prepared alloy. At 0.4 g/L dosage, it could remove over 98% of 2,6-DCBA during 5 hour run (191 mg of 2,6-DCBA/1 L). Other materials needed at least 0.8 g/L alloy dosage to reach the same removal efficiency. Nevertheless, the concentration levels shown within this thesis are much higher than the ones usually investigated [81-84, 103-104].

Table 18. The results for hydrodechlorination of 2-chlorobenzoic acid (2-CBA) in aqueous solution (1 mmol/dm^3) with the studied alloy materials.

alloy (mg)	NaOH (mg)	molar ratio Cl:Al:OH^-	Entry #	commercial Raney Al-Ni 50:50 wt.%		Entry #	mechano-thermal Al-Ni 50:50 wt.%	
				removal	Al leached (mg/L)		removal	Al leached (mg/L)
270	400	1 : 47 : 100	**1**	>99%	690	**9**	>99%	1045
135	400	1 : 23: 100	**2**	99%	350	**10**	>99%	553
135	200	1 : 23 : 50	**3**	97%	319	**11**	>99%	533
80	200	1 : 14 : 50	**4**	97%	201	**12**	>99%	350
80	100	1 : 14 : 25	**5**	94%	189	**13**	>99%	313
40	100	1 : 7 : 25	**6**	66%	104	**14**	>99%	168
40	50	1 : 7 : 12.5	**7**	55%	86	**15**	97%	153
20	50	1 : 3.5 : 12.5	**8**	26%	57	**16**	72%	88
				commercial Raney Al-Ni 58:42 wt.%			mechano-thermal Al-Ni 58:42 wt.%	
80	200	1 : 17 : 50	**17**	>99%	421	**22**	>99%	396
80	100	1 : 17 : 25	**18**	>99%	378	**23**	>99%	375
40	100	1 : 9 : 25	**19**	83%	224	**24**	97%	211
40	50	1 : 9 : 12.5	**20**	91%	210	**25**	98%	194
20	50	1 : 4 : 12.5	**21**	55%	135	**26**	70%	106

reaction conditions: 100 mL of ca 1 mM aqueous solution of 2-CBA + powder alloy + solid NaOH, 25 °C, 1 atm, 300 RPM, reaction time 5 hrs. Higher dosages of 58:42 wt.% were excluded due to reproducible high removal efficiency at <0.8 g/L.

Table 19. The results for hydrodechlorination of 2,6-dichlorobenzoic acid (2,6-DCBA) in aqueous solution (1 mmol/dm^3) with the studied alloy materials.

alloy (mg)	NaOH (mg)	molar ratio Cl:Al:OH^-	Entry #	commercial Al-Ni 50:50 wt.%	Entry #	mechano-thermal Al-Ni 50:50 wt.%	Entry #	commercial Al-Ni 58:42 wt.%	Entry #	mechano-thermal Al-Ni 58:42 wt.%
			removal efficiency							
270	400	1 : 47/58 : 100	**1**	>99%	**9**	>99%	**17**	n.p.	**25**	n.p.
135	400	1 : 23/29: 100	**2**	90%	**10**	>99%	**18**	n.p.	**26**	n.p.
135	200	1 : 23/29 : 50	**3**	90%	**11**	>99%	**19**	n.p.	**27**	n.p.
80	200	1 : 14/17 : 50	**4**	86%	**12**	>99%	**20**	>99%	**28**	>99%
80	100	1 : 14/17: 25	**5**	84%	**13**	99%	**21**	>99%	**29**	>99%
40	100	1 : 7/9 : 25	**6**	59%	**14**	83%	**22**	83%	**30**	97%
40	50	1 : 7/9 : 25	**7**	51%	**15**	79%	**23**	91%	**31**	98%
20	50	1 : 3.5/4 : 25	**8**	37%	**16**	30%	**24**	55%	**32**	70%

reaction conditions: 100 mL of ca 1 mM aqueous solution of 2,6-DCBA + powder alloy + solid NaOH, 25 °C, 1 atm, 300 RPM, reaction time 5 hrs, n.p. = not performed, Al quantities are expected to be close to that in Table 18 and were not determined. Cl:Al:OH- molar ratios are given for 50:50 wt.% and 58:42 wt.% alloy, respectively.

If the concentration levels of the contaminants were increased 10-fold (10 mmol per dm^3), after overnight mixing (Table 20), the same dosages of alloy (0.8 g/L) were sufficient to dehalogenate almost all amount of the present 2-CBA (ca 97-98%). This represents a significant reduction and is caused more like by the principles of heterogeneous catalysis (the probability of bimolecular reaction) than the amount of leached aluminum from the alloy. In concentrated solutions, the hydrogen gas evolved is being utilized more effectively for the HDH reaction. Comparing the found minimum molar excess for the successful HDH reaction with the reaction stoichiometry, at least 2 times molar excess was needed to complete the removal of chlorobenzoic acids. The molar excess determined within the present work in accordance with the previously published results and can be taken as a rule of thumb for the HDH of Ar-X contaminants. Surprisingly, the phase composition of the used mechano-thermally prepare materials revealed that for 2,6-DCBA at higher concentration levels, utilization of the 50:50 wt.% Al-Ni alloy provides higher removal. The phase composition and the kinetics of 2,6-DCBA (ca. two times slower compared to 2-CBA) can explain this observation. While observed decomposition rate is higher for 58:42 wt.% Al-Ni alloy, the aluminum leaching rate is rapid. In case of incomplete conversion (Table 20, Entries **#16-18** and **#22-24**), 50:50 wt.% Al-Ni composition, can in the end provide more hydrogen for the reaction in the course of 17 hours due to slower aluminum leaching.

Table 20. Application of mechano-thermally prepared alloys for decomposition of 10 mM solutions.

alloy (mg, mmol Al)	NaOH (mg)	mechano-thermal alloys			
		Entry #	50:50 wt.%	Entry #	58:42 wt.%
			removal		removal
270 (4.66)	400	**1**	>99%	**7**	>99%
135 (2.33)	400	**2**	>99%	**8**	>99%
135 (2.33)	200	**3**	>99%	**9**	>99%
80 (1.38)	200	**4**	97%	**10**	81%
80 (1.38)	100	**5**	98%	**11**	97%
40 (0.69)	100	**6**	41%	**12**	45%
			removal		removal
270 (4.66)	400	**13**	>99%	**19**	>99%
135 (2.33)	400	**14**	90%	**20**	92%
135 (2.33)	200	**15**	90%	**21**	90%
80 (1.38)	200	**16**	86%	**22**	51%
80 (1.38)	100	**17**	84%	**23**	57%
40 (0.69)	100	**18**	59%	**24**	25%

*entries 1-12 correspond to 2-CBA, entries 13-24 to 2,6-DCBA, reaction conditions identical with experiments in Table 18.

Due to their submicronic character, mechano-thermally prepared materials showed superior dehalogenation properties, other bases were tested as well. For example, calcium hydroxide and sodium salt of ethylenediaminotetraacetic acid showed good HDH efficiency before [12, 13]. The results for fixed alloys dosage of 0.8 g/L are listed in Table 21. The test of various bases gives a clear overview about the system and its behavior. Calcium hydroxide used as a leaching reagent provided complete dechlorination in the course of 20 hours with significantly smaller fraction of leached aluminum (0-70 mg/L). The efficiency comparable to that of sodium hydroxide is given by the pH levels securing solubility of the aluminum specimen. The reaction runs better in more diluted $Ca(OH)_2$ suspension (Figure 39a). At higher dosages, hydrocalumite $Ca_2Al(OH)_6 \bullet 3(H_2O)$ was found to precipitate out form the suspensions. The reaction kinetics is however limited by the very low water solubility of $Ca(OH)_2$.

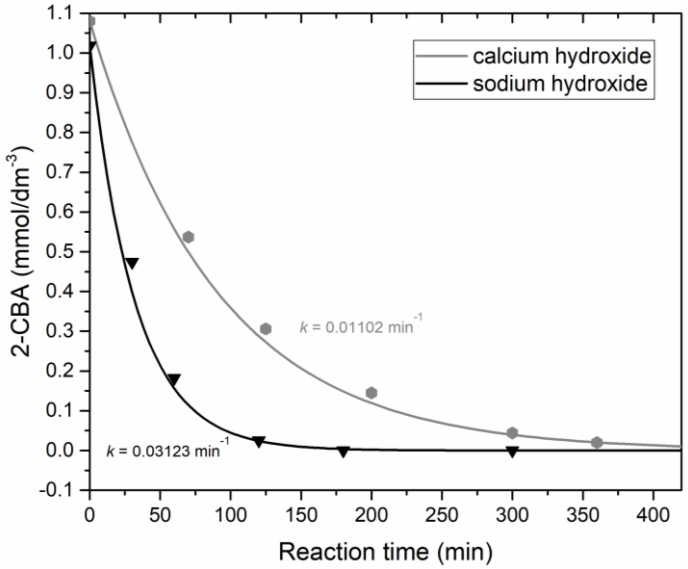

Figure 39. Comparison of the decomposition kinetics $Ca(OH)_2$ vs. NaOH studied at the same alloy dosage.

Surprisingly, utilization of potassium carbonate in the case of aluminum-rich alloy (58:42 wt.%) provided 100% removal even at lower pH levels (around 10.5). Compared to $Ca(OH)_2$, K_2CO_3 has 10x higher solubility in water and is able to promote the reaction via the following equilibrium

$$CO_3^{2-} + H_2O \leftrightarrow HCO_3^- + OH^-$$

The lowest efficiency was observed for ammonium hydroxide, which also showed the lowest values of pH and the precipitation of $Al(OH)_3$. Experiments including NH_4OH also showed great variability in total removal (by 40-50%), probably due to its volatile nature.

While complexing agents, such as herein used EDTA provides reasonable efficiency at higher dosages, their utilization is mostly precluded by slow leaching of nickel metal as detected by visual inspection (the solutions have slightly blueish color) and ICP-OES measurement (conc. over 50 mg/L). Due to the complexing effect of similar compounds, this would result in carcinogenic Ni^{2+} ions leaching into the water, which makes their use improper for water treatment applications.

In comparison, utilization of various bases at higher concentration level of 2-CBA (10 $mmol/dm^{-3}$) was verified. An observed decrease in the total removal was significant. The removal of 2-CBA at 10 $mmol/dm^3$ concentration did not proceed more than 50% at 0.8 g/L alloy dosage for $Ca(OH)_2$, whereas it was considered complete when NaOH was used as a base. For other bases, efficiency of only up to 40% was obtained. Here, the limited aluminum leachability is clearly the limitation.

The obtained data led to a conclusion that the decomposition of chlorinated contaminants in the environments with not sufficiently high pH or with bases, which extracts nickel, is not feasible. For most of the bases, after 17 hours reaction time, precipitation of aluminum hydroxide (Figure 40a) appeared. Once $Al(OH)_3$ precipitates, it hinders the hydrodehalogenation reaction due to its crystals growing on alloy´s particles. For further HDH tests, minimal attention was paid to the application of other bases for the HDH reaction.

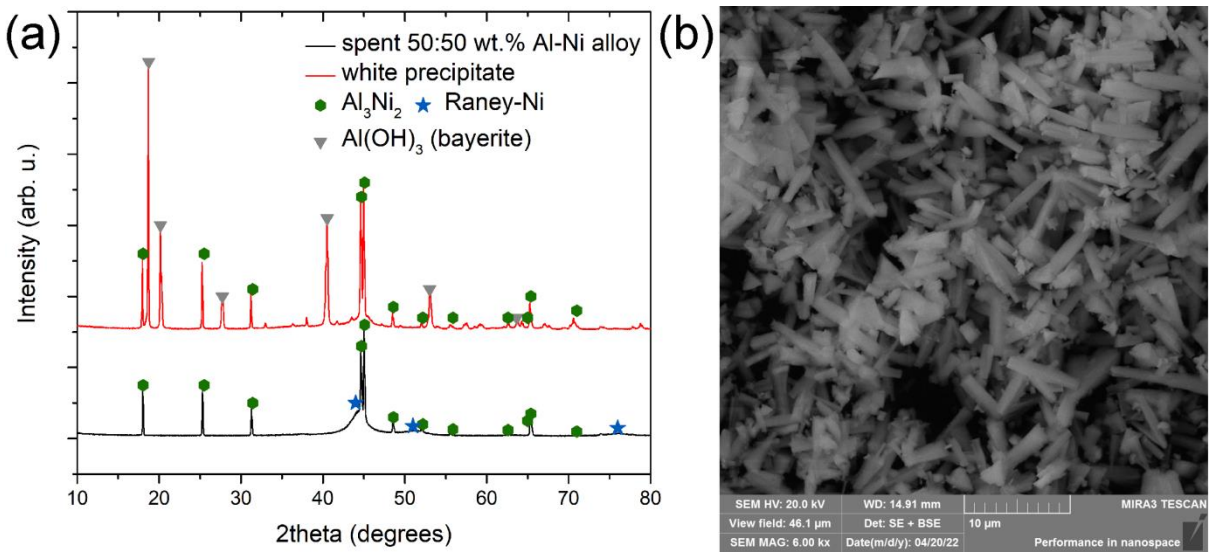

Figure 40. The XRPD pattern of the precipitated $Al(OH)_3$ phase (bayerite) (a) along with the SEM image of formed crystals (b).

Table 21. Utilization of various bases for hydrodehalogenation of 2-chlorobenzoic acid and 2,6-dichlorobenzoic with mechano-thermally prepared alloy materials.

			2-chlorobenzoic acid				2,6-dichlorobenzoic acid			
base	base (mg)	molar ratio CBA:base	Entry #	mechano-thermal Al-Ni 50:50 wt.%	Entry #	mechano-thermal Al-Ni 58:42 wt.%	Entry #	mechano-thermal Al-Ni 50:50 wt.%	Entry #	mechano-thermal Al-Ni 58:42 wt.%
				removal		removal		removal		removal
$Ca(OH)_2$	185	25	**1**	>99%	**9**	98%	**17**	53%	**25**	64%
$Ca(OH)_2$	375	50	**2**	89%	**10**	98%	**18**	70%	**26**	78%
K_2CO_3	265	25	**3**	53%	**11**	>99%	**19**	62%	**27**	70%
K_2CO_3	530	50	**4**	72%	**12**	>99%	**20**	67%	**28**	72%
NH_4OH	0.375	50	**5**	54%	**13**	20%	**21**	34%	**29**	39%
NH_4OH	0.198	25	**6**	21%	**14**	21%	**22**	30%	**30**	35%
Na_4EDTA	460	25	**7**	68%	**15**	68%	**23**	54%	**31**	60%
Na_4EDTA	980	50	**8**	85%	**16**	>99%	**24**	47%	**32**	62%

reaction conditions: 100 mL of ca 1 mM aqueous solution of CBA + fixed alloy dosage of 0.8 g/L (performed at fixed CBA:Al molar ratio of 1:14 (50:50 wt.% alloy) or 1:17 (58:42 wt.% alloy) + solid NaOH, 25 °C, 1 atm, 300 RPM, reaction time 20 hrs

When the efficiency of the removal of 2-CBA and 2,6-DCBA was verified, 2,3,6-trichlorobenzoic acid (2,3,6-TCBA) was inspected. The molecule is also known as *trysben*, which was commercially sold and used as a pesticide. The molecule of trysben contains three atoms of chlorine per molecule and its hydrogen demand is three-fold compared to its monochlorinated analogue. The position of chlorine atoms on benzene ring respective to carboxylic group may alter the decomposition. The compound can be degraded but at considerably lower reaction rates. In this case, the superiority of the mechano-thermally prepared alloy material was pronounced. A dosage of the alloy of 0.8 g/L was the lowest amount capable of decomposing a chlorine-rich benzoic acid, with the kinetic rate constant of 0.01215 min^{-1}. The commercial product failed to provide full dechlorination under the same reaction conditions. The dosage of the alloy was increased 0.135 g/L and followed the decomposition. At this reagent dosage, it followed approximately the kinetics studied with the mechano-thermally prepared alloy material. Due to the limited supply of reagents, 58:42 wt.% alloys were not applied for the studied pesticides. In the end, it was shown that particularly for higher concentrations of pollutants, containing several chlorine atoms, fast leaching of aluminum from the alloy becomes a disadvantage.

Except for 2,3,6-TCBA, a mixture of 2,3,6-TCBA with other trichlorobenzoic acids isomers (technical grade quality) was obtained from the supplier. At the time, analytical standards for the quantification of each compound were not available. Decomposition was evaluated in a sum (assuming similar absorption coefficients). The results were similar to that of pure compound with 0.8 g/L of alloy leading to close-to-complete dehalogenation.

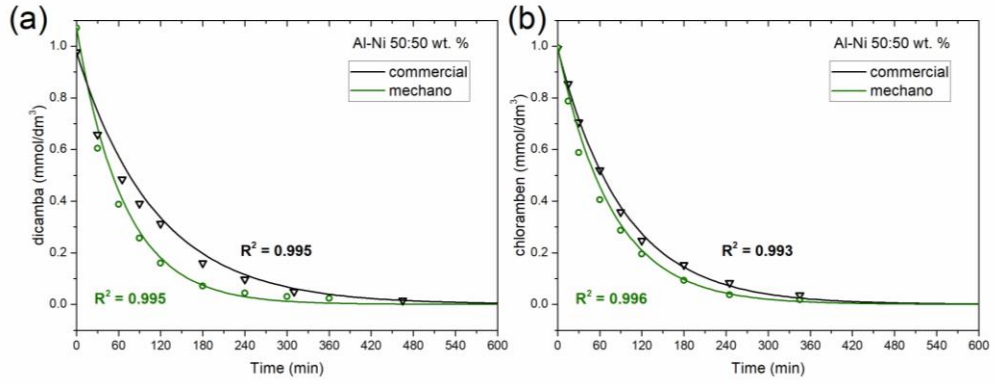

Figure 41. The decomposition kinetics of *dicamba* and *chloramben* under identical conditions (0.135 g/L 50:50 wt.% Al-Ni alloy + 2 g/L NaOH).

Two other studied analogs (*dicamba* and *chloramben*), containing only two chlorine atoms in different positions) provided good removal rates and acceptable reagent dosing (Table 23). The decomposition curves for chlorobenzoic benzoic acids derivates are given in Figure 42. The observed difference lies mostly in a number of halogen atoms bound to the aromatic benzene ring. There was no significant deviation among any of the studied compound. Removal rates were similar to that of 2,6-DCBA and are very favorable for applications. The conclusion is that while structural aspects may play a role in the reaction kinetics, for derivates containing only one type of halogen, the removal rates will be alike and depend more on a number of halogen-bound atoms. The observed removal rates for all studied compounds herein showed similar values to catalyst based on supported-Pd/Pt. We presume direct reduction of the compounds into their non-halogenated analogs. However, especially for *chloramben*, we were not able to spot it on HPLC. The product of dehalogenation was detected in dead-time. Also, for *dicamba*, we noticed that two HPLC peaks were always detected in chromatograms. Additional HPLC-MS analysis did not solve the puzzle. We consider inability to assign the reaction products to be a minor drawback, since for HDH reaction the formation of unwanted halogenated by-products is improbable.

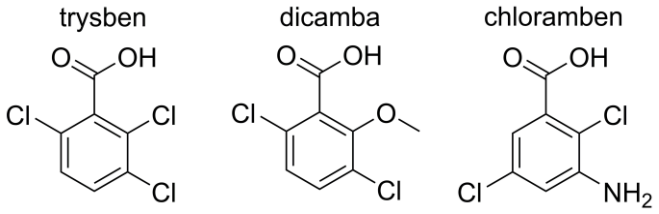

Figure 42. Chemical structures of pesticides under investigation - 2,3,6-TCBA (*trysben*), 3,6-dichloro-2-methoxybenzoic acid (*dicamba*), and 3-Amino-2,5-dichlorobenzoic acid (*chloramben*).

Table 22. The results for hydrodechlorination of chlorinated pesticides *trysben* (entries #1-8), *dicamba* (entries #9-16), and *chloramben* (entries #17-24) upon identical conditions using selected alloy material (50:50 wt.% Al-Ni).

			mechano-thermal Al-Ni 50:50 wt.%					
alloy (mg)	NaOH (mg)	*molar ratio CBA:Al:OH^-	Entry #	*trysben* removal	Entry #	*dicamba* removal	Entry #	*chloramben* removal
270	400	1 : 47/58 : 100	1	100%	9	100%	17	99%
135	400	1 : 23/29: 100	2	100%	10	98%	18	99%
135	200	1 : 23/29 : 50	3	100%	11	97%	19	99%
80	200	1 : 14/17 : 50	4	89%	12	92%	20	99%
80	100	1 : 14/17: 25	5	97%	13	85%	21	95%
40	100	1 : 7/9 : 25	6	59%	14	36%	22	96%
40	50	1 : 7/9 : 25	7	46%	15	39%	23	77%
20	50	1 : 3.5/4 : 25	8	10%	16	15%	24	24%

reaction conditions: : 100 mL of ca 1 mM aqueous solution of the corresponding CBA, stirred at 25 °C and 300 RPM for 5 hrs.
*CBA:Al molar ratio is given for the 50:50 wt.% Al-Ni alloy and 58:42 wt.% Al-Ni alloy, respectively

Table 23. The kinetic rate constants based on the pseudo-first order kinetic model applied for the fitting of decomposition of studied compounds.

compounds	commercial		mechano-thermal	
	50:50 wt.% Al-Ni	58:42 wt.% Al-Ni	50:50 wt.% Al-Ni	58:42 wt.% Al-Ni
2-chloorbenzoic acid	8.5	18.1	29.1	35.0
2,6-dichlorobenzoic acid	5.0	11.1	12.2	21.1
trysben	11.4	-	12.2	-
*dicamba**	8.9	-	14.8	-
*chloramben**	10.7	-	12.0	-

reaction conditions: 100 mL of ca 1 mM aqueous solution of CBA + fixed alloy dosage of 0.8 g/L and 1 g/L of NaOH, stirred at 25 °C and 300 RPM; *increased dosage of reagents to 1.35 g/L pf the alloy and 2 g/L of NaOH

5.3.4 The mechanism of Al-Ni alloys dehalogenation and factors affecting the process

The 50:50 wt.% Al-Ni alloy was identified to contain primarily Al_3Ni and Al_3Ni_2 phases (unreacted Al might be present as well), which is in accordance with the binary Al-Ni phase diagram. Kinetics of the dissolution of these two phases plays crucial role in utilization of the alloy for the HDH reactions. According to the XRPD results after the reaction, it can be seen that primarily Al_3Ni phase is being consumed in diluted sodium hydroxide solution, whereas the kinetics of Al_3Ni_2 phase leaching is much slower at ambient temperature. This is demonstrated by the XRPD pattern of a leached alloy after 5 hours in 0.1 wt.% NaOH solution and ambient conditions (Figure 43b). Clearly, diffraction peaks assigned to nano-crystalline, in-situ formed, Raney nickel can be identified, while the rest of the peaks is assigned solely to Al_3Ni_2 phase. By this time, Al_3Ni phase has already disappeared and transformed fully into the nickel metal. Although the Raney nickel prepared by leaching of the two crystallographically different intermetallic phases can possess different solid-state properties, the change in the reaction rate cannot be observed. This is given by the complexity of the system and simultaneous leaching of the two phases. It is possible that in a pure sample of Al_3Ni phase the true reaction rate for this phase could be measured. The nickel formed by leaching of the Al_3Ni phase was found to be more brittle and disintegrate to provide higher surface area [57]. It is supported also by the observed differences in the reaction kinetics for 2-CBA and 2,6-DCBA compounds. The materials containing higher mass fraction of the Al_3Ni (equal to 58:42 wt.% Al-Ni) showed in all cases faster decomposition rates. On the other hand, for concentrated solutions of contaminants, slow dissolution of Al_3Ni_2 phases provided higher % removal in long runs (17 hours) as seen in Table 20. Another factor that will affect the process from the material´s side, in combination with the phase composition, is the grain size of the used alloy. Since the leaching of aluminum is a diffusion controlled process, the grain size can have a significant effect on the total fraction of aluminum leached, and therefore on hydrogen gas evolution. Especially for the Al_3Ni_2 phase, this plays the crucial role. Within the performed experiments, a difference of 20-30% of aluminum fraction leached between the commercial and the mechano-thermally prepared 50:50 wt.% alloy was observed. The materials also showed significantly diverse particle size distribution curves. Therefore, maintaining defined particle size class and a phase composition are the key components of the Al-Ni alloys design for the HDH application.

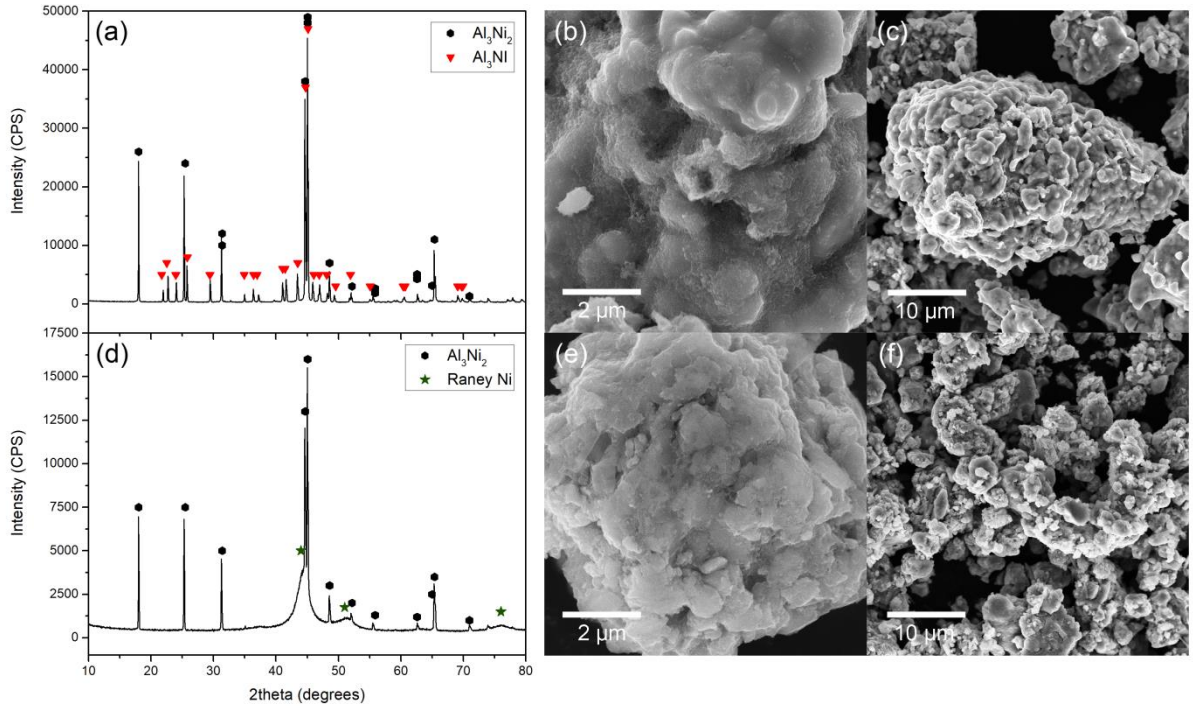

Figure 43. The XRPD pattern of the mechano-thermal 50:50 wt.% Al-Ni alloy composed of Al_3Ni and Al_3Ni_2 phases (a) and its detailed morphology (b, c), the XRPD pattern after leaching (d) and disintegrated particle of porous Raney nickel metal (e, f).

While the particle size appeared to have a significant effect on the total efficiency, unreliable results were obtained when comparing three different batches of the 50:50 wt.% alloy. The material obtained from unknown supplier, with d_{90} = 70 µm (as defined by supplier), showed hydrophobic behavior and was found to provide far worse results. The XRPD pattern of the material showed no difference from the other alloys and according the SEM images, it was prepared by the same method as the commercial 50:50 wt.% alloy obtained from Sigma-Aldrich (cast-and-crush). When inspected by thermogravimetric analysis, out of the three tested alloys, the highest mass loss was measured, close to 0.5 wt.%. The mass loss could be assigned to the unwashed PCA used in the crushing step of the alloy preparation. The presence of such coating, especially in the case of required wettability of the material is crucial. In comparison, the mechano-thermally prepared alloy, showed mass loss of only 0.04%, since volatile PCA was implemented in the process of the preparation.

While it might seem obvious, in many studies, only the optimal conditions were discussed and the effect of parameters such as temperature, scale, and stirring are skipped. From the technological point of view, these are the key factors affecting the process in real working conditions. Although temperature will affect the leaching of aluminum from the alloy, stirring is responsible for mass transfer inside a reactor, to secure efficient collisions

and promote the HDH reaction. We determined to what extent the HDH reaction is affected by these two factors.

Besides the abovementioned factors, one must be aware that the hydrodehalogenation reaction is a highly heterogeneous process comprising all physical states (solid/liquid/gas). Since the Al-Ni alloys are much heavier than the aqueous phase containing contaminants, a strong tendency for settling will be observed and the reagent will not be available for the chemical reaction. To avoid heterogeneity as a limiting factor of the process, the stage of complete suspension should be reached. This lies in a correct design of the batch reactor. The kinetics of 2-chlorobenzoic acid decomposition using 1 L reagent bottle is shown in Figure 44a. Several different scenarios were compared to explicitly show how big the impact on the dehalogenation reaction is at ambient temperature. It is clear that when no stirring is involved, all alloy particles are settled and slowly, during the reaction progress, they get saturated with hydrogen gas bubbles. This creates impermeable interface and the reaction practically stops. When a magnetic stirring bar is applied to the vessel, the reaction proceeds, however, at comparably slower rates than in the case of 100 mL reaction volume (under the same reaction conditions; dosage 0.8 g/L alloy + 1 g/L NaOH). This is due to the missing horizontal drag responsible for uplifting the alloy´s particles. Such drag can be only created with mechanical stirrers of suitable shape. Here, four blade turbine with was utilized to secure sufficient axial drag. This allowed to achieve the same reaction kinetics while maintain the same stirring rate. For scale-up, the reactor design and stirring should be carefully specified so as to maintain expected reaction times and good aluminum leachability.

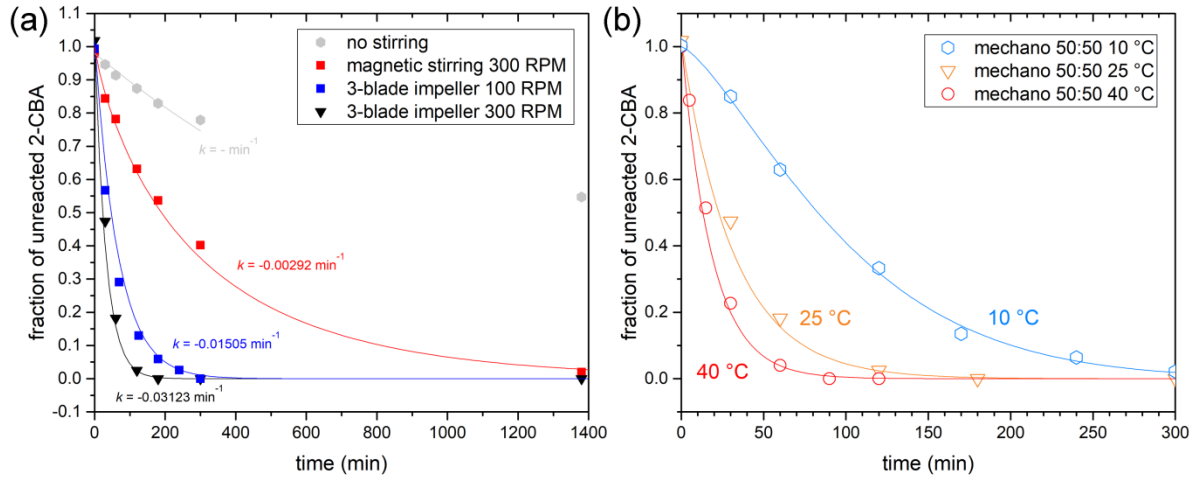

Figure 44. The comparison of 1 L scale experiment under the identical reaction conditions using different stirring (a); the decomposition kinetics of 2-CBA at different temperatures (b).

Once sufficient stirring is secured, the temperature parameter was varied at 1 L scale as seen in Figure 44b. The experiment was checked with the kinetic rate constant obtained at a small scale. The kinetic rate in this case was rapidly affected by lowering the temperature to 10 °C and the process was prolonged several-fold time. In addition, the kinetics could not be simply described by the pseudo-first kinetic order model. It showed sigmoidal character. For this, Avrami model was implemented as it was usually implemented for the leaching kinetics processes. According to the measured data points, it seems that in the very beginning of the HDH reaction, an induction period appears which is not resolved for room temperature and can be ignored. On the other hand, increasing temperature up to 40 °C led to an increase in the decomposition rate by 1.7 times, which might be beneficial for the process.

5.3.5 Recycling of the used alloy

The Raney type Al-Ni alloys cannot be classified as catalysts, per se. Since the material reacts with the environment and chemically changes (refer to parts 2.7.1 and 2.7.2), it eventually steps out of the reaction as chemically new entity. The Raney nickel, as a catalyst, is formed while aluminum is leached out of the structure. Therefore, materials can be only used on a limited basis and the reactions cannot be cycled. Instead, commercially available catalysts based on precious metals (Pd/C or Pt/C), provide the possibility of re-use; if the catalyst is not destroyed or poisoned (organic products, chloride ions) during the reaction. The question about sustainability arises at this point. First of all, while the reaction itself is not repeatable with the same reagents, in-situ formed Raney nickel is industrially valuable product. This can be further processed and used in catalytic hydrogenation. It is noted that such use within one commercial subject is improbable. After use, the material would be preferentially disposed, which is of a big concern due to the current nickel/alloy prices. Here, a potential sustainability plan is demonstrated utilizing easy and inexpensive reprocessing of the alloy after use. The main point of the process is re-milling of the spent alloy with aluminum powder (approx. $1/10^{th}$ of nickel price) and subsequent thermal treatment of the physical mixture. The regeneration route is basically identical to the preparation method. Figure 45a shows the XRPD pattern of leached alloy after 5 hours reaction time (black line) and the same material remilled with aluminum (red line). The SEM picture of the milled mixture is shown in Figure 45b. After milling, a physical mixture of unreacted Al_3Ni_2 phase with aluminum and nano-crystalline Raney nickel formed. We processed this mixture at three different temperatures in an argon atmosphere. In this case, the crystallization appeared above the melting point of aluminum. Annealing at 700 °C for

period of two hours allowed for the formation of alloy (with nominal amounts of unreacted aluminum metal) (Figure 45a, green).

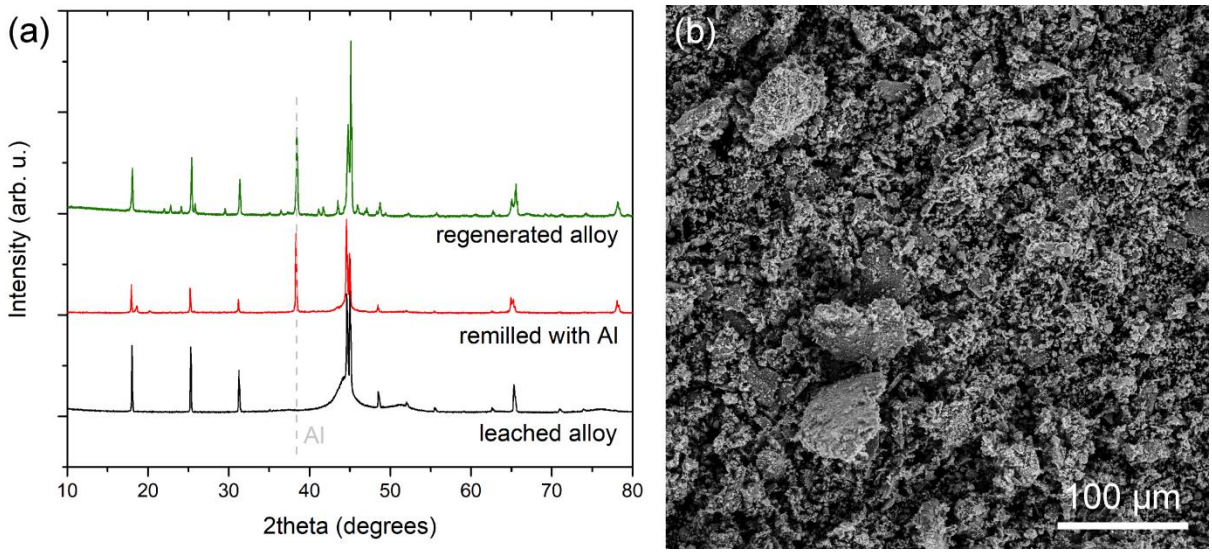

Figure 45. The XRPD pattern of the spent alloy, alloy remilled with Al powder, and thermal-processed product (a), SEM picture of the spent alloy re-milled with Al powder (b).

This material can be used again in the hydrodehalogenation process. The result for use of the reprocessed alloy material on the model solution of 2-CBA or 2,6-DCBA at two concentration levels. The suggested method is considered to be a ground-breaking discovery in terms of applicability of the Al-Ni alloys for hydrodehalogenation reaction. It only includes short remilling of the spent alloy with cheap aluminum powder and thermal treatment at still relatively low temperatures. Molten metal work-up is for this process completely avoided and it only concerns technologically not demanding requires simple equipment. It is highlighted that mechano-thermal preparation of the Al-Ni alloys, proposed herein, is superior to any other published methods for Al-Ni alloys preparation so far. It is faster, performed at temperatures as low as 500 °C, and does not need any additional processing. On the top of that, for the HDH reaction at high pH, technical grade metals are of sufficient purity and represent no danger for its use. For commercial application, continuous feed ball-mills attached to continuously operating furnace are an economically feasible option for a large-scale alloy production via proposed methodology. Combined with the regeneration plan, it allows for relatively simple recycling of the materials and minimizing of the total costs for technology.

Table 24. The results for 2-CBA and 2,6-DCBA hydrodehalogenation with the regenerated alloy material at two concentration levels.

2-chlorobenzoic acid				
alloy (mg)	NaOH (mg)	2-CBA (mM)	removal (%)	removal (%)[#]
135	200	2.965*	71	>99
80	200	6.302*	49	97.1
80	100	0.044	96	>99
40	100	0.530	45	>99
2,6-dichlorobenzoic acid				
alloy (mg)	NaOH (mg)	2,6-DCBA (mM)	removal (%)	removal (%)[#]
135	200	5.951*	42	90
80	200	7.530*	27	86
80	100	0.400	60	89
40	100	0.697	28	79

[#]originally mechano-thermally prepared 50:50 wt.% Al-Ni alloy material
*starting concentration was set to 10 mM of contaminats (2-CBA or 2,6-DCBA).

6 CONCLUSION

The main aim of this thesis was to develop an easy and scalable preparation for Al-Ni alloys preparation via a low-temperature mechanochemical method. The Raney type Al-Ni alloys were shown previously to be powerful reducing reagents in basic aqueous environments. The fabrication of these materials was in the end achieved by a combination of mechanical activation of powder metal mixtures in a ball mill and their thermal processing at temperatures 500-700 °C. Nano-crystalline, air-stable, alloy materials were obtained via this process. As expected, the materials were composed of nano-crystalline intermetallic Al_3Ni_2 and Al_3Ni phase. Through aluminum leaching in basic aqueous environment, these provided highly active Raney nickel. The Raney nickel catalyst is widely used porous structure for catalytic hydrogenation reactions.

Prepared materials were applied for hydrodechlorination of various environmental pollutants in a basic environment. The efficiency of dehalogenation was compared to the commercially available analogues with the identical Al-Ni wt.% composition. As demonstrated in the experimental part, mechano-thermally prepared alloys showed superior hydrodehalogenation properties due to their unique microstructure. The robustness of the HDH technology using prepared Al-Ni alloys was verified based upon several observations

1. The reaction itself is not compound specific but rather C-Cl bond specific. The number of halogen atoms and the compound´s structure will affect the kinetics of removal.
2. The reaction conditions for specific contaminant studied can be optimized experimentally in a few steps, for complex systems design of experiments (DoE) can be implemented.
3. Regardless of the contaminant, the reaction will be affected by temperature and stirring.
4. The reaction can be scaled up several fold time but the process parameters will need to be adjusted in order to reach the same removal efficiency.
5. The reaction can be applied to samples of real wastewater showing high efficiency for halogenated benzenes removal.
6. The Raney type Al-Ni alloys provide an alternative to less efficient bimetallic couples or costly precious metal based hydrogenation catalysts.

Although the technology is robust and fast, it has several drawbacks. The main drawback lies in the post treatment of cleaned water and regeneration of the reagents. Sodium hydroxide, found as an ideal leaching agent, is a relatively cheap chemical. However, it creates an environment with high pH values. In the neutralization step, a relatively large amount of acid is needed to neutralize the mixture. This should not be of a big concern if technology is applied for industrial effluents. High pH values can potentially represent a risk for natural waters containing living organisms. The use of other bases at lower pH was shown to be not as efficient. The aluminum leaching was the limiting step.

The current market prices of Al-Ni alloys are even of more concern regarding the economical sustainability of the process. Recently, the nickel metal price has grown significantly. To cut down on total costs of the HDH technology, a suitable way for the preparation has to be developed on a large scale. This may be possible by designing a continuous milling process followed by thermal treatment as outlined within this thesis. In the last part of the thesis, a simple plan for regeneration of the alloy materials was outlined. The materials can be regenerated by simple re-milling of the spent alloy material with fresh aluminum powder followed by thermal processing. This process is similar to the alloy preparation. The regenerated material showed promising hydrodehalogenation properties as well. Along the mechano-thermal preparation process for Al-Ni alloys, outlined regeneration plan can help to considerable decrease material costs. Overcoming material price problems may attract more attention for the HDH technology based on Al-Ni alloys.

LIST OF REFERENCES

[1] FIEDLER, Heidelore, Roland KALLENBORN, Jacob de BOER and Leiv K. SYDNES. The Stockholm Convention: A Tool for the Global Regulation of Persistent Organic Pollutants. *Chemistry International*. 2019, **47**(2).

[2] PANAGOS, Panos, Marc VAN LIEDEKERKE, Yusuf YIGINI and Luca MONTANARELLA. Contaminated sites in Europe: Review of the current situation based on data collected through a European network. *Journal of Environmental and Public Health*. 2013.

[3] ALONSO, Francisco, Irina P BELETSKAYA and Miguel YUS. Metal-Mediated Reductive Hydrodehalogenation of Organic Halides. Chemical *Reviews*. 2002, **102**, 4009-4091.

[4] BELL, M. The Reduction of Organic Halogen Compounds by Sodium Borohydride. *The Journal of Organic Chemistry*. 1969, **34**(12), 1967–1970.

[5] HE, Pan Pan, Chuan Shu HE, Qi LIU and Yang MU. Dehalogenation of diatrizoate using nanoscale zero-valent iron: Impacts of various parameters and assessment of aerobic biological post-treatment. *RSC Advances*. 2017, **7**(44), 27214–27223.

[6] MINES, Paul D., Kamilla M.S. KAARSHOLM, Ariadni DROUMPALI, Henrik R. ANDERSEN and Yuhoon HWANG. Estimating dehalogenation reactivity of nanoscale zero-valent iron by simple colorimetric assay by way of 4-chlorophenol reduction. *Environmental Engineering Research*. 2019, **25**(2), 197–204.

[7] JING, Ran, Soliver FUSI and Birthe V KJELLERUP. Remediation of Polychlorinated Biphenyls (PCBs) in Contaminated Soils and Sediment : State of Knowledge and Perspectives. *Frontiers in Environmental Science*. 2018, **6**(July), 1–17.

[8] JOVANOVIC, Goran N., James E. ATWATER, Polona ŽNIDARŠIČ-PLAZL and Igor PLAZL. Dechlorination of polychlorinated phenols on bimetallic Pd/Fe catalyst in a magnetically stabilized fluidized bed. *Chemical Engineering Journal*. 2015, **274**, 50–60. ISSN 13858947.

[9] SHIH, Yang hsin, Yao Cyong CHEN, Meng yi CHEN, Yu tsung TAI and Chih Ping TSO. Dechlorination of hexachlorobenzene by using nanoscale Fe and nanoscale Pd/Fe bimetallic particles. *Colloids and Surfaces A: Physicochemical and Engineering Aspects*. 2009, **332**(2–3), 84–89.

[10] COUTTS, Janelle L., Robert W. DEVOR, Brian AITKEN, Michael D. HAMPTON, Jacqueline W. QUINN, Christian A. CLAUSEN and Cherie L. GEIGER. The use of mechanical alloying for the preparation of palladized magnesium bimetallic particles for the remediation of PCBs. *Journal of Hazardous Materials*. 2011, **192**(3), 1380–1387.

[11] ENGELMANN, Mark D., John G. DOYLE and I. Francis CHENG. The complete dechlorination of DDT by magnesium/palladium bimetallic particles. *Chemosphere*. 2001, **43**(2), 195–198.

[12] WEIDLICH, Tomáš, Anna KREJČOVÁ and Lubomír PROKEŠ. Study of dehalogenation of halogenoanilines using Raney Al-Ni alloy in aqueous medium at room temperature. *Monatshefte fur Chemie*. 2010, **141**, 1015-1020.

[13] WEIDLICH, Tomáš and Lubomír PROKEŠ. Facile dehalogenation of halogenated anilines and their derivatives using Al-Ni alloy in alkaline aqueous solution. *Central European Journal of Chemistry*. 2011, **9**(4), 590–597.

[14] WEIDLICH, Tomáš, Lubomír PROKEŠ and Dagmar POSPÍŠILOVÁ. Debromination of 2,4,6-tribromophenol coupled with biodegradation. *Central European Journal of Chemistry*. 2013, **11**(6), 979–987.

[15] WEIDLICH, Tomáš, Jakub OPRŠAL, Anna KREJČOVÁ and Bohumil JAŠÚREK. Effect of glucose on lowering Al-Ni alloy consumption in dehalogenation of

halogenoanilines. *Monatshefte fur Chemie*. 2015, **146**(4), 613–620.
[16] PÉRKO, Jan, Barbora KAMENICKÁ and Tomáš WEIDLICH. Degradation of the antibacterial agents triclosan and chlorophene using hydrodechlorination by Al-based alloys. *Monatshefte fur Chemie*. 2018. **149**, 1777–1786.
[17] HEGEDUS, Michal, Petr LACINA, Miroslav PLOTĚNÝ, Jaroslav LEV, Barbora KAMENICKÁ and Tomáš WEIDLICH. Fast and efficient hydrodehalogenation of chlorinated benzenes in real wastewaters using Raney alloy. *Journal of Water Process Engineering*. 2020, **38**, 101645.
[18] WEIDLICH, Tomáš, Barbora KAMENICKÁ, Klára MELÁNOVÁ, Veronika ČIČMANCOVÁ, Alena KOMERSOVÁ and Jiří ČERMÁK. Hydrodechlorination of different chloroaromatic compounds at room temperature and ambient pressure—differences in reactivity of Cu-and Ni-based Al alloys in an alkaline aqueous solution. *Catalysts*. 2020, **10**(9), 994.
[19] BENDOV, Helena, Barbora KAMENICK, Milan VLČEK and Petr ŠVEC. Application of Raney Al-Ni Alloy for Simple Hydrodehalogenation of Diclofenac and Other Halogenated Biocidal Contaminants in Alkaline Aqueous Solution under Ambient Conditions. *Materials*. 2022, **15**(11), 3939.
[20] LIU, Guo-Bin, Takehito TSUKINOKI, Tadashige KANDA, Yoshiharu MITOMA and Masashi TASHIRO. Organic Reaction in Water. Part 2. A New Method for Dechlorination of Chlorobiphenyls Using a Raney Ni-AI Alloy in Dilute Aqueous Alkaline Solution. *Tetrahedron Letters*. 1998, **39**, 5991–5994.
[21] LIU, Guo-bin, Lu DAI, Xiang GAO, Miao-kui LI and Thies THIEMANN. Reductive degradation of tetrabromobisphenol A (TBBPA) in aqueous medium. *Green Chemistry*. 2006, **9**, 781–783.
[22] JAMES, Stuart, J. Chrostopher ADAMS, Carsten BOLM, Dario BRAGA, Paul COLLIER and Tomislav FRIŠČIC. Mechanochemistry: opportunities for new and cleaner synthesis. *Chemical Society reviews*. 2012, **41**, 413–447.
[23] BALÁŽ, Peter. *Mechanochemistry in nanoscience and minerals engineering*. Springer-Verlag Berlin Heidelberg, 2008. ISBN 9783540748540.
[24] BALÁŽ, Peter, Marcela ACHIMOVIČOVÁ, Matej BALÁŽ, Peter BILLIK, Zara CHERKEZOVA-ZHELEVA, José Manuel CRIADO, Francesco DELOGU, Erika DUTKOVÁ, Eric GAFFET, Francisco José GOTOR, Rakesh KUMAR, Ivan MITOV, Tadej ROJAC, Mamoru SENNA, Andrey STRELETSKII and Krystyna WIECZOREK-CIUROWA. Hallmarks of mechanochemistry: from nanoparticles to technology. *Chemical Society reviews*. 2013, **42**(18), 7571–637.
[25] JAMES, Stuart and Tomislav FRIŠČIC. Mechanochemistry. *Chemical Society reviews*. 2013, **42**(18), 7494–7496.
[26] TÓTHOVÁ, E., M. SENNA, A. YERMAKOV, J. KOVÁČ, E. DUTKOVÁ, M. HEGEDÜS, M. KAŇUCHOVÁ, M. BALÁŽ, Z.L. BUJŇÁKOVÁ, J. BRIANČIN and P. MAKRESKI. Zn source-dependent magnetic properties of undoped ZnO nanoparticles from mechanochemically derived hydrozincite. *Journal of Alloys and Compounds*. 2019, **787,** 1249-1259.
[27] CHAURUKA, S. R., A. HASSANPOUR, R. BRYDSON, K. J. ROBERTS, M. GHADIRI and H. STITT. Effect of mill type on the size reduction and phase transformation of gamma alumina. *Chemical Engineering Science* [online]. 2015, 134, 774-783.
[28] HEGEDÜS, M., Matej BALÁŽ, M TEŠINSKÝ, M SAYAGUES, P. SIFFALOVIC, M KRUĽAKOVÁ, Mária KAŇUCHOVÁ, Jaroslav BRIANČIN, M. FABIÁN and Peter BALÁŽ. Scalable synthesis of potential solar cell absorber Cu_2SnS_3 (CTS) from nanoprecursors. *Journal of Alloys and Compounds*. 2018, **768**, 1006.
[29] HEGEDÜS, M., P. BALÁŽ, M. BALÁŽ, P. SIFFALOVIC, N. DANEU, M.

KAŇUCHOVÁ, J. BRIANČIN and M. FABIÁN. Mechanochemical approach to a Cu_2ZnSnS_4 solar cell absorber via a „micro-nano" route. *Journal of Materials Science*. 2018, **53**, 13617–13630.
[30] JEONG, Haneul and Junhyung LEE. 3D-Superstructured Networks Comprising Fe-MIL-88A Metal-Organic Frameworks Under Mechanochemical Conditions. *European Journal of Inorganic Chemistry*. 2019, **2019**(42), 4597–4600.
[31] CHEN, Kunfeng and Dongfeng XUE. A chemical reaction controlled mechanochemical route to construction of CuO nanoribbons for high performance lithium-ion batteries. *Physical Chemistry Chemical Physics*. 2013, **15**(45), 19708–19714.
[32] DE OLIVEIRA, Paulo F.M., Jhon QUIROZ, Daniela C. DE OLIVEIRA and Pedro H.C. CAMARGO. A mechano-colloidal approach for the controlled synthesis of metal nanoparticles. *Chemical Communications*. 2019, **95**.
[33] EINFAL, Tomaž, Odon PLANINŠEK and Klemen HROVAT. Methods of amorphization and investigation of the amorphous state. *Acta pharmaceutica*. 2013, **63**(3), 305-334.
[34] ELISEI, Elena, Jean François WILLART, Florence DANÈDE, Jürgen SIEPMANN, Florence SIEPMANN and Marc DESCAMPS. Crystalline Polymorphism Emerging From a Milling-Induced Amorphous Form: The Case of Chlorhexidine Dihydrochloride. *Journal of Pharmaceutical Sciences*. 2018, **107**(1), 121–126.
[35] OLIVEIRA, Paulo F.M., Jean François WILLART, Juergen SIEPMANN, Florence SIEPMANN and Marc DESCAMPS. Using Milling to Explore Physical States: The Amorphous and Polymorphic Forms of Dexamethasone. *Crystal Growth and Design* [online]. 2018, **18**(3), 1748-1757.
[36] EL-ESKANDARANY, M. Sherif. Introduction. *Mechanical Alloying*. William Andrew Inc. 2001. ISBN 978-0-8155-1462-6.
[37] IMAMURA, Kenichi and Mamoru SENNA. Change in the phase stability of zinc blende and wurtzite on grinding. *Journal of the Chemical Society, Faraday Transactions 1: Physical Chemistry in Condensed Phases* [online]. 1982, **78**(4).
[38] SENNA, M. Problems on the mechanically induced polymorphic transformation. *Crystal Research and Technology*. 1985, **20**(2), 209–217.
[39] REN, Ruiming, Zhenguo YANG a L. L. SHAW. Polymorphic transformation and powder characteristics of TiO_2 during high energy milling. *Journal of Materials Science* [online]. 2000, **35**, 6015-6026.
[40] NEIKOV, OLEG, NABOYCHENKO, STANISLAV. Chapter 2: Mechanical Crushing and Grinding. *Handbook of Non-Ferrous Metal Powders*. Elsevier. 2018. ISBN 978-0-0810-0543-9.
[41] NEIKOV, Oleg D. *Mechanical Crushing and Grinding*. 2. edition. Elsevier Ltd., 2019. ISBN 9780081005439.
[42] LÜ, L and M O LAI. *Mechanical Alloying*. Springer New York, NY, 1998. ISBN 978-0-7923-8066-5.
[43] DUROUDIER, Jean-Paul. Ball and Rod Mills. In: *Size Reduction of Divided Solids*. Elsevier. 2016. ISBN 978-1-78548-185-7.
[44] GOCK, Eberhard and Karl Eugen KURRER. Eccentric vibratory mills - Theory and practice. In: *Powder Technology*. 1999, 302–310.
[45] SIDOR, J. A mechanical layered model of a vibratory mill. *Mechanics and Control*. 2010, **29**(3), 138–148.
[46] SONI, P.R. *Mechanical Alloying: Fundamentals and Applications*. Cambridge International Science Publishing. 1999. ISBN 978-1-8983-2656-4.
[47] WEIDENTHALER, Claudia. In Situ Analytical Methods for the Characterization of Mechanochemical Reactions. *Crystals*. 2022, **12**(3), 345.

[48] MAURICE, D. R. and T. H. COURTNEY. The physics of mechanical alloying: A first report. *Metallurgical Transactions A*. 1990, **21**(1), 289–303.
[49] GONZÁLEZ, Gema, L. D'ANGELO, J.L. OCHOA, B. LARA and E. RODRIGUEZ. The Influence of Milling Intensity on Mechanical Alloying. *Journal of Metastable and Nanocrystalline Materials*. 2002, **13**, 159–164.
[50] BURGIO, N., A. IASONNA, M. MAGINI, S. MARTELLI and F. PADELLA. Mechanical alloying of the Fe-Zr system. Correlation between input energy and end products. *Il Nuovo Cimento D*. 1991, **13**(4), 459–476.
[51] GIL-GONZÁLEZ, Eva, Luis A. PÉREZ-MAQUEDA, Pedro E. SÁNCHEZ-JIMÉNEZ and Antonio PEREJÓN. Paving the Way to Establish Protocols: Modeling and Predicting Mechanochemical Reactions. *Journal of Physical Chemistry Letters*. 2021, **12**(23), 5540–5546.
[52] DEEVI, S. C. and V. K. SIKKA. Nickel and iron aluminides: An overview on properties, processing, and applications. *Intermetallics*. 1996, **4**(5), 357–375.
[53] HUANG, W. and Y. A. CHANG. A thermodynamic analysis of the Ni-Al system. *Intermetallics*. 1998, **6**(6), 487–498.
[54] BRAMMER, Travis Michael. Improving the phase stability and oxidation resistance of β-NiAl by. 2011. 90 pages. Master thesis. Iowa State University.
[55] TAYLOR, A. and N. J. DOYLE. Further studies on the nickel–aluminium system. I. β-NiAl and δ-Ni_2Al_3 phase fields . *Journal of Applied Crystallography*. 1972, **5**(3), 201–209.
[56] URRUTIA, Andrea, Silvana TUMMINELLO, Diego Germán LAMAS and Silvana SOMMADOSSI. X-Ray Characterization of Intermetallic Phases in Al/Ni Multilayer System. *Procedia Materials Science*. 2015, **8**, 1150–1159.
[57] BAKKER, M. L., D. J. YOUNG and M. S. WAINRIGHT. Selective leaching of $NiAl_3$ and Ni_2Al_3 intermetallics to form Raney nickels. *Jounal of materials science*. 1988, **23**, 3921–3926.
[58] LIU, Z. G., J. T. GUO, L. L. HE and Z. Q. HU. Formation of B2 Intermetallic NiAl and FeAl By Mechanical Alloying. *Nanostructured Materials*. 1994, **4**(7), 787–794.
[59] ATZMON, Michael. In situ thermal observation of explosive compound-formation reaction during mechanical alloying. *Physical Review Letters*. 1990, **64**(4), 487–490.
[60] CARDELLINI, F, G MAZZONE, A MONTONE, M Vittori ANTISARI and Centro Ricerche Energia CASACCIA--DIVISIONE. Solid state reactions between Ni and Al powders induced by plastic deformation. 1994, **42**(7), 2445–2451.
[61] RAFIEI, Mahdi, Hossein MOSTAAN, Farshid ABBASI, Ali HAMZELU and Mahdi ORAEI. Mechanochemical assisted synthesis of NiAl and Ni_2AlSi intermetallic: A comparative study on the corrosion behavior. *Materials Research Express*. 2019.
[62] NAEEM, Haider T., Kahtan S. MOHAMMAD and Azmi RAHMAT. Synthesis of Al–Ni Intermetallic Compounds by Mechanical Alloying. *Metallurgist*. 2014, **58**(7–8), 615–621.
[63] VUONG, Quang Tran, Phan Quang THANG, Takeshi OHURA and Sung Deuk CHOI. Chlorinated and brominated polycyclic aromatic hydrocarbons in ambient air: seasonal variation, profiles, potential sources, and size distribution. *Reviews in Environmental Science and Biotechnology* [online]. 2020, **19**(2), 259–273.
[64] JIN, Rong, Minghui ZHENG, Gerhard LAMMEL, Benjamin A.Musa BANDOWE and Guorui LIU. Chlorinated and brominated polycyclic aromatic hydrocarbons: Sources, formation mechanisms, and occurrence in the environment. *Progress in Energy and Combustion Science*. 2020, **76**, 100803.
[65] FIELMAN, Kevin T., Sarah A. WOODIN, Michael D. WALLA and David E. LINCOLN. Widespread occurrence of natural halogenated organics among temperate marine infauna. *Marine Ecology Progress Series*. 1999, **181**, 1–12.

[66] XU, Ranyun, Yawei XIE, Jinping TIAN and Lyujun CHEN. Adsorbable organic halogens in contaminated water environment: A review of sources and removal technologies. *Journal of Cleaner Production*. 2021, **283**, 124645.
[67] BORJA, Josephine, Donna Marie TALEON, Joseph AURESENIA and Susan GALLARDO. Polychlorinated biphenyls and their biodegradation. *Process Biochemistry*. 2005, **40**(6), 1999–2013.
[68] CSUROS, Z., J. PETRO and J. VOROS. Investigations With the Use of Raney Nickel Catalyst. *Periodica Polytechnica Chemical Engineering*. 1957, **1**(3), 153–185.
[69] WEIDLICH, Tomáš, Petr LACINA and Michaela ŠTĚPÁNKOVÁ. Effective destruction of (poly)chlorinated aromatic compounds using aluminium alloys. *Proceedings of the 42nd InternationalConference of the Slovak Society of Chemical Engineering*. 2016. ISBN 978-80-89597-35-2.
[70] YIN, Lifeng, Yunrong DAI, Junfeng NIU, Yueping BAO and Zhenyao SHEN. Rapid dechlorination of chlorophenols in aqueous solution by [Ni|Cu] microcell. *Journal of Hazardous Materials*. 2012, **209**–**210**, 414–420.
[71] DUAN, Jiangtao, Hong ZHU, Fuyuan XU and Jianzhuang ZHAO. A new approach to 4-chlorophenol dechlorination on monometallic copper compared to its Cu/Fe bimetallic system. *Chemical Engineering Journal*. 2016, **304**, 282–288.
[72] HUANG, Qiang, Wen LIU, Ping'an PENG and Weilin HUANG. Reductive dechlorination of tetrachlorobisphenol A by Pd/Fe bimetallic catalysts. *Journal of Hazardous Materials* [online]. 2013, **262**, 634–641.
[73] RAUT, Sandesh S., Rohit SHETTY, Nikhi Maria RAJU, Sanjay P. KAMBLE and Prashant S. KULKARNI. Screening of zero valent mono/bimetallic catalysts and recommendation of Raney Ni (without reducing agent) for dechlorination of 4-chlorophenol. *Chemosphere*. 2020, **250**, 126298.
[74] HAN, Yi, Wei LI, Minghui ZHANG and Keyi TAO. Catalytic dechlorination of monochlorobenzene with a new type of nanoscale Ni(B)/Fe(B) bimetallic catalytic reductant. *Chemosphere*. 2008, **72**(1), 53–58.
[75] MITOMA, Yoshiharu, Yumi KATAYAMA and Cristian SIMION. Chapter: Mechanistic Considerations on the Hydrodechlorination Process of Polychloroarenes. *Organochlorine*. IntechOpen. 2018. ISBN 978-1-78984-263-0.
[76] TASHIRO, Masashi, Akio IWASAKI and Gouki FUKATA. Studies on the Selective Preparation of Aromatic Compounds. An Attempt to Prepare All the Possible Deuterated Phenols by the Reductive Dehalogenation of the Corresponding Halophenols with Raney Alloys in an Alkaline Deuterium Oxide Solution. 1978, **43**(2), 1976–1979.
[77] TASHIRO, M. and K. NAKAYAMA. Preparation of All the Possible Ring-deuteriated Benzoic Acids by Reductive Dehalogenation of the Corresponding Halogenobenzoic Acids with Raney Alloys in an Alkaline Deuterium Oxide Solution. *Journal of Chemical Society*. 1983, 2315–2318.
[78] TASHIRO, Masashi, Hiroshi NAKAMURA and Kouji NAKAYAMA. Reductive dehalogenation of haloacetophenones with raney alloys in alkaline solution. *Organic Preparations and Procedures International*. 1987, **19**(6), 442–446.
[79] TASHIRO, Masashi, Hiroshi NAKAMURA and Kouji NAKAYAMA. Preparation of Deuteriated 1 -Phenylethanols. *Journal of Chemical Society. Perkin Trans.* 1988, 179–181.
[80] CHOUDHARY, Vasant R., Sudhakar K. CHAUDHARI and Ashok N. GOKARN. A Kinetic Model for Leaching Process in Preparation of Raney Nickel Catalyst. *Industrial and Engineering Chemistry Research*. 1989, **28**(1), 33–37.
[81] JUNG, Haeryong and Heechul CHOI. Catalytic decomposition of ozone and para-Chlorobenzoic acid (pCBA) in the presence of nanosized ZnO. Applied Catalysis B: Environmental. 2006, **66**(3–4), 288–294.

[82] LAN, Bingyan, Ruihuan HUANG, Laisheng LI, Huihua YAN, Gaozu LIAO, Xi WANG and Qiuyun ZHANG. Catalytic ozonation of p-chlorobenzoic acid in aqueous solution using Fe-MCM-41 as catalyst. *Chemical Engineering Journal*. 2013, **219**, 346–354.
[83] PARK, Jong Sup, Heechul CHOI and Jaewon CHO. Kinetic decomposition of ozone and para-chlorobenzoic acid (pCBA) during catalytic ozonation. Water Research. 2004, 38(9), 2285–2292.
[84] HUANG, Yiyang, Hui WANG, Kai HUANG, Donggen HUANG, Shuang YIN and Qin GUO. Degradation kinetics and mechanism of 3-Chlorobenzoic acid in anoxic water environment using graphene/TiO_2 as photocatalyst. Environmental Technology (United Kingdom). 2020, 41(17), 2165–2179.
[85] LIU, Guo-bin, Hong-yun ZHAO, Lu DAI and Thies THIEMANN. A convenient method for the reductive degradation of mono-, di-, and tribromodiphenyl ethers, tetrabromo- and tetrachlorobisphenol A with Raney Ni-Al alloy. 2009, **2009**(xiii), 211–226.
[86] LIU, Guo Bin, Hong Yun ZHAO, Jie ZHANG and Thies THIEMANNB. Raney Ni-Al alloy mediated hydrodehalogenation and aromatic ring hydrogenation of halogenated phenols in aqueous medium. *Journal of Chemical Research*. 2009, **6**, 342–344.
[87] YANG, Bo, Fengzhen ZHANG, Shubo DENG, Gang YU, Hong ZHANG, Jianzhong XIAO, Lili SHI and Jincan SHEN. A facile method for the highly efficient hydrodechlorination of 2-chlorophenol using Al-Ni alloy in the presence of fluorine ion. *Chemical Engineering Journal*. 2012, **209**, 79–85.
[88] YANG, Bo, Jiaxing ZHANG, Yunfei ZHANG, Shubo DENG, Gang YU, Jinhua WU, Hong ZHANG and Jianhong LIU. Promoting effect of EDTA on catalytic activity of highly stable Al-Ni bimetal alloy for dechlorination of 2-chlorophenol. *Chemical Engineering Journal*. 2014, **50**, 222-229.
[89] CAGNETTA, Giovanni, John ROBERTSON, Jun HUANG, Kunlun ZHANG and Gang YU. Mechanochemical destruction of halogenated organic pollutants: A critical review. *Journal of Hazardous Materials*. 2016, **313**, 85–102.
[90] BIRKE, V., J. MATTIK and D. RUNNE. Mechanochemical reductive dehalogenation of hazardous polyhalogenated contaminants. *Journal of Materials Science*. 2004, **39**(16–17), 5111–5116.
[91] NAH, In Wook, Kyung Yub HWANG and Yong Gun SHUL. Effect of metal and glycol on mechanochemical dechlorination of polychlorinated biphenyls (PCBs). *Chemosphere*. 2008, **73**(1), 138–141.
[92] BALÁŽ, M., P. BALÁŽ, Z. BUJŇÁKOVÁ, Z. PAP, D. KUPKA and A. ZORKOVSKÁ. Mechanochemical dechlorination of PVC by utilizing eggshell waste. *Proceedings of the 8th International Conference on Mechanochemistry and Mechanical Alloying, INCOME 2014*. 2014, **126**(4), 884–887.
[93] HEGEDÜS, Michal, Marcela ACHIMOVIČOVÁ, Hongjue HUI, Gabin GUÉLOU, Pierric LEMOINE, Ismail FOURATI, Jean JURASZEK, B. MALAMAN, Peter BALÁŽ and Emmanuel GUILMEAU. Promoted crystallisation and cationic ordering in thermoelectric $Cu_{26}V_2Sn_6S_{32}$ colusite by eccentric vibratory ball milling. *Dalton Transactions*. 2020, 49(44), 15828-15836.
[94] BALÁŽ, P., E. GUILMEAU, N. DANEU, O. DOBROZHAN, M. BALÁŽ, M. HEGEDUS, T. BARBIER, M. ACHIMOVIČOVÁ, M. KAŇUCHOVÁ and J. BRIANČIN. Tetrahedrites synthesized via scalable mechanochemical process and spark plasma sintering. *Journal of the European Ceramic Society*. 2020, **40**(5), 1922-1930.
[95] ZHU, Ping, J. C.M. LI and C. T. LIU. Reaction mechanism of combustion synthesis of NiAl. *Materials Science and Engineering A*. 2002, **329**–**331**, 57–68.
[96] CHRIFI-ALAOUI, F. Z., M. NASSIK, K. MAHDOUK and J. C. GACHON. Enthalpies of formation of the Al-Ni intermetallic compounds. *Journal of Alloys and*

Compounds. 2004, **364**(1–2), 121–126.
[97] GATES-RECTOR, S. D. and T. N. BLANTON. The Powder Diffraction File: A Quality Materials Characterization Database. *Powder Diffraction*. 2019, **34**, 352–360.
[98] CHEN, H. L., E. DOERNBERG, P. SVOBODA and R. SCHMID-FETZER. Thermodynamics of the Al_3Ni phase and revision of the Al-Ni system. *Thermochimica Acta*. 2011, **512**(1–2), 189–195.
[99] XIAO, Jiang, Rui HU and Guangcai CHEN. Micro-nano-engineered nitrogenous bone biochar developed with a ball-milling technique for high-efficiency removal of aquatic Cd(II), Cu(II) and Pb(II). *Journal of Hazardous Materials*. 2020, **387**, 121980.
[100] BALÁŽ, Matej, Anna ZORKOVSKÁ, Farit URAKAEV, Peter BALÁŽ, Jaroslav BRIANČIN, Zdenka BUJŇÁKOVÁ, Marcela ACHIMOVIČOVÁ and Eberhard GOCK. Ultrafast mechanochemical synthesis of copper sulfides. *RSC Advances*. 2016, **6**(91), 87836–87842.
[101] HAM, Hyung Chul, Anatoly P. MAGANYUK, Jonghee HAN, Sung Pil YOON, Suk Woo NAM, Tae Hoon LIM and Seong Ahn HONG. Preparation of Ni-Al alloys at reduced temperature for fuel cell applications. *Journal of Alloys and Compounds*. 2007, **446**–**447**, 733–737.
[102] LEE, Yu Jin, Yong Seok LEE, Jun Young CHA, Young Suk JO, Hyangsoo JEONG, Hyuntae SOHN, Chang Won YOON, Yongmin KIM, Kwang Bum KIM and Suk Woo NAM. Development of porous nickel catalysts by low-temperature Ni–Al chemical alloying and post selective Al leaching, and their application for ammonia decomposition. *International Journal of Hydrogen Energy*. 2020, **45**(38), 19181–19191.
[103] ZHANG, Shuo Shuo, Ning YANG, Shou Qing NI, Vinothkumar NATARAJAN, Hafiz Adeel AHMAD, Shiping XU, Xu FANG and Jinhua ZHAN. One-pot synthesis of highly active Ni/Fe nano-bimetal by simultaneous ball milling and in situ chemical deposition. *RSC Advances*. 2018, **8**(47), 26469–26475.
[104] GALLEGO, Alfredo, Virginia L. GEMINI, Ariana A. ROSSEN, Susana L. ROSSI, Valeria TRÍPODI, Daniel CORACH, Estela PLANES and Sonia E. KOROL. Aerobic degradation of 3-chlorobenzoic acid by an indigenous strain isolated from a polluted river. *World Journal of Microbiology and Biotechnology*. 2012, **28**(3), 1245–1252.